UNIVERSITÀ
DEGLI STUDI
FIRENZE

DOCTOR OF PHILOSOPHY IN
INDUSTRIAL ENGINEERING

XXIX CYCLE

PhD COURSE COORDINATOR
Prof. Maurizio DE LUCIA

Development of a radial piston expander for vapor compression cycles

Scientific Sector ING-IND/09

PhD Student
Dott. Giovanni Galoppi

Tutor
Prof. Giovanni Ferrara

Co-tutor
Ing. Lorenzo Ferrari

PhD Course Coordinator
Prof. Maurizio De Lucia

2013/2016

ISBN XXX–XX–XXXX–XXX–X
D/XXXX/XXXX/XX

Ai miei genitori

Ai miei nonni

Ringraziamenti

Desidero ringraziare i Proff. Ennio Antonio Carnevale e Giovanni Ferrara che mi hanno dato la possibilità di seguire il percorso del dottorato di ricerca, offrendomi così un'enorme opportunità per crescere sia dal punto di vista professionale che personale. In particolare, un sentito ringraziamento al Prof. Giovanni Ferrara, sempre pronto a dare preziosissimi consigli nonostante i numerosi impegni. Un enorme grazie anche all'Ing. Lorenzo Ferrari per avermi seguito e supportato con disponibilità, pazienza e dedizione durante questo percorso.

Grazie al Prof. Daniele Fiaschi ed all'Ing. Riccardo Secchi con cui ho condiviso questo lavoro di tesi, passando dai momenti difficili a quelli più felici.

Ringrazio fortemente tutti i colleghi, o meglio amici, del gruppo di ricerca REASE, Alessandro, Alfonso, Andrea F., Andrea T., Fabio, Francesco, Giulio, Giovanni, Isacco, Luca, Michele e Niccolò che hanno reso piacevoli tutte le giornate passate sia in Facoltà che in laboratorio. Non posso non rivolgere uno speciale ringraziamento a Isacco e Luca che hanno speso gran parte del loro tempo, specialmente nei primissimi periodi, per condividere le loro conoscenze e competenze nelle attività svolte.

Un sentito ringraziamento a Francesca per essermi sempre stata vicina, per avermi trasmesso allegria e spensieratezza quando ne avevo più bisogno, e per farmi sempre sentire importante.

Infine, un forte ringraziamento ai miei genitori e tutta la mia famiglia, che mi hanno supportato durante tutto il percorso svolto, e che mi hanno permesso di raggiungere questo importante traguardo.

Table of contents

List of figures

List of tables

List of symbols and acronyms

Nomenclature

A	Area	[m^2]
Bo	Bond number	
c_p	Heat capacity	[$kJ\ kg^{-1}\ K^{-1}$]
D	Diameter	[m]
e	Eccentricity	[m]
g	Gravity acceleration	[$m\ s^{-2}$]
h	Specific enthalpy	[$kJ\ kg^{-1}$]
Ja	Jakob number	
K	Flow coefficient	
l_v	Latent heat	[$kJ\ kg^{-1}$]
M	Mass	[kg]
$\dot{m}$	Mass flow rate	[$kg\ s^{-1}$]
P	Power	[W]
p	Pressure	[Pa]
Q	Heat flow	[W]
R	Radius of the shaft	[m]
	Determination coefficient	
R_v	Volumetric expansion ratio	
rpm	Rotational speed	[rpm]
s	Specific entropy	[$kJ\ kg^{-1}\ K^{-1}$]
T	Temperature	[K]
	Torque	[N m]

U	Specific internal energy	[kJ kg^{-1}]
u	Velocity	[m s^{-1}]
V	Volume	[m^3]
V_0	Dead volume	[m^3]
V_s	Displacement volume	[m^3]
x	Piston displacement	[m]
z	Height	[m]

Greek symbols

β	Agitation factor	
ε	Void fraction	
η	Efficiency	
θ	Crank angle	[rad]
λ	Thermal conductivity	[W m^{-2} K^{-1}]
μ	Viscosity	[Pa s]
ρ	Density	[kg m^{-3}]
σ	Surface tension	[N m^{-1}]
χ	Vapor quality	

Subscripts

b	Bubble
built	built
comp	Compressor
cond	Condenser
cool	Cooling
cyl	Cylinder
des	Desired
disch	Discharge
down	Downstream
eff	Effective
ev	Evaporated
eva	Evaporator

exp	Expander
frict	Friction
heat	Heating
in	Inlet
ind	Indicated
is	Isentropic
liq	Liquid
meas	Measured
mec	Mechanical
mom	Momentum
num	Numerical
out	Outlet
p	Piston
static	Static
suc	Suction
th	Theoretical
thr	Throttling
tot	Total
up	Upstream
v	Valve
vap	Vapor
vol	Volumetric

Abbreviation

BDC	Bottom Dead Centre
CFC	Chlorofluorocarbons
COP	Coefficient Of Performance
GHG	Greenhouse Gas
GWP	Global Warming Potential
HCFC	Hydro-chlorofluorocarbons
HFC	Hydrofluorocarbons
ODP	Ozone Depletin Potential

SLHX	Suction Line Heat Exchanger
TDC	Top Dead Centre
VCC	Vapor Compression Cycle

Introduction

In both residential and industrial applications, the need of thermal and cooling production is fulfilled by the use of heat pumps and refrigeration systems that, in general, operate in base of Vapor Compression Cycles (VCC). Enhancing the energy efficiency of these cycles has been a widespread concern over the last decades. In the global energy field, the continuous increasing of the energy consumption, especially supplied by the burning of fossil fuels, has caused serious environmental problems. The resulting CO_2 emissions lead to global warming, ozone layer depletion, air pollution and acid rain. This issue can be solved either by finding new technologies or by improving the efficiencies of the existent technologies.

In a VCC unit, the losses that cause deviations from the ideal reversed Carnot cycle are due to the non-isothermal heat rejection in the condenser and the non-isentropic expansion through the throttling valve. For these reasons, in order to improve the efficiency of this cycle, many researchers investigated strategies for reducing the discharge compressor temperature and for improving the throttling process. The reduction of the discharge compressor temperature for lowering the heat rejection losses during the condensation has been investigated by using an inter-cooled multi-stage compression. However, it must be considered that most of the cycle irreversibilities comes from the throttling valve, which wastes up to 20% of the compressor input. In addition to the use of internal heat exchangers and ejectors, a practicable solution to increase the energy efficiency of such system by improving the expansion process is to replace the throttling valve with a two-phase expander, leading to a recovery of the expansion work by exploiting the pressure drop between the condenser and the evaporator. In this way, the power required to the cycle decreases so that to obtain an enhancement of the coefficient of performance (COP). Moreover, when the expander works in a refrigeration cycle, the COP further improves due to the increase of the cooling capacity in the evaporator.

The use of an expander is substitution of the throttling valve is more efficient and leads to higher COP improvements with greater pressure levels as thermodynamic conditions at the condenser and the evaporator. For this reason, this technology is studied mainly in CO_2 cycles, where high pressure values are reached and the COP of the basic cycle is lower in comparison to the traditional HFC cycles.

In this work, an expander in place of the throttling valve in a common VCC unit has been developed. The results present in this Thesis are part of a more extended research carried out in a European Project for the promotion of technological and economic advantages for the SMEs in collaboration with the RTD performers of KTH (Stockholm) and NTUA (Athens) and four SMEs from Greece, Italy and Sweden. The main purpose of the research is the development of an expander in a vapor compression cycle by using an existing machine already present in the market for other applications. In this way, an expander has been developed with low manufacturing costs. In particular, the investigated expander is derived by a radial piston motor for hydraulic applications that works with oil.

Among the expanders studied in literature, radial piston expanders were investigated in very few cases in comparison to other technologies as scroll, screw and vane expanders. These studies have showed the difficulty of using this technology in the present application because of the low efficiency obtained by expanding a liquid and the low produced powers. As concern piston type expanders, whereas the large number of interacting surfaces causes high friction losses and torque pulsations are produced, great advantages due to the very low starting torque and the ability to work in off-design conditions justify the use of this type of motors for small size and seasonal applications.

In order to evaluate the issues that affect the expander performance inside a VCC unit, a fast and flexible numerical model is needed leading to reduce the computational costs. Because of the lack of models on expansion of wet fluids in literature, an approach based on simplified numerical models used in the reciprocating compressor field has been developed. In particular, a 0D quasi-steady model has been implemented into EES® environment to evaluate the variation of the thermodynamic parameters in the cylinders with time-step progress. The accuracy of this model has been assessed by comparing it with the commercial software AMESim® that contains validated libraries on specific components. The numerical analysis has allowed to identify the needed small modifications to be made on the expander without changing its architecture.

An extensive experimental activity on the modified expander has been necessary to characterize it in detail and evaluate the effective performance. With this aim, a dedicated test rig and a measurement system have been developed. The expander has been rigidly connected to an electric motor, which regulates the rotational speed. In addition to the standard instruments needed to calculate the power output and the isentropic efficiency, the machine has been also equipped with dynamic pressure sensors to determine the indicate power. The acquisition of the measurements has been performed by using two different purposely developed LabVIEW® software in order to generate the indicated cycles and to control the brushless.

The large use of VCC units working with HFCs, and in particular R134a, which is being phased out, but has some practical undoubtable advantages like safety, low cost and large availability, has led to evaluate the effective performance of the expander in these systems. The tests with R134a have been performed in a DORIN test rig, where the influence of the thermodynamic conditions at the expander inlet and the rotational speed on the performance in terms of isentropic efficiency and COP improvement of the cycle has been evaluated in detail. The issues that affect negatively the performance, related to the mechanical losses and the leakages, have been evaluated in order to assess the effective potential of the expander without these sources of losses.

Afterwards, the strong interest of the industrial and research fields in carbon dioxide as a refrigerant has brought to test the proposed expander also in a cycle working with this fluid. The results obtained in a test rig working with CO_2 developed at the Department of Industrial Engineering of the University of Florence have showed that higher performance in comparison to the tests with R134a could be obtained due to the lower volumetric expansion ratio required by the fluid. On the other hand, the higher pressures reached in these systems lead to greater mechanical losses. The presence of high mechanical losses and leakages is inevitably due to the original application of the machine, which must work with a higher viscosity fluid withstanding higher values of pressure (i.e. up to 300 bar) in comparison to the application studied in this work.

The high potential of the expander, especially in terms of indicated cycles, has suggested redesigning and manufacturing the machine, retaining its overall architecture so that to keep the design and production costs down. The interest on the efficiency improvement of HFC cycles due to their current wide application has brought to focus the redesign on the increase of the built-in volumetric expansion ratio and the reduction of the mechanical losses.

The problems of regulation and reaching stable conditions in the traditional VCC units for testing the expander, as those used in the previous tests that are composed of too many components and are too big, has brought to design and built a new dedicated test rig with the aim of only creating the desired boundary conditions. The developed cycle, called "hot-gas bypass cycle", has some advantages for the tests of compressors and expanders in comparison to the traditional VCCs. In this cycle, the use of the evaporator is avoided and the thermodynamic conditions at the compressor inlet are obtained by mixing the cold two-phase fluid with part of the hot gas coming from the compressor discharge. The consequent lack of the evaporator leads to a lower size, lower costs and higher stability of the cycle. The cycle has been designed in order to work with R404A and R404A, which are HFC refrigerants with a lower required volumetric expansion ratio than R134a. The improvement of the expander performance after the redesign has been analyzed in this cycle.

Finally, a comparison between the experimental P-V cycles obtained with R134a and the results obtained by using the 0D numerical model has been required so that to evaluate the accuracy of the developed model and analyze in depth the thermo-fluid dynamic behavior of the fluid inside the cylinder. Despite a good matching during the suction and discharge phases, a difference of the pressure trend in the expansion phase has been noticed due to the lack of phase change that causes a temperature difference between the liquid and vapor phases. Focusing only on the expansion phase of a two-phase fluid, the process has been mainly analyzed in a constant volume flash chamber without power generation. By taking inspiration from a study on a two-phase adiabatic expansion in a cylinder with a moving piston operating with water at atmospheric pressure, a 1D thermal conduction model has been developed to study the two-phase expansion with R134a with an improved accuracy.

The present Thesis examines in detail the use of an existing machine as expander in substitution of the throttling valve in VVC unit, by performing both numerical and experimental analyses and highlighting the main outcomes of the research.

Chapter 1 is an overview of the vapor compression cycles and describes some methodologies to enhance the efficiency of such systems. In particular, the advantages resulting from the use of an expander in substitution of the throttling valve are highlighted and the studies found in literature on the technologies used on this topic are presented.

In Chapter 2, the proposed radial piston expander and its theoretical thermodynamic cycle are described. Moreover, the developed numerical model is presented and the modifications on the expander as a result of the numerical analysis are reported.

In Chapter 3, the test rig and the measurement system developed for the experimental tests are described in detail. Particular attention is paid to the experimental setup for the acquisition of the P-V cycles.

Chapter 4 reports the experimental activities on the expander working with both R134a and CO_2. The results are presented in order to evaluate the influence of the thermodynamic conditions and the rotational speed on the performance. In particular, the isentropic efficiency and the consequent COP improvement of the cycle are evaluated with the measured and the indicated power in order to assess the influence of the mechanical losses.

In Chapter 5, the assessment of the losses that affect negatively the expander performance, due to the low built-in volumetric expansion ratio, the mechanical losses and the leakages, is presented. In addition, the redesign of the expander made for improving these issues is described.

In Chapter 6, the hot-gas bypass cycle designed and built for testing the expander is described. The advantages of using this cycle in comparison to the traditional VCC unit are presented. Moreover, the experimental results obtained by using the expander in this cycle are highlighted.

In conclusion, Chapter 7 describes the improved numerical model for the prediction of the expansion phase because of the difference between the pressure trends obtained from the experimental tests and the previous developed 0D numerical model. The results that show a strong improvement of the accuracy are reported.

1 Vapor compression cycles

1.1 History of refrigeration and heat pumps

Nowadays, refrigeration systems and heat pumps are widely used in both commercial and specific industrial applications. The production of cold by using the current known technologies starts in the beginning of the 20th century, due to the ease to extract heat energy, especially from fossil hydrocarbons, and the lack of an analogous direct method to produce cold.

The first attempt goes back to ancient times, when the demand of cold, mainly for food storage, was satisfied by using stored ice, vaporization of water and other evaporative processes. In the Roman period, ice-cabinets existed and until the last half of the 19th century, systems of ice distribution to households were present in many European cities. Moreover, ancient Egyptians were already aware that the evaporative cooling represents a form of natural production of cold; in fact, the evaporation of water in air leads to a reduction of the temperature of the remaining liquid. They stored water in clay vases, which were not glazed. The porosity of the material allowed a diffusion of water through the vase wall and its successive evaporation on the outer surface. For this reason, the water was kept fresher than ambient air also in hot and dry climates.

In the 1600s and 1700s, numerous researchers from different countries studied phase-change physics that led to the foundation of artificial refrigeration. At first, Oliver Evans proposed a system that is the basis of the actual common refrigeration processes with the use of a volatile fluid in a closed loop to freeze water into ice. In such system, the water was evaporated in a vacuum chamber producing refrigeration and the produced vapor was pumped to a water-cooled heat exchanger to condense for re-use. In 1828, its idea probably influenced Richard Trevithick, who proposed an air-cycle system for refrigeration. The first working machine was built in 1834 by Jacob Perkins, which patent describes an apparatus and means using "volatile fluids for the purpose of producing the cooling or freezing of fluids, and yet at the same time constantly condensing such volatile fluids, and bringing them into operation without waste" [1]. The invention of the vapor compression machine (Figure 1.1) represents the basic principle of currently employed refrigeration cycles and introduced actual refrigerants. Although the volatile fluid refereed in its patent was sulfuric ether, its use could cause unpleasant explosions and the first tests were carried out with caoutchoucine, an industrial solvent.

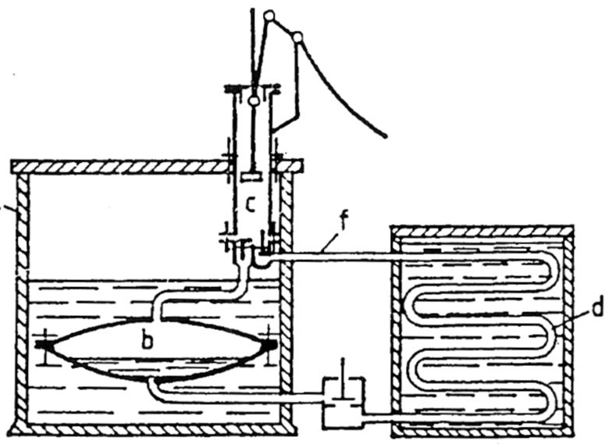

Figure 1.1 - Perkin's machine for compression refrigeration.

The above mentioned researchers led to the successive large scale employment of cooling. In 1861, the first refrigerated storage house was built by Thomas Mort and Eugéne Nicolle, followed by the first refrigerated steamship – *la Frigorifique* - and the process for condensing air into liquid developed by Carl Linde at the end of 1800s. In the beginning of the 20th century, the first hermetic refrigeration unit was built and new methods were invented for the freezing of foods. Finally, in 1939 the first commercial heat pump, which showed a different way to exploit the thermodynamic cycle, was installed to heat the erected town hall of Zurich by using the river Limmat as a heat source and obtaining coefficients of performance up to 3. Successively, in the second half of the 20th century, the main innovations concerned the substances used as working fluid and many technological advances were achieved.

1.1.1 Refrigerant progression

The use of water to produce cold impedes the reaching of lower temperatures below 0 °C due to its fixed melting point. To overcome this issue, after the observation that by adding salt to the ice the melting temperature could be changed, since the 16th century "freezing mixtures" were invented. The evolution of refrigerants from their advent is depicted in Figure 1.2 [2].

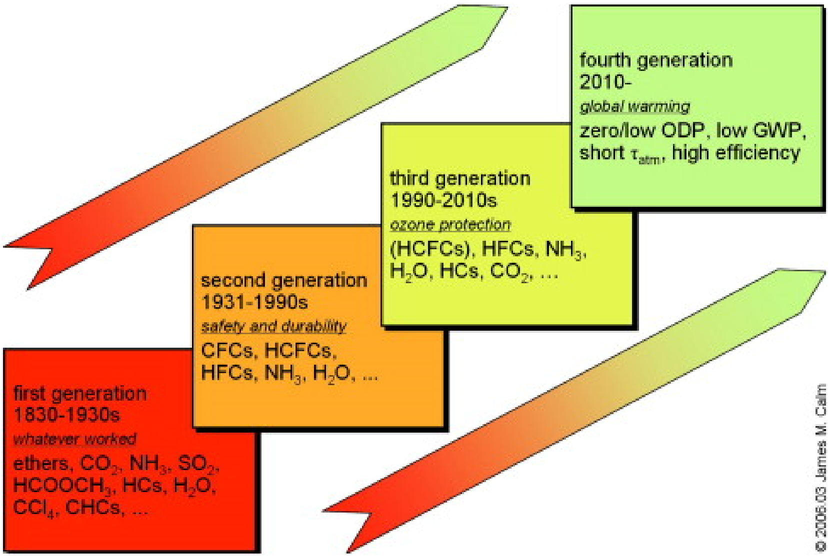

Figure 1.2 - Evolution of refrigerants [2].

For the first 100 years, familiar solvents and other volatile fluids were used as refrigerants. This "first generation" of refrigerants caused commonly accidents due to the flammability, toxicity and, sometimes, reactivity. Successively, a shift to fluoro-carbons was made for safety and durability. The "second generation" was constituted by chlorofluorocarbons (CFCs) and, above all, by hydro-chlorofluorocarbons (HCFCs) that were neither toxic nor flammable. The commercial production of R12 began in 1931, whereas ammonia was, as today, the most popular refrigerant in large industrial systems. Later, the issue about the depletion of protective ozone led to the Vienna Convention and the resulting Montreal Protocol (1987) that forced the participating countries to first reduce, and then totally stop the production of CFC compounds. A renewed interest was placed on "natural refrigerants" such as ammonia, carbon dioxide, hydrocarbons and water. In 1990s, the first alternative refrigerants were commercialized and introduced in substitution of the ozone-depleting refrigerants. As required by the Montreal Protocol, the use of CFC refrigerants in new equipment was phased out by 1996 in Non-Article 5 countries (mostly developed) and by 2010 in the others. The limitation of HCFCs is still continuing. The Montreal Protocol limited the consumption of HCFCs in steps and expected the stop of the consumption by 2030 in non-Article 5 countries and by 2040 in the others.

At the beginning of the 2000s, concerns have been raised related to the global climate change due to the absorption of infrared emissions from the earth that causes an increase of the earth surface temperature. The refrigerants with long atmospheric lifetimes and high numbers of carbon-fluorine bonds have been identified as greenhouse gases (GHGs). The parameters that measure the environmental friendliness of a refrigerant are the ozone depleting potential (ODP) and the global warming potential (GWP). The first indicates the ability to destroy stratospheric ozone (relative to trichlorofluoromethane R-11 with unity ODP), whereas the latter measures the potential contribution to global warming. Figure 1.3 reports a table that summarizes the properties of some refrigerants. It can be seen that no progress has been made for the GWP when switching from HCFCs to HFCs and natural refrigerants are highly competitive for environmental issues [3].

Refrigerant	ODP	GWP	Flammable	Toxic
CFCs and HCFCs				
R12	0,9	8100	No	No
R22	0,055	1500	No	No
Pure HFCs				
R32	0	650	Yes	No
R134a	0	1200	No	No
R152a	0	140	Yes	No
HFCs mixtures				
R404A	0	3300	No	No
R407C	0	1600	No	No
R410A	0	1900	No	No
Natural refrigerants				
Propane (R290)	0	3	Yes	No
Isobutane (R600a)	0	3	Yes	No
Ammonia (R717)	0	0	Yes	Yes
Carbon dioxide (R744)	0	1	No	No

Figure 1.3 - Environmental properties of some refrigerants.

During the formulation of Kyoto Protocol, many countries have committed to reduce the GHG emissions forcing shifts to the fourth generation of refrigerants.

1.2 The vapor-compression refrigeration cycle

Usually, commercial refrigeration and heat pump units operate in base of Vapor Compression Cycles (VCC) that use mechanical work to transfer the heat from a cold to a hotter heat source [4]. In these cycles, the fluid is subjected to four processes, as shown in the scheme of Figure 1.4. At the lower temperature, the fluid vaporizes by means of the latent heat provided by the heat source. Then, the vapor is compressed to a higher pressure by an electricity-powered compressor. The heat is then rejected so that the fluid changes back to a liquid. In general, the fluid pressure is reduced by expanding through a lamination valve in order to obtain the same initial thermodynamic conditions. The cooling effect is represented by the heat transferred to the working fluid in the evaporation process, whereas the heating effect by the heat transferred by the working fluid in the condensation process.

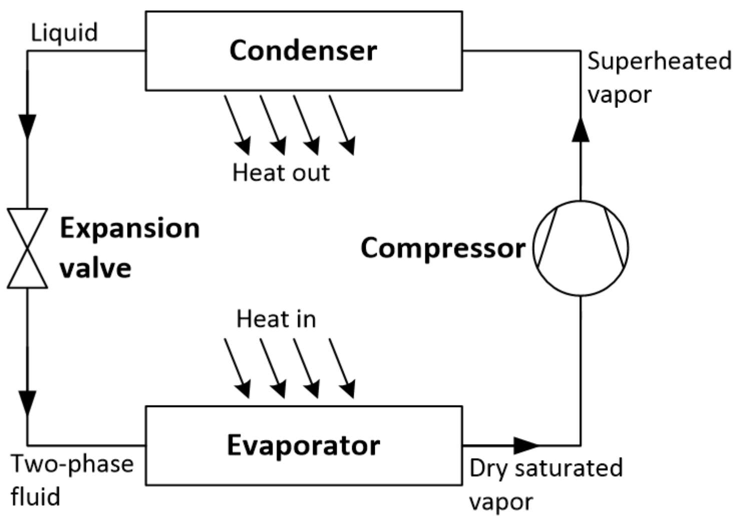

Figure 1.4 - Simple layout of a vapor compression cycle.

In Figure 1.5, the simple vapor compression cycle is shown on the temperature-entropy diagram showing the deviations from the ideal reversed Carnot cycle identified by shaded areas. The adiabatic compression process reaches a temperature greater than the condenser one. The extra work is represented by the shaded triangle and it could be avoided with an isothermal compression at the point where the condensing temperature is reached until the condensing pressure is attained. The expansion through a valve is a constant enthalpy process without heat absorption or rejection that causes a corresponding drop in temperature by flashing some of the fluid into vapor. The shaded rectangle indicates the second deviation from the ideal cycle and it represents the work potentially recoverable.

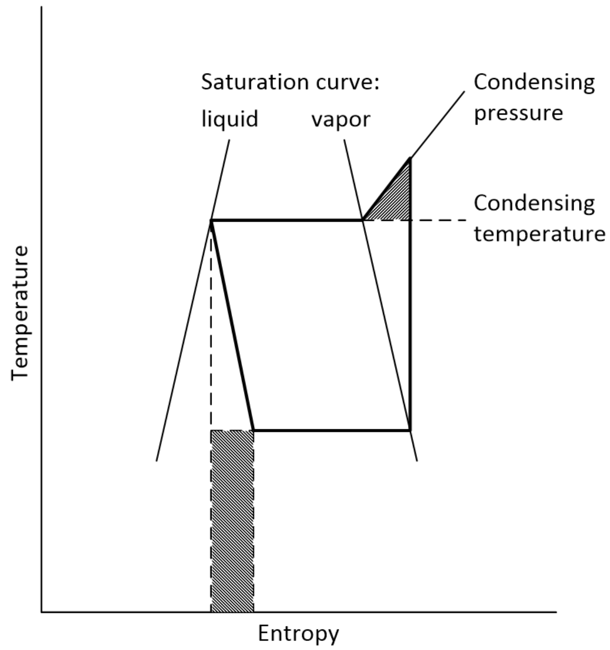

Figure 1.5 - Temperature-entropy diagram for ideal compression cycle.

The performance of the system is measured as the ratio of the cooling/heating effect to the compressor input power that is called as Coefficient of Performance (COP) (Eq. 1.1).

$$COP = \frac{Q_{cool/heat}}{W_{comp}} \tag{1.1}$$

Due to the deviations from ideal processes, the theoretical COP is less than the Carnot COP, where the compression and expansion processes take place at constant entropy and the addition and rejection of heat take place at constant temperature. The ideal COP depends on the properties of the refrigerant. In addition, in a real circuit the COP is further lower because of the mechanical and the thermal losses.

1.2.1 Transcritical carbon dioxide cycle

Since the invention of the vapor compression cycle by Evans and Perkins, CO_2 has been a candidate as refrigerant. In 1850, Alexander Twining was the first to propose the use of CO_2 as refrigerant using a steam compression system in his British patent. The carbon dioxide gained its popularity in food industries and human comfort applications in 1900s because of the toxicity and flammability of NH_3 and SO_2. Its disadvantages mainly due to the difficulties of handling the high pressure and the higher efficiency of the newly conceived refrigerants led to lose its importance in the 1930s. Decades later, the discovery of the adverse effects of synthetic refrigerants caused a renewed interest in the CO_2 as refrigerant. In the 1990s, Lorentzen carried out many studies on its improvement and suggested that motor vehicles, air-conditioning systems and heat pumps are suited for CO_2 refrigeration [5]. In addition to having important advantages in terms of ODP and GWP as reported in Figure 1.3, its non-toxicity and non-flammability allowed its use in those places where refrigerant leak could represent an issue (i.e. inside supermarkets or food storages).

The low critical temperature of the carbon dioxide equal to 31.1 °C leads to the use of transcritical cycles. In these cycles, the condenser is replaced by a gas cooler where the heat rejection transformation takes place at variable temperature. The main drawback of a CO_2 transcritical cycle is the high pressure of the fluid by considering that the critical pressure is 73.7 bar so that it necessitates a redesign of the equipment to handle such high pressures. The variation of the temperature during the gas cooling process causes a strong deviation from an ideal Carnot cycle worsening the attainable performance index. Figure 1.6 shows the comparison between the R134a and CO_2 cycles on a temperature-entropy diagram with the same cooling capacity. The high temperature at the compressor discharge and the large pressure difference between the gas cooler and the evaporator that causes higher throttling losses lead to a much bigger area for CO_2. For these reasons, the transcritical CO_2 cycle has lower efficiency compared to the HFC refrigeration systems causing the research on strategies to improve the performance.

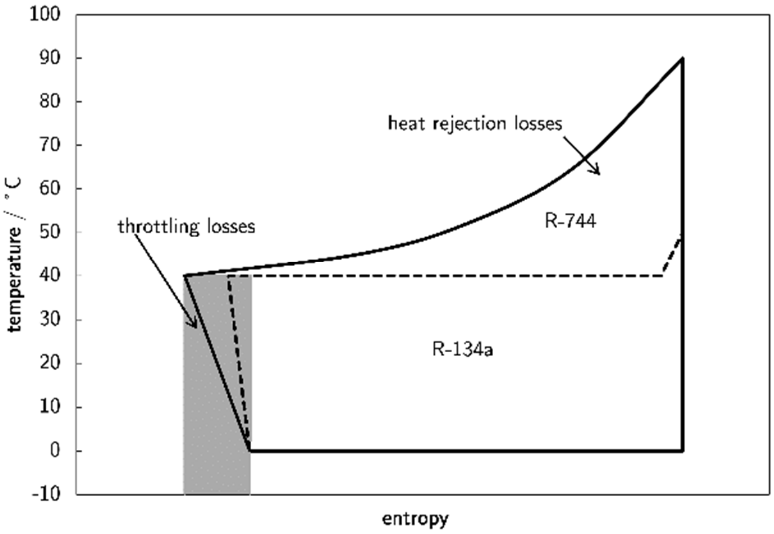

Figure 1.6 - Comparison between the R134a and CO_2 cycles.

1.2.2 Improved single stage cycles

Over the last decades, enhancing the energy efficiency of vapor compression cycles has been a widespread concern. In order to improve the performance of the cycle, strategies are investigated for reducing the discharge compressor temperature and for improving the throttling process. The reduction of the temperature could be obtained with the use of an inter-cooled multi-stage compression. On the other hand, the use of internal heat exchangers, ejectors and expanders is investigated to improve the throttling process [6]. A suction line heat exchanger (SLHX) between gas cooler outlet and evaporator outlet increases the degree of subcooling and protects the compressor from two-phase flow. Preissner [7] analyzed the effect of the internal heat exchanger at various temperature of the heat sink in a CO_2 cycle and he measured an improvement of the COP up to 13%. The use of an ejector as a lamination valve reduces the irreversibilities in the expansion process by using the kinetic energy of the gas to increase the suction pressure at the compressor inlet. Domansky [8] analyzed the behavior of 38 different refrigerants in an ejector cycle showing a theoretical COP improvement between 10% and 30%. The replacing of the throttling device with an expander not only performs the isentropic expansion ideally but also recovers the work of expansion.

1.3 Energy recovery with expander

In a conventional vapor compression cycle, most of the irreversibilities come from the throttling valve that wastes up to 20% of the compressor input. The use of an expander in substitution of the throttling valve (Figure 1.7a) leads to a recovery of the expansion work by exploiting the pressure drop from the condenser to the evaporator and a consequent increase of the COP of the entire cycle. As shown in the pressure-enthalpy (P-h) diagram (Figure 1.7b), with the integration of an expander the enthalpy difference h_{4h}-h_{4e} can be extracted in the form of expansion work decreasing the power required to the cycle. Moreover, the cooling capacity is increased (i.e. the enthalpy difference is h_1-h_{4e}) leading to a further COP improvement of the cycle in the cooling operation compared to the conventional cycle. It is worth pointing out that the maximum COP improvement can be reached ideally with an isentropic expansion (h_{4h}-h_{4s}).

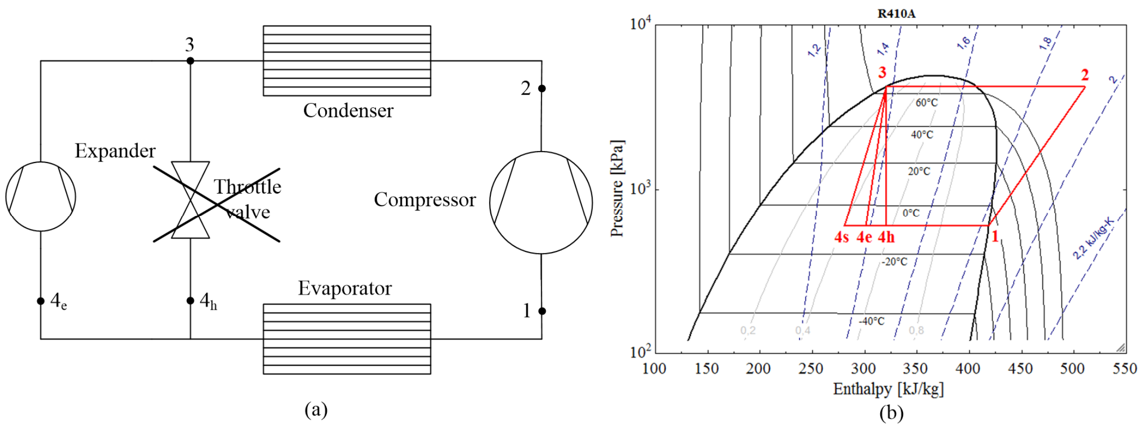

Figure 1.7 - Vapor compression cycle with an expander (a); P-h diagram of a vapor compression cycle (b).

The potential energy recovery in a VCC depends especially on the working fluid and the working conditions at the condenser and the evaporator. A series of preliminary thermodynamic calculations were performed to determine the theoretical performance improvement. By fixing the temperatures of the cold and the hot heat sinks to 0 °C and 53 °C respectively, and the heat exchangers effectiveness-capacitance rate product at 0.75 for the evaporator and 1.75 for the condenser, the cycle performance was evaluated. By considering an isentropic efficiency of the compressor equal to 0.6, which represents a lower value than an average value of these kinds of machines, the COP improvement was calculated with both an isentropic expansion and an isentropic efficiency of the expander equal to the compressor one. The COP improvement compared to the simple throttle valve cycle (COP_{thr}) is calculated as:

$$\Delta COP = \frac{COP_{\exp} - COP_{thr}}{COP_{thr}} \tag{1.2}$$

where COP_{exp} is the COP of the cycle with the expander and is calculated as:

$$COP_{\exp} = \frac{Q_{cool/heat}}{W_{comp} - W_{\exp}} \tag{1.3}$$

The reference heat pump power is fixed at 20 kWth, considering a medium-high domestic size. As reported in Table 1.1, three different working fluids were analyzed (i.e. R134a, R407C and R410A). The maximum power output of the expander is 2.1 kW leading to a maximum COP increase of about 30%. However, by considering the real expansion, the theoretical COP increase is reduced to 12-15% and it is higher for R410A. The main parameter that influences the cycle performance is the expander isentropic efficiency: the higher the isentropic efficiency, the closer the process to the isentropic process and the larger COP improvement of the cycle (Figure 1.8). The different results obtained by using different fluids is justified by the fluid properties; in particular, the R410A reaches higher values of pressure and the pressure difference between the condenser and the evaporator is greater. For this reason, the simple throttle cycle has higher expansion losses and a lower COP; consequently, the integration of an expander leads to a higher improvement of the cycle efficiency.

Table 1.1 - Performance improvement of the cycle with the use of an expander.

Parameter	**R134a**	**R410A**	**R407C**
Ideal expander power [kW]	1.659	2.142	1.845
Real expander power [kW]	0.995	1.301	1.107
Ideal COP increase [%]	23.1	28.3	24.1
Real COP increase [%]	12.7	15.2	13.1
Volumetric expansion ratio	49.57	17.6	32.8
Mass flow rate [kg/s]	0.114	0.105	0.104

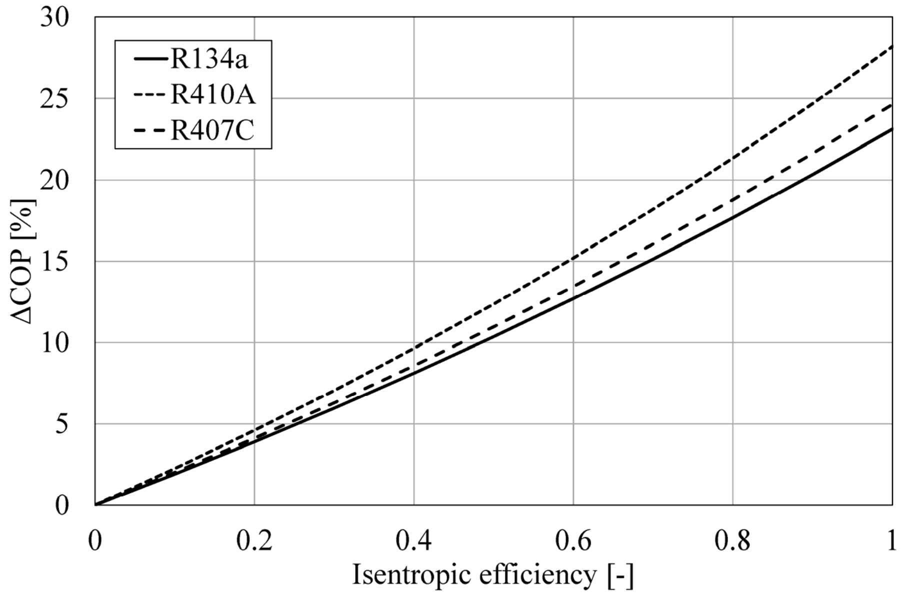

Figure 1.8 - COP improvement as a function of the isentropic efficiency for different fluids.

It is interesting to observe that high values of the expansion ratio are shown for all fluids. This parameter varies within a relatively wide range for the different fluids, with the lowest end for R410A and highest end for R134a. The expansion volumetric ratio is an issue for the adoption of volumetric expanders. In addition, the cycle flow rate is within the range 0.10 – 0.12 kg/s. This parameter plays a key role on the choice of the type of expander and its size.

The other main operational parameters are the evaporation and condensation temperatures that, depending on the operating mode, are related to the ambient temperature. In heating mode, by considering the same temperature of the hot heat sink equal to 53 °C, the evaporation temperature depends on the ambient one. Figure 1.9a shows the influence of the evaporation temperature on the COP improvement for the different refrigerants. The higher improvement obtained by using an isentropic efficiency of the expander equal to 0.6 is observed for low evaporation (and, consequently, ambient) temperatures because of the higher pressure ratio and work-recovery potential. As explained previously, the highest improvement is observed for R410A, which has the lower COP of the simple throttle cycle. In cooling mode, the ambient temperature affects the condensation temperature and its influence on the COP improvement, by considering the same temperature cold heat sink of 0 °C, is shown in Figure 1.9b. In this case, the

COP increases with decreasing the evaporation temperature due to the increase of the pressure ratio, in an analogous way of the previous case. For these reasons, the use of an expander in a VCC can lead to greater benefit in less favorable conditions, where the performance are significantly improved.

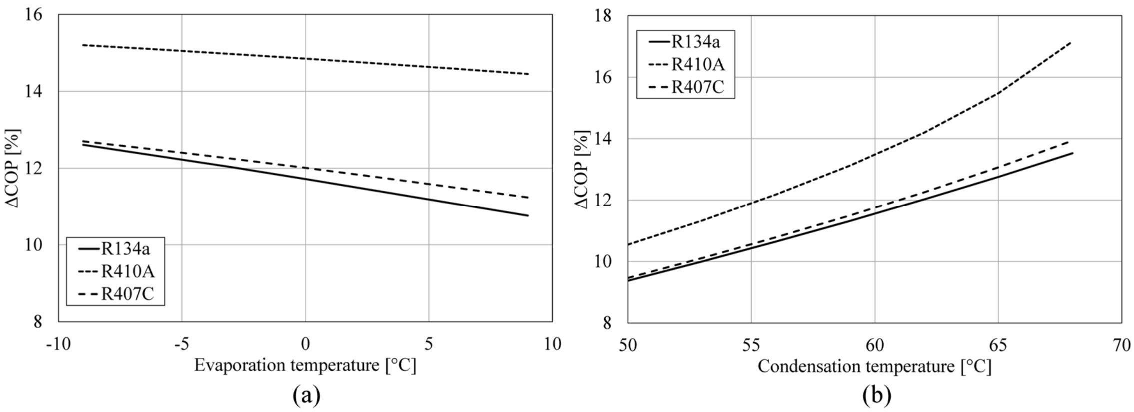

Figure 1.9 - COP improvement as a function of the evaporation (a) and condensation (b) temperatures for different fluids.

1.4 Overview on expanders

The use of an expander to recover a part of the work in a VCC unit is getting more interesting with the continuous increasing of both the cost of electricity and the global energy consumption, leading to considerable economic and environmental advantages. Many researchers investigated the possibility of recovering the expansion work by replacing the throttling valve with a two-phase expander.

The expanders can be classified in two main categories: velocity types, such as turbines, and volumetric types, such as rotary vane, piston, screw and scroll expanders. For medium and low size systems, especially if operating with two-phase fluids, turbines are not suitable because they suffer strong surface wearing and other dynamic issues due to the high rotational speed and the high volumetric difference between the two phase. On the other hand, the volumetric expanders, which are characterized by lower flow rates and higher-pressure ratios, are generally preferred [9].

Most of the studies were carried out on transcritical systems with CO_2 as refrigerant due to the lower original COP compared to the HFC systems and the higher condensation pressure (exceeding 100 bar) that would lead to a remarkable COP improvement [10].

Salehi et al. [11] studied a turbocharger where a turbine is coupled to the compressor on the same shaft. They had problems with leakage of refrigerant through the shaft and with the heat transfer between the expander and the compressor. Tøndell [12] tested a radial outflow impulse turbo expander for mobile air conditioning systems that showed low efficiency due to the extra fluid friction losses and extra exit losses caused by the large diameter of the turbine and the principle outflow turbine. They concluded that this type of expander is inapplicable in these systems.

Stosic et al. [13] investigated the use of twin screw machines to fulfil both the expansion and compressor processes and showed an overall 55% expansion-compression isentropic efficiency. Huff et al. [14] proposed a scroll expander derived from an unmodified scroll compressor. The test results showed an isentropic efficiency of 42% in the speed range between 1400 and 2200 rpm. Other studies on this technology were carried out theoretically by Kim et al. [15], who analyzed the influence of the working thermodynamic conditions on the in-cylinder pressure trend, and experimentally by Fukuta et al. [16], who evaluated the influence of the expander rotational speed, controlled by an oil pump, on its efficiency; the results showed a total efficiency of the expander equal to 54% and 55% respectively. Vane expanders were examined by means of dedicated test rigs by Fukuta et al. [17] (Figure 1.10) and Yang et al. [18], who achieved a total efficiency of 60% at 2000 rpm and an optimal isentropic efficiency of 23% at 800 rpm respectively; in these studies, the expander rotational speed was controlled by an oil pump in the first case, whereas an adjustable electrical resistance load was used in the other one. A detailed modelling of this technology was done by Jia et al. [19], who studied the influence of the rotational speed and the thermodynamic operating conditions on the expander performance in terms of volumetric and isentropic efficiencies. In particular, the results showed an isentropic efficiency of 45% and a maximum COP improvement potential of 27.2% compared to the simple throttle valve cycle.

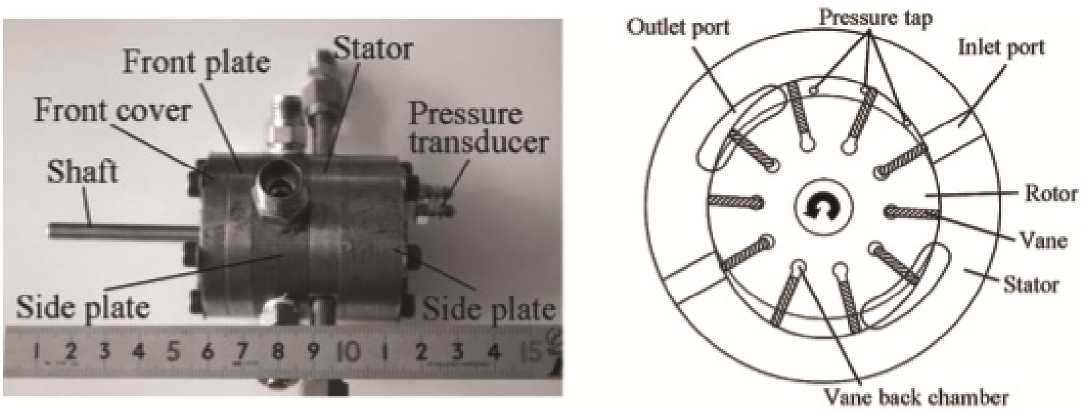

Figure 1.10 - Schematic of a rotary vane expander [17].

Li et al. [20] investigated experimentally the performance of a rolling-piston type expander, whose principle is shown in Figure 1.11a, and they reported a maximum isentropic efficiency of 58.7% with a COP improvement of at least 10%. A CO_2 rolling piston expander was tested also by Tian et al. [21], who dissipated the power output by using a light box and found a maximum total efficiency of the machine equal to 45%. Jiang et al. [22] developed a two-rolling piston expander and showed an isentropic efficiency of about 28 - 33% in the rotational speed range from 850 to 1000 rpm. Guan et al. [23] tested a swing expander prototype (Figure 1.11b) that has advantages in comparison to a rolling-piston type, including less leakages and less poorly lubricated parts. The experimental results indicated an isentropic efficiency up to 44%.

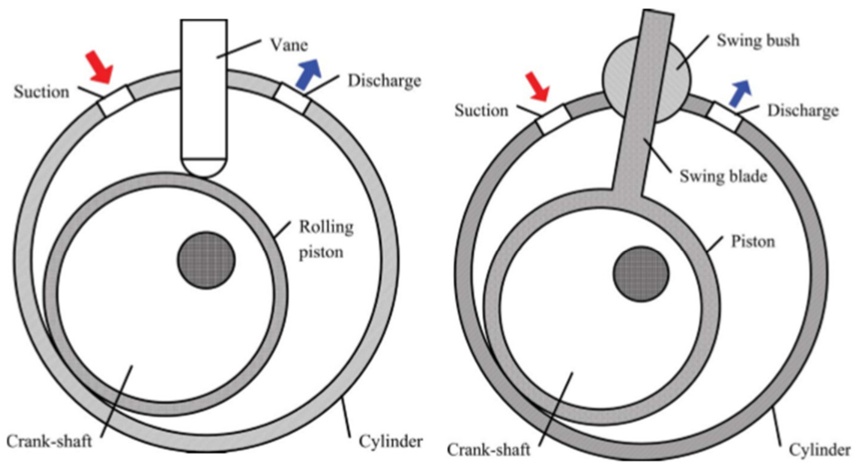

(a) (b)

Figure 1.11 - Principle of a rolling-piston expander (a) and a swing-piston expander (b) [9].

A free piston compressor-expander was developed by Nickl et al. [24] with three expansion stages coupled with a one-stage compression, as shown in Figure 1.12. The test results indicated that an isentropic efficiency of 70% was reached, with at least 40% COP improvement over the cycle with throttle. Zhang et al. [25] developed a double effect free piston expander where the compressor should be combined with the expander on a common shaft to effectively utilize the work extracted from the expansion process. The results showed an isentropic efficiency of about 62% by referring to the P–V diagram.

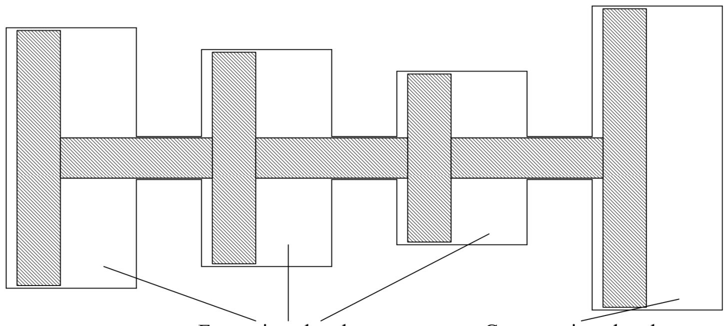

Figure 1.12 - Principle of a free piston expander-compressor.

Baek et al. [26] developed a piston-type expander, which was a small two-cylinder machine modified from a four-stroke two-piston engine, and they reported an isentropic efficiency less than 10%. A radial piston type reciprocating expander (Figure 1.13) was investigated by Fukuta et al. [27], who analyzed the P-V diagrams and indicated an overall 40% efficiency level.

Due to the highest COP of conventional cycles with HFCs, the COP improvement related to the replacement of the throttling valve with the expander is much less remarkable in these cycles compared to the CO_2 cycles. Therefore, very few experimental studies were carried out on applications of expanders in subcritical cycles.

He et al. [28] developed a Pelton-type expander for energy recovery in a domestic R410A refrigeration system. Even though the improvement of COP and isentropic efficiency were fair values (5.4% and 32.8% respectively), the high rotational speed of 26500 rpm was a serious factor reducing the Pelton-type expander's life span. Zhang et al. [29] designed a turbo expander that reached the maximum isentropic efficiency of 10% at 2000 rpm. Xia et al. [30] developed and tested a sliding vane expander for the replacement of the throttle valve in R410A refrigerant system. The results showed that the expander has a maximum isentropic efficiency of 32.7%. A two-stage rotary vane expander was developed by Wang et al. [31] in a R410A air conditioning system. A maximum isentropic efficiency and COP improvement of 31.5% and 10.3% respectively were measured through the variable speed test.

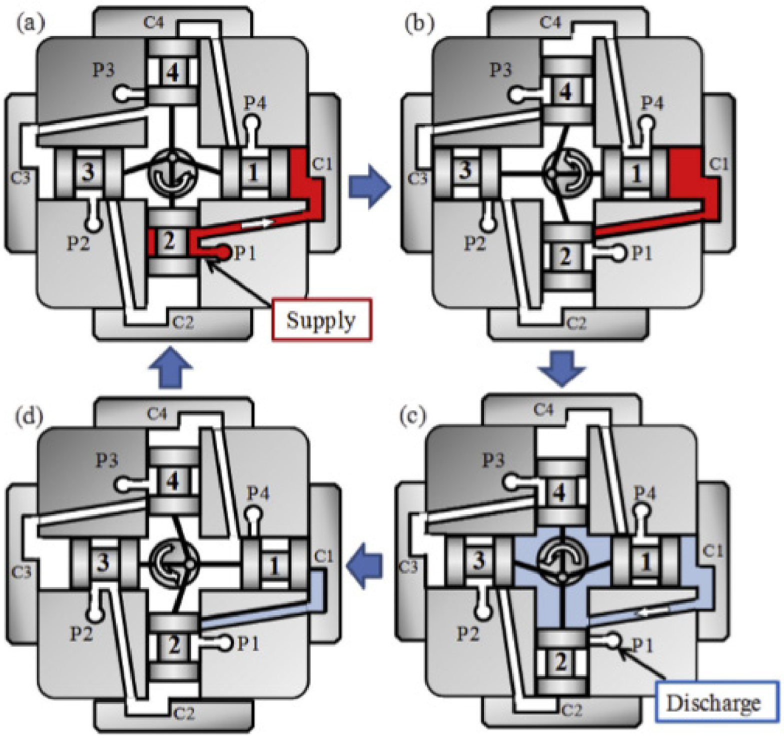

Figure 1.13 - Scheme of a reciprocating expander and working principle [27].

A relevant issue related to the integration of an expander in a commercial refrigeration system is the additional cost involved. As discussed in an editorial of Hwang [32], the expander efficiency is a crucial factor. Subiantoro and Ooi [33] carried out a theoretical analysis to investigate the benefits of using an expander in a refrigeration system using various refrigerants. The results demonstrated that expanders are financially feasible and, assuming an expander efficiency of 50%, the payback periods are less than 5 years for all systems studied and, in particular, less than 1 year for CO_2.

2 Reciprocating expander

Among all the expanders studied so far, radial piston ones were investigated in very few cases. The large number of interacting surfaces (i.e. piston rings, piston and cylinder walls) leads to high friction losses that adversely influence the performance. In addition, the precise timing of the suction and discharge valves makes this type of expander structurally complex and the finite number of pistons and the fixed displacement cause torque pulsations. However, this technology, mainly used in hydraulic applications, has some interesting features and advantages compared to the other ones. Radial piston expanders have very low starting torque, which is a great advantage for small size and seasonal applications. In fact, the expander generally works in off-design conditions (low flow rate and low-pressure drops available) several days per year; therefore, it is important that it is able to produce power even in the less favorable conditions, which take place most of time. In addition, it is important to underline that, in contrast to other technologies, the volumetric ratio of radial piston expanders can be easily scaled up or down without any significant problem (i.e. by modifying the dead volume or, in case, the stroke), either on the production or in the design process.

In this work, an existing machine for a different application was used as expander in a vapor compression cycle in order to examine if considerable performance can be obtained by means of an already known technology leading to obtain an expander with limited manufactured costs.

2.1 Original expander

The here investigated expander is derived by a hydraulic motor manufactured by

Italgroup® that has some interesting features which make it suitable for the expansion of a two-phase fluid. It can handle liquids/fluids at very low temperatures (even at -40 °C) and it can deal with very high pressure (300 bar). Its lifetime is long and, due to its reliability, its maintenance requirements are negligible.

In particular, a radial piston type motor was selected and modified in order to improve the performance when used in a heat pump cycle.

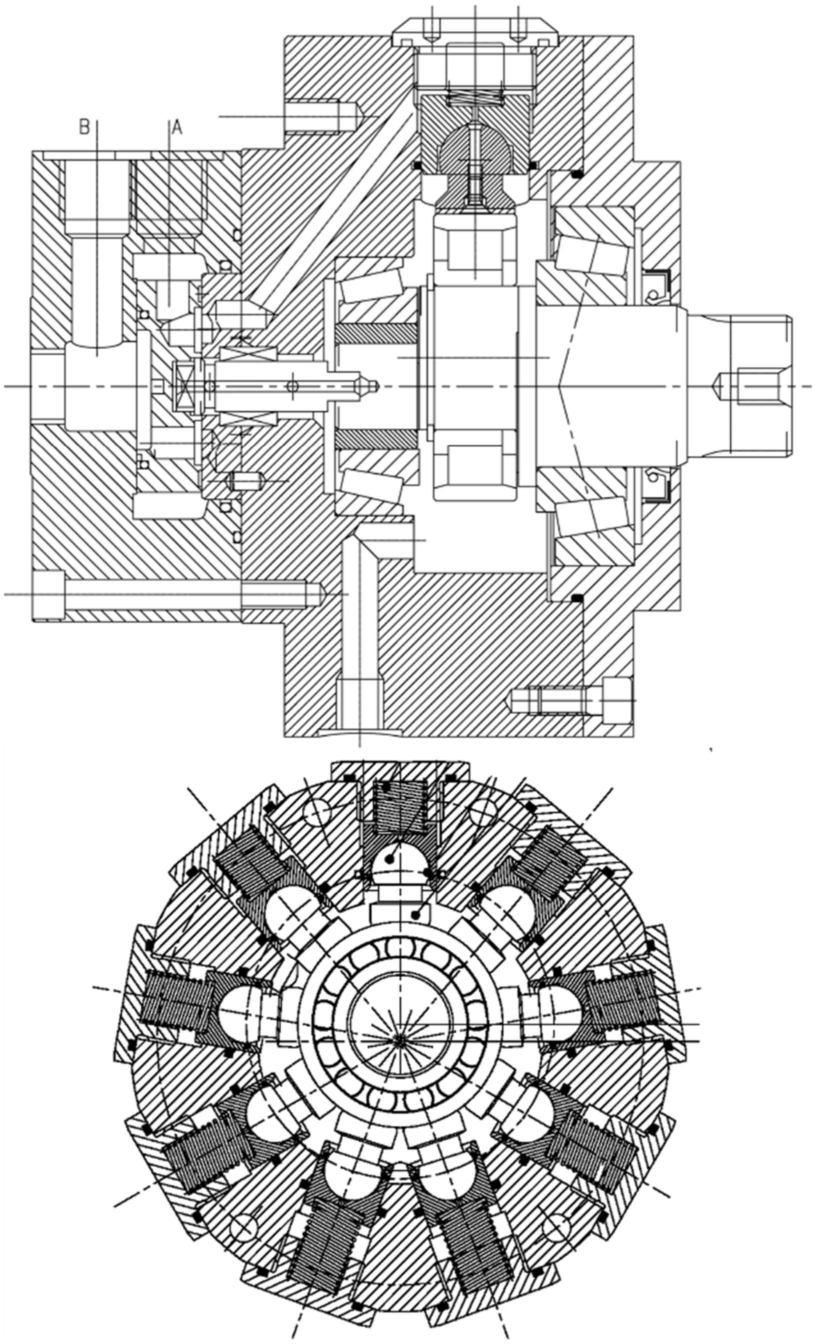

Figure 2.1 - Axial and cross-section views of the manufactured expander.

Figure 2.1 shows the axial and the cross-section views of the original expander. The motor has 9 pistons with a total 102 cm^3 displacement volume. From the high-pressure side, the working fluid enters each cylinder through an intake duct and moves the piston downward: the piston is connected through a valve stem to the tappet, which moves the eccentric cam connected to the shaft. The forces of the pistons on the eccentric shaft are directed radially and produce a torque, driving it to rotation. The stroke of the pistons is determined by the eccentricity of the shaft. The pistons are pushed and kept in contact with the bearing on the shaft by means of springs at the top of each cylinder.

The fluid intake/output mechanism is a key aspect of the expander. Figure 2.2 shows a scheme of the expander with the distribution. The mechanism is influenced by the relative movement of a rotating plate driven by the shaft to a stationary plate fixed on the case. The latter has a hole for each piston with the same diameter of the intake duct, whereas the size of the holes on the rotating plate determines the timing of the suction and discharge phases. When the hole of the rotating plate linked to the suction side overlaps the hole of the stationary plate, the pressurized fluid enters into the intake duct and, consequently, the cylinder. The behavior in the discharge phase is the same, except for the fact that the fluid inside the cylinder flows towards the lower pressure side. In order to minimize the sliding friction between the plates, the stationary plate is made of brass.

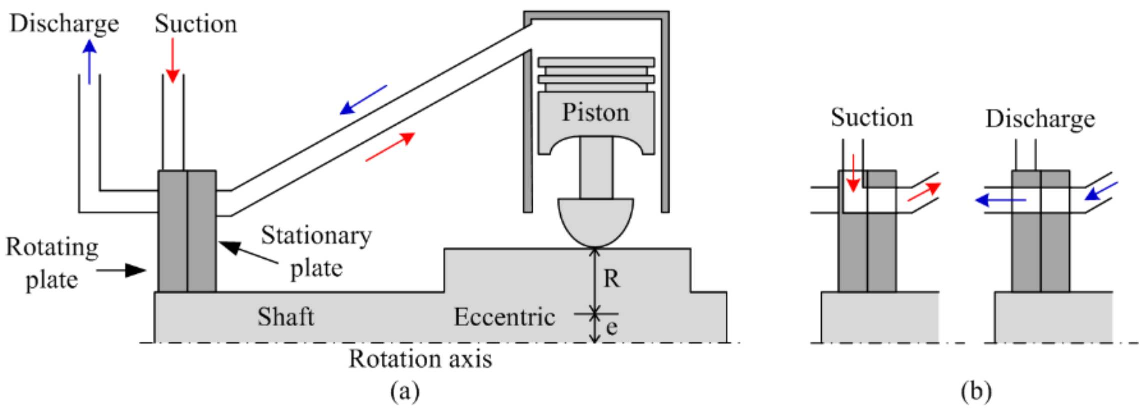

Figure 2.2 - Schematic of the expander (a) and scheme of the distribution (b).

The piston displacement law, as a function of the crank angle, is calculated with the following equation (Eq. 2.1), referred to the schematic of Figure 2.2:

$$x(\theta) = -e \cdot \cos(\theta) + \sqrt{e^2 \cdot \left(\cos^2(\theta) - 1\right) + R^2} \tag{2.1}$$

The geometrical data are summarized in Table 2.1.

Table 2.1 - Expander technical data.

Parameter	**Value**
Number of cylinders	9
Bore (mm)	30
Stroke (mm)	16

2.2 Thermodynamic cycle

The reciprocating expander is a machine that produces work by expanding a pressurized fluid from the suction side to the discharge one. The evaluation of the thermodynamic cycle is fundamental to predict the expander performance in terms of adsorbed power, volumetric efficiency, mass flow rate, etc.

The thermodynamic cycle of a reciprocating expander can be evaluated on different levels of detail, considering various effects acting on the cycle. In the following paragraphs, two different levels of cycle description (i.e. ideal and theoretical) will be described.

2.2.1 Ideal cycle

The different states of the working fluid during its expansion are presented in Figure 2.3 that represents the Clapeyron diagram. In this diagram, the trend of the in-cylinder pressure in function of the displacement volume is shown.

Starting from the top dead center (TDC) position, the ideal cycle is composed by the following phases:

- Suction (1-2) – the high pressurized fluid enters the cylinder at a constant pressure equal to the suction pressure, as the piston moves towards the bottom dead center (BDC). In this phase, the suction valve is opened and the admission work is produced.

- Expansion (2-3) – during this phase the valves are closed. The fluid inside the cylinder is expanded from the suction pressure leading to a reduction of the in-cylinder pressure up to a value that depends on the fluid and the geometry of the expander. Ideally, this phase is represented by an adiabatic expansion.
- Thermodynamic discharge (3-4) – it is assumed that the discharge valve opens at the BDC. At this point, the fluid instantaneously exits the cylinder and the in-cylinder pressure equalized the discharge pressure. In this case, the “under-expansion” phenomenon occurs (i.e. the discharge pressure is lower than the in-cylinder pressure at point 3). Otherwise, the “over-expansion” occurs.
- Discharge (4-5) – the piston moves toward the TDC forcing the remaining fluid out of the cylinder through the discharge valve. The in-cylinder pressure equalizes the discharge pressure.
- Compression (5-6) – if the discharge valve opens before the piston reaches the TDC, the remained mass is compressed.
- Thermodynamic admission (6-1) – when the piston is at TDC, the suction valve opens, the fluid instantaneously enters the cylinder and the in-cylinder pressure equalizes the discharge pressure. This phase is similar to the “thermodynamic discharge”.

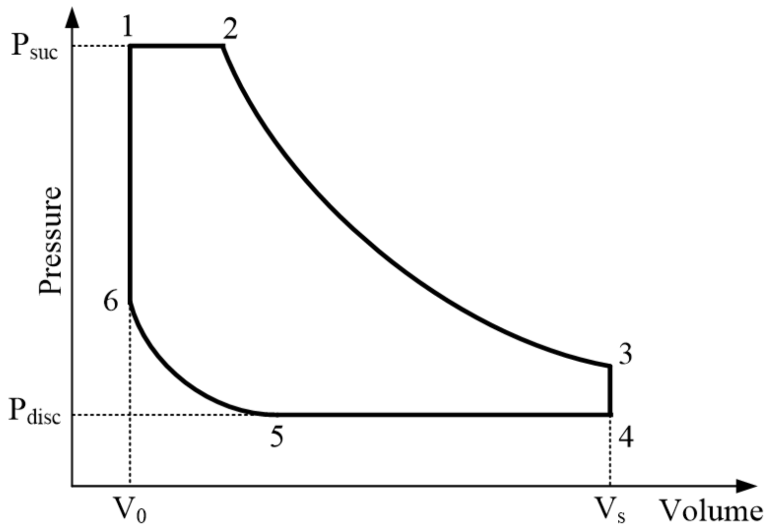

Figure 2.3 - P-V diagram of the ideal thermodynamic cycle.

The closed area of the ideal cycle represents the work produced by one cylinder of the expander without considering the effects of the pressure losses through the valves and the non-isentropic effects during the phases of the cycle.

2.2.2 Theoretical cycle

The influence of the pressure losses through the valves is taking into account in the theoretical cycle. This phenomenon leads to a modified P-V cycle (Figure 2.4) that differs from the ideal one on the following phases:

- Suction (1'-2') – when the suction valve opens, the in-cylinder pressure increases with a slope that depends on the pressure losses (i.e. the "thermodynamic admission" phase disappears): the higher the pressure losses, the lower the slope of the in-cylinder pressure increase. For this reason, when the suction valve closes, the cylinder can reach a lower peak pressure (P'_{suc}) than the suction pressure. It is worth noticing that this phase also depends on the dead volume that decreases the peak pressure.
- Free discharge (3'-4') – similarly to the suction phase, the pressure losses causes the absence of the "thermodynamic discharge" and the in-cylinder pressure, when the discharge valve opens, does not decrease instantaneously. In order to allow the free discharge of the fluid and, consequently, reduce the work absorbed in the discharge phase, the discharge valve can open slightly before the TDC.
- Discharge (4'-5') – during this phase, the in-cylinder pressure remains slightly higher than the discharge pressure due to the pressure losses through the discharge valve. The advance of the discharge valve closing in respect to the TDC represents a compromise between the consequent increase of the peak pressure reached during the suction phase and the work lost by the compression of the remained fluid inside the cylinder.

The work produced in the theoretical cycle is lower than the ideal one, as shown by the closed areas of the cycles in Figure 2.4, due to the pressure drop caused by the gas flowing through the valves.

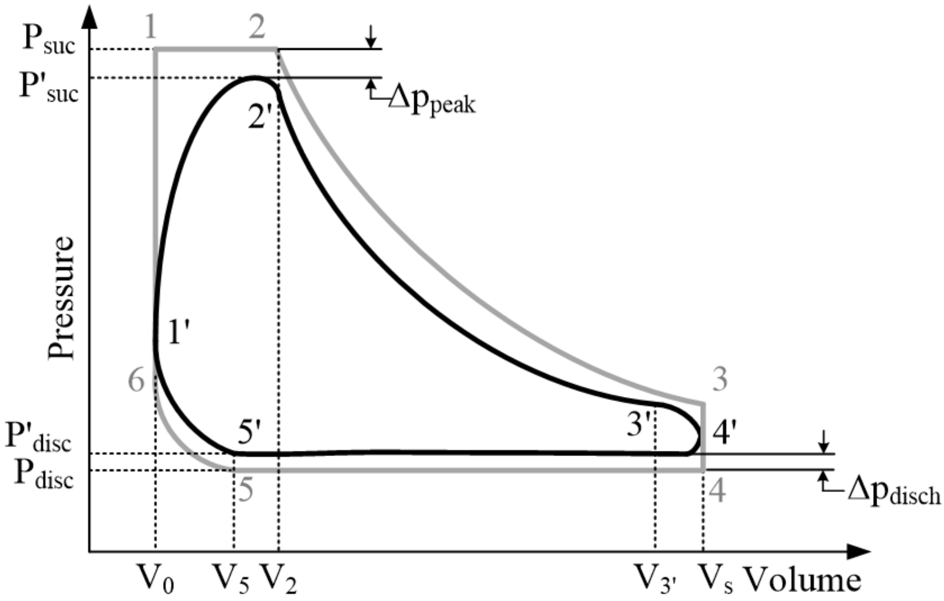

Figure 2.4 - P-V diagram of the theoretical cycle (black line) compared to the ideal one (gray line).

2.2.3 Performance parameters

Some different definitions of the volumetric and energy efficiency can be used in a similar way of the reciprocating compressor field by taking into account different parameters and phenomena.

The *volumetric efficiency* quantifies the abilities of the expander to fill the cylinder as the piston moves from the TDC to the BDC. By considering the swept volume equal to the displacement volume, the volumetric efficiency is defined as the ratio between the measured mass elaborated in each cycle on the theoretical mass calculated from the displacement volume and the density at the suction side (Eq. 2.2).

$$\eta_{vol} = \frac{m_{meas}}{m_{th}} = \frac{m_{meas}}{\rho_{suc} V} \tag{2.2}$$

It is the traditional and most common definition of volumetric efficiency.

By considering the swept volume by the piston during the suction phase, the *suction volumetric efficiency* can be defined. Its definition is analogous to the precedent definition, but the theoretical mass is calculated from the suction swept volume instead of the displacement volume (Eq. 2.3).

$$\eta_{vol,suc} = \frac{m_{meas}}{\rho_{suc} V_{suc}} \tag{2.3}$$

In addition to the pressure losses through the valves, also leakages inside the expander worsen the values of both definitions of the volumetric efficiency. This phenomenon inevitably occurs due to the clearances between the components inside the expander, when the seals can not assure perfect gas tight. More in detail, the leakages can be addressed to imperfect sealing between the moving elements and to the piston rings. The amount of leakage is connected to the following parameters:

- gas molecular weight – lower molecular weights bring to greater leakages
- expansion ratio – greater expansion ratios (i.e. suction/discharge pressure ratio) lead to higher leakages
- rotational speed – the leakages are higher at low rotational speed
- operating hours – when the wear rate of the elements inside the expander is at a maximum level, the leakages are greater.

A geometrical parameter that influences the filling of the cylinder is related to the dead volume by defining the following ratio (Eq. 2.4):

$$C = \frac{V_0}{V_s} \tag{2.4}$$

The inverse of this ratio represents the expansion volumetric ratio.

The geometrical parameter that indicates the difference between the two definitions of volumetric efficiency can be expressed as (Eq. 2.5):

$$f_a = \frac{V_2}{V_s} \tag{2.5}$$

As this ratio rises, the suction valve remains open for longer time leading to an increase of the mass flow and, consequently, of the admission work and the produced torque. On the other hand, the expansion work is reduced due to the reduction of the piston stroke at closed valves and the specific work (i.e. the ratio between the produced work and the mass elaborated in each cycle) decreases. It is one of the main optimization parameters of a piston expander.

In a similar way, it can be defined the following ratio by considering the cylinder volume when the outlet valve closes (Eq. 2.6):

$$f_p = \frac{V_5}{V_s} \tag{2.6}$$

This ratio should be as low as possible to reduce the amount of the remaining mass that gets trapped in the cylinder and, therefore, gets compressed causing work losses. On the other hand, the compression of the remaining mass allows to begin the suction phase with an initial higher pressure and to reach a greater in-cylinder pressure at the beginning of the expansion phase.

As for what concerns volumetric efficiency, also energy efficiency can be expressed in different ways.

The *isentropic efficiency* is defined as the ratio between the power output measured on the shaft on the isentropic power calculated from the mass flow rate and the isentropic enthalpy difference (Eq. 2.7).

$$\eta_{is} = \frac{W_{meas}}{\dot{m}\Delta h_{is}} \tag{2.7}$$

Such efficiency is the figure which final users are more interested in. It is directly related to the specific work: the higher its value, the greater the recovered cost on the plant. The friction losses inside the machine influence the power measured on the shaft of the expander and, consequently, the value of the isentropic efficiency.

The *isentropic indicated efficiency* can be defined in order to avoid the influence of the mechanical losses. It is calculated analogously to the precedent definition, but the indicated power (i.e. calculated from the area of the measured P-V diagram), which indicates the power on the fluid, is used instead of the measured power. (Eq. 2.8).

$$\eta_{is,ind} = \frac{W_{ind}}{\dot{m}\Delta h_{is}} \tag{2.8}$$

It is important to notice that both definitions of the isentropic efficiency take into account the measured mass flow rate that includes the leakages through the expander. Thus, the increase of the leakages leads to a reduction of the isentropic efficiency.

The *mechanical efficiency* evaluates the effect of the friction losses inside the expander and it is expressed as the ratio between the measured power to the indicated power (Eq. 2.9).

$$\eta_{mec} = \frac{W_{meas}}{W_{ind}} \tag{2.9}$$

These presented parameters evaluate how the expander works and give information on which phenomena most influence the expander performance.

2.3 Numerical model

In order to obtain the optimum design of the expander when used in a vapor compression cycle and assess the main aspects to modify, its performance was evaluated numerically. In this stage, it is fundamental to study the expander performance by means of a fast and flexible model. It is important to point out that the redesign was carried out as the right compromise between the performance improvement and the manufacturing costs/constraints.

The model was first developed into EES® environment, which is equipped with many reliable libraries of real fluid properties. The developed model was compared with the commercial code LMS Imagine Lab AMESim in order to validate the obtained results. The EES model is purposely developed and thus highly customizable, whereas the AMESim model is realized by using the pre-defined and validated components available from its wide library, but it has a modest level of customizability; both calculation codes have many libraries with Equations Of State of real fluids.

2.3.1 The quasi-steady model

The EES model was based on a 0D quasi-steady approach to evaluate the time variation of the thermodynamic parameters with time-step progress. An analogous model was developed with a good agreement with experimental results in the reciprocating compressor field for refrigerating applications [34]. Conversely, in case of an expansion of wet fluids, no models are present in the literature.

In the definition of the cycle inside the cylinder, the leakages, the friction losses and the eventual heat transfer through the expander walls are neglected, whereas the non-negligible effects of friction losses through the input/output ducts are considered separately.

For each time step, corresponding to a well-defined crank angular position, the mass flow rate through the valves is calculated by considering an isentropic flow in a simple nozzle. In addition, the fluid is considered as incompressible in according to the theory of isentropic flows of ideal gases that justifies this assumption for Mach numbers under 0.3. Thus, the mass flow rate is given by Eq. 2.10.

$$\dot{m} = K \cdot A_v \cdot \rho_{up} \cdot \sqrt{\frac{2 \cdot (p_{up} - p_{down})}{\rho_{up}}} \tag{2.10}$$

where the path area A_v is determined by the valve timing, the diameters of the holes in the rotating/stationary plates and the piston displacement law. When the piston is at the TDC, it must be considered that the area at the end of the intake duct A_{cyl} is masked by the piston, as shown in Figure 2.5. For this reason, the effective passage area A_v varies with the piston stroke over a shaft rotation angle corresponding to the travelling of the piston in front of the related bore on the cylinder surface. When the holes in the rotating plate are closed, the mass flow rate is null and the value of the in-cylinder mass is kept constant. The non-isentropic behavior of the mass flow is taken into account using the flow coefficient *K*. This parameter is unknown and it has to be determined from experimental data.

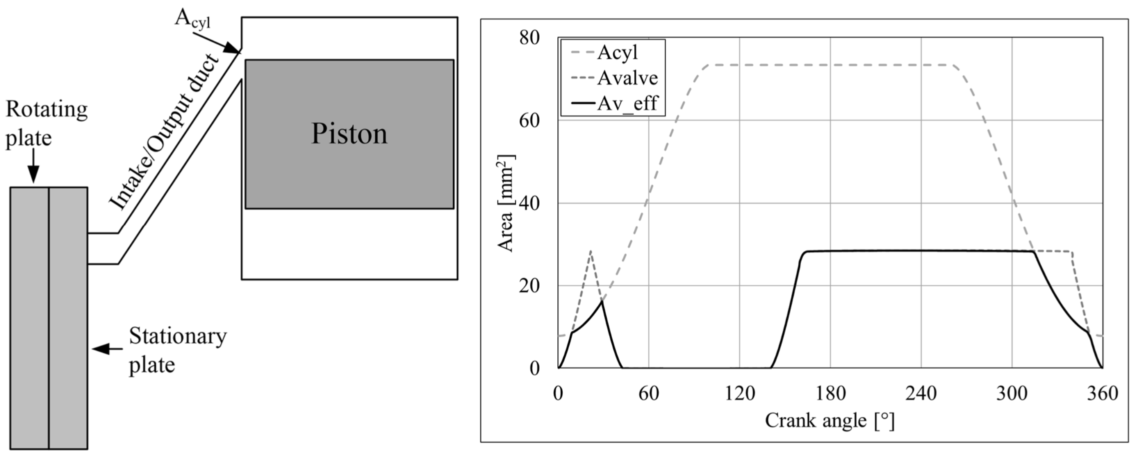

Figure 2.5 - Distribution system in the expander and effective passage area.

After having calculated the mass flow rate, the mass continuity equation (Eq. 2.11) and the entropy balance in the cylinder (Eq. 2.12) are solved.

$$\rho_{cyl}^{i} = \frac{V_{cyl}^{i-1} \cdot \rho_{cyl}^{i-1} + \sum_k \dot{m}_k^i}{V_{cyl}^{i}} \tag{2.11}$$

$$s_{cyl}^{i} = \frac{s_{cyl}^{i-1} \cdot M_{cyl}^{i-1} + s_{suc}^{i-1} \cdot M_{in}^{i} - s_{cyl}^{i-1} \cdot M_{out}^{i}}{M_{cyl}^{i}} \tag{2.12}$$

The computed density and the specific entropy allow the calculation of the in-cylinder pressure from the real gas property tables. The procedure is repeated iteratively, for each defined angular step (1°), until the convergence is reached over a whole cycle.

The calculation of the pressure drops inside the intake/output ducts is considered crucial in this model, as the diameter of the ducts, fluid velocities and flow path length make these losses not negligible, especially at relatively high rotational speeds. According to [35], the total static pressure drop of a fluid flowing inside a pipe can be calculated as the sum of three terms (Eq. 2.13):

$$\Delta p_{tot} = \Delta p_{mom} + \Delta p_{frict} + \Delta p_{static} \tag{2.13}$$

which are the momentum, friction and static pressure drops respectively. The latter, which depends on the head loss due to variation of quote, is reasonably neglected in this model. The momentum pressure drop is related to the change in kinetic energy of the flow and is given by:

$$\Delta p_{mom} = u_{tot}^2 \left[(R_1 + R_2)_{out} - (R_1 + R_2)_{in} \right] \tag{2.14}$$

where R_1 and R_2 are defined as:

$$R_1 = \frac{(1-\chi)^2}{\rho_{liq} \cdot (1-\varepsilon)} \tag{2.15}$$

$$R_2 = \frac{\chi^2}{\rho_{vap} \cdot \varepsilon} \tag{2.16}$$

The void fraction ε is calculated with the following expression:

$$\varepsilon = \frac{\chi}{\rho_{vap}} \left[(1 + 0.12(1-\chi)) \left(\frac{\chi}{\rho_{vap}} + \frac{1-\chi}{\rho_{liq}} \right) + \frac{1.18(1-\chi)\left[g\sigma(\rho_{liq} - \rho_{vap}) \right]^{0.25}}{m_{tot}\,\rho_{liq}^{0.5}} \right]^{-1} \tag{2.17}$$

Finally, the friction pressure drop is calculated by the Muller-Steinhagen correlation [36]:

$$\left(\frac{dP}{dz}\right)_{frict} = RS(1-\chi)^{1/3} + b\chi^{3} \tag{2.18}$$

where

$$RS = a + 2(b-a)\chi \tag{2.19}$$

where a and b are the monophasic frictional pressure gradients for the liquid and vapor phases respectively. Since this correlation is semi–empirical and interpolates the two-phase frictional pressure losses from the full liquid flow (χ=0) and full vapor flow (χ=1), it is applicable only inside the two phase field.

In reference to Eq. 2.10, the pressure drop reduces the value of the upstream pressure p_{up} that is equal to the suction pressure during the suction phase and the in-cylinder pressure during the discharge phase.

In Figure 2.6 the computational logic flow-chart is shown.

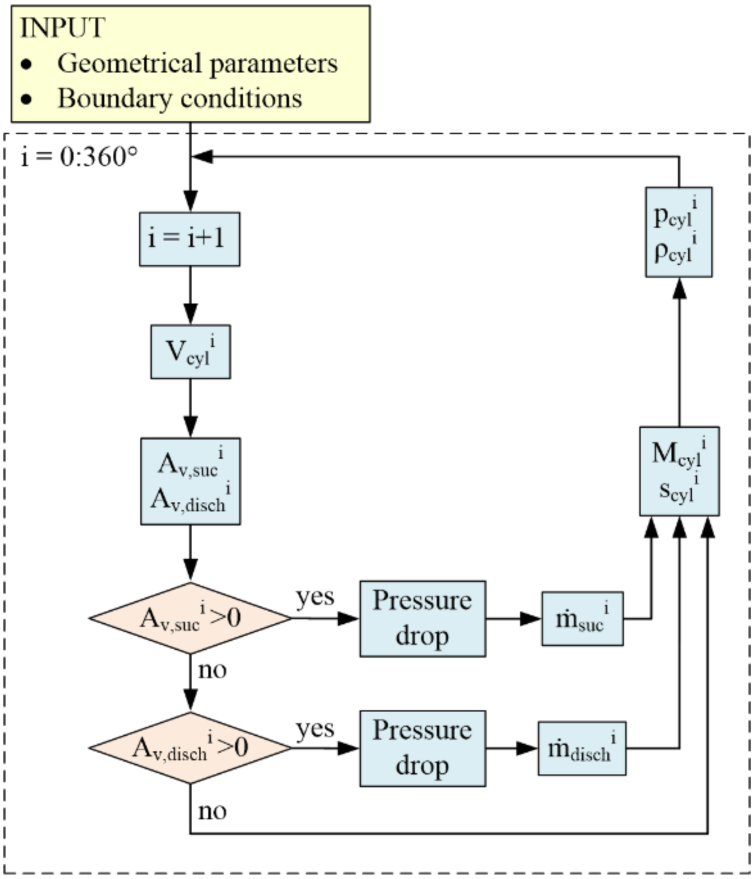

Figure 2.6 - Flow chart of the numerical model.

2.3.2 Numerical model comparison

The reliability of the developed model was assessed by comparing the obtained results with those provided by the commercial 1D code AMESim. The comparison was carried out with the same valve timing and boundary conditions in both models. It was considered the R134a as working fluid and the values of suction and discharge pressures equal to 15 bar and 2.94 bar respectively, corresponding to a saturation temperature of 55.2 °C and 0.1 °C; in addition, the fluid at the suction side is liquid (χ=0). Tests with different values of the flow coefficient were performed (i.e. from 0.6 to 1).

The tested configuration modeled in AMESim is depicted in Figure 2.7. The boundary conditions are represented by the pressure and the enthalpy of the fluid at the expander suction and discharge. The valve timing is simulated by using a “variable cross-section orifice” and a duct is inserted between the orifice and the cylinder. It is important to underline that the thermodynamic parameters inside the cylinder were calculated in AMESim by means of the same equations of the EES model. Conversely, the intake duct is modeled in AMESim with a 1D time-domain approach by considering the Muller-Steinhagen correlation, as in EES model, for the evaluation of the pressure drop.

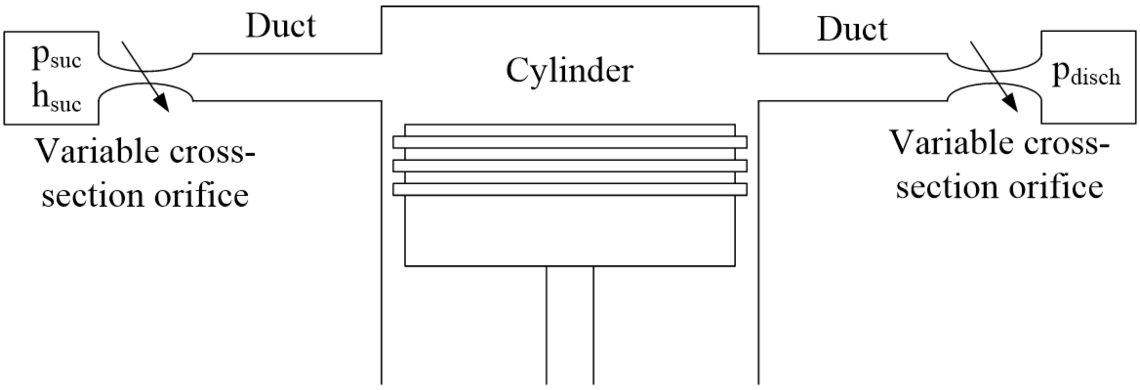

Figure 2.7 - Scheme of the AMESim model configuration.

Figure 2.8 and Figure 2.9 show the good agreement between the two models. In particular, Figure 2.8 depicted the P-V diagrams obtained with both models with a flow coefficient of 0.7, whereas Figure 2.9 reported the specific power obtained at different values of the flow coefficient. The good agreement allows using the quasi-steady model to study the performance of the expander in order to obtain the optimum redesign.

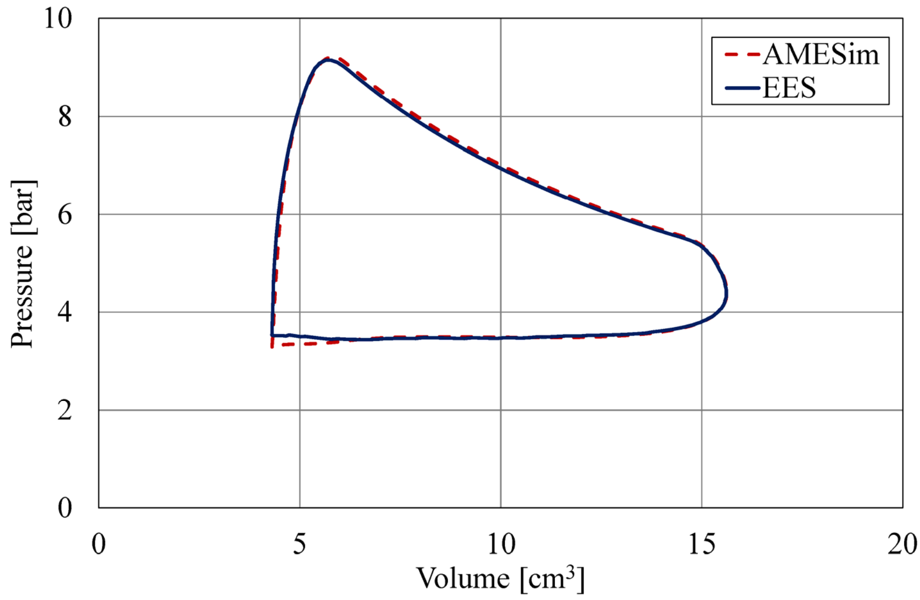

Figure 2.8 - Comparison between the P-V diagrams obtained by EES an AMESim with a flow coefficient of 0.7.

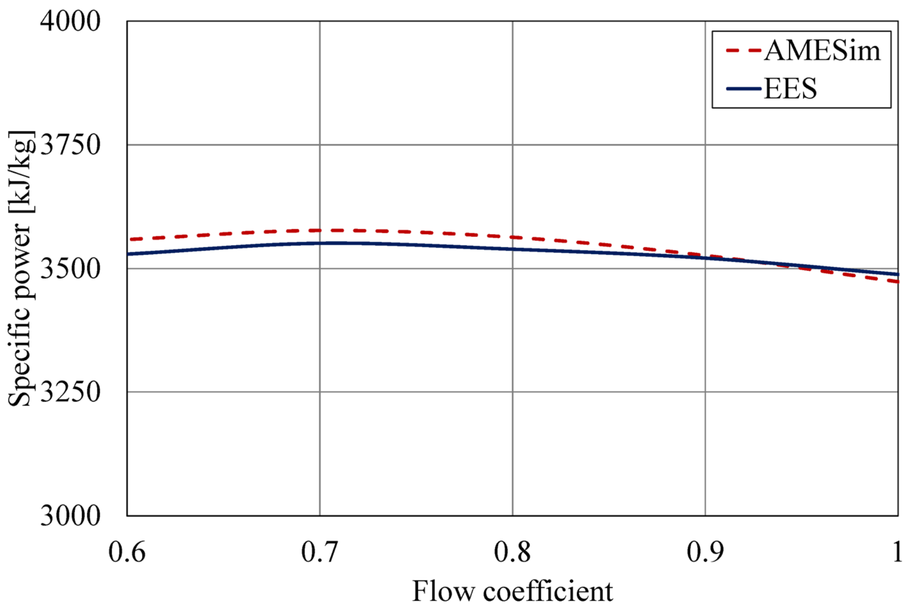

Figure 2.9 - Comparison between EES and AMESim in terms of specific power at different values of the flow coefficient.

2.4 First redesign of the expander

The development of the numerical model allows evaluating the main issues of the commercial version of the expander that influence its performance when used in place of the throttling valve in a vapor compression cycle. Some changes of the original version were necessary as a compromise between the performance and the manufacturing costs.

The simulations were carried out with R134a as working fluid by considering a heat pump power of 20 kW_{th} and the condenser and evaporator temperatures of 65 °C and -10 °C respectively.

As explained in the following paragraphs, the two main critical issues are related to the valve timing and the high dead volume of the cylinders. The main changes were done in order to improve these aspects.

2.4.1 Influence of the valve timing

In the original version of the expander, the geometry of the rotating plate led to a valve timing of 0°-180° for the suction phase and 180°-360° for the discharge phase, starting from the TDC. With this configuration, each cylinder would be always connected to the input/output pipeline of the VCC unit and it would never be closed. Therefore, the contribution of the expansion work would be null. In order to maximize the specific work, the valve timing was changed by modifying both the angular positioning and the size of the holes on the plates. A preliminary analysis (Table 2.2) shows that strong improvements are achieved at lower suction angle and higher discharge angle. At higher suction angle, the power increases together with the mass flow rate: however, the lower angle available for the expansion phase leads to lower specific power. In addition, by considering to open the discharge valve before the BDC to allow the free discharge of the working fluid, the influence of the duration of this phase is very low.

Table 2.2 - Performance of the expander with different valve timing.

	Suct: 0°-45° **Disch: 140°-270°**	**Suct: 0°-30°** **Disch: 140°-270°**	**Suct: 0°-30°** **Disch: 140°-360°**
Mass flow rate [kg/s]	0.761	0.408	0.413
Power [kW]	2.225	1.712	1.745
Specific work [kJ/kg]	2.922	4.196	4.222

In order to decrease the timing of the suction phase as much as possible, the diameter of the holes on the plates were reduced. It is important to point out that the reduction of the holes leads to lower suction angle and higher pressure losses through the valves. A right compromise was chosen by reducing the diameters from 8 mm to 6 mm in both the rotating and stationary plates. The following valve timing was achieved:

- Suction phase: from 0 to 43 degrees
- Discharge phase: from 140 to 360 degrees

Figure 2.10 shows the original and the modified rotating plate. For the suction phase, the buttonhole became a single hole with a lower diameter: whereas, for the discharge side, the buttonhole, made of ten holes because of manufacturing constraints, was slightly extended. The stationary plate was modified only by reducing the diameter of the nine holes.

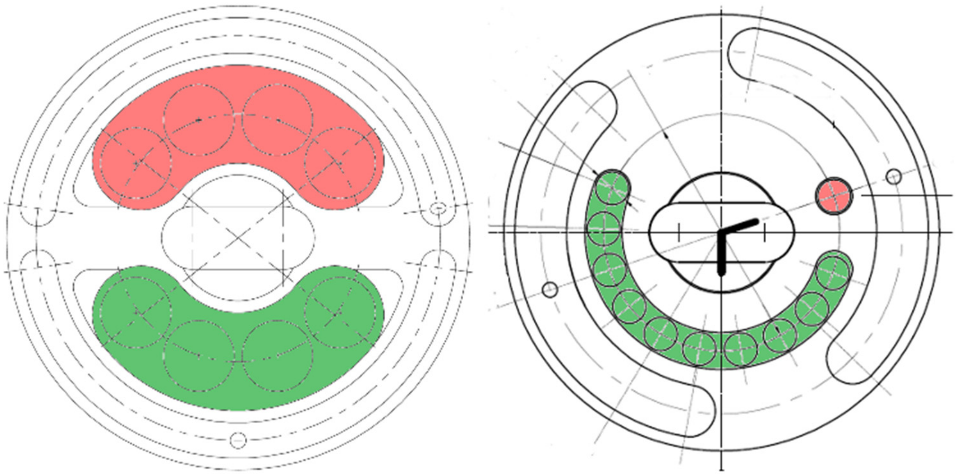

Figure 2.10 - Scheme of the original (left) and modified (right) rotating plate: the holes linked to the suction and discharge sides are colored in red and green respectively.

2.4.2 Influence of the dead volume

Another important aspect for the improvement of the expander performance was the reduction of the dead volume. In the proposed expander, the dead volume is constituted by the volume of the intake duct and the space above the piston at the TDC, the latter mainly occupied by the volume inside the spring. The influence of both contributions was analyzed by performing a preliminary analysis without these volumes, as reported in Table 2.3. The high dead volume, which is approximately the 79% of the displacement volume, reduces strongly the expander performance. In fact, without the two contributions, the specific work increases twice. The reduction of the dead volume leads to both the decrease of the mass flow rate and the enhancement of the power.

Table 2.3 - Comparison between current and modified geometries of the expander.

	Current	**No duct**	**No spring**	**No duct No spring**
Mass flow rate [kg/s]	0.413	0.361	0.397	0.262
Power [kW]	1.745	2.080	1.950	2.100
Specific work [kJ/kg]	4.222	5.762	4.912	8.015

Consequently, two modifications were done to the original design:

- The space inside the spring above the piston was filled with a screw under the cover head (Figure 2.11)
- The diameter of the intake duct was reduced to the same diameter of the holes on the plates as a trade-off between the expansion ratio and the friction losses of the fluid inside the duct.

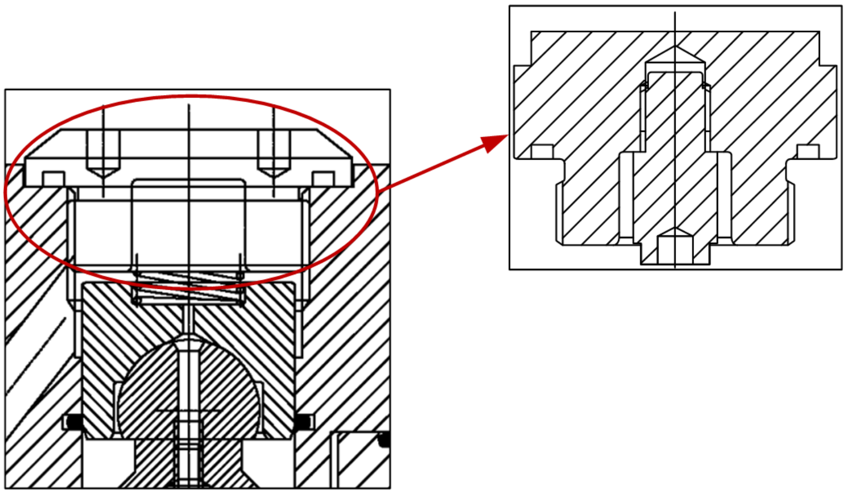

Figure 2.11 - Original (left) and modified cover head (right).

As a result, the dead volume was reduced from 79% to 34% of the displacement. The influence of the diameter of the intake duct and the holes on the plate was analyzed, as reported in Table 2.4 that shows the best performance with a diameter of 5 and 6 mm.

It is important to remember that the reduction of these diameters leads to the increase of the expansion ratio; on the other side, the pressure losses enhances.

Table 2.4 - Specific works with different values of holes and duct diameters.

Diameter [mm]	8	7	6	5	4
Specific work [kJ/kg]	5.856	6.392	6.768	6.956	6.092

These changes on the expander led to an increase of the expansion ratio and, therefore, the specific work without big changes on the design and a strong increase of the manufacturing costs; only some components has to be changed (i.e. the plates and the cover heads), whereas the case is the same as the original version except for the diameters of the intake ducts.

2.5 Preliminary analyses

After evaluating the main issues to be modified in the original machine, preliminary numerical analyses were performed by considering the redesigned expander in two different seasonal conditions with R134a as working fluid:

- case 1: suction pressure (from the condenser of the heat pump) of 10 bar, corresponding to a saturation temperature of 39.4 °C; discharge pressure (to the evaporator of the heat pump) of 3.5 bar, corresponding to a saturation temperature of 5 °C;
- case 2: suction pressure of 15 bar (corresponding saturation temperature of 55.2 °C) and discharge pressure of 2.94 bar (corresponding to a saturation temperature of 0.1 °C).

It was considered that the fluid enters the expander in saturation conditions with a quality of 0 and the rotational speed of the machine was 1450 rpm. Due to the unknown value of the flow coefficient, the simulations were performed at different flow coefficients.

Figure 2.12 shows the trends of the power produced by the expander and its isentropic efficiency at different flow coefficients in the two analyzed working conditions. In each case, the power output is greater at higher values of the flow coefficient due to the decrease of the pressure losses through the valve. In addition, the power is higher for the working condition in which the pressure ratio between the suction and the discharge side is greater (i.e. case 2). In spite of the trend of the power output, the isentropic efficiency remains almost unchanged (i.e. in the range 0.43-0.48) with varying the flow coefficient. Moreover, its values are similar also at different working conditions.

The COP improvement obtained by introducing the analyzed expander into the heat pump cycle in place of the throttling valve was calculated (Figure 2.13). Higher values are found in case 2 (6.5 - 6.8% vs 4 - 4.8%) where the contribution of the expander is more important due to the higher expansion ratio.

It is important to point out that these results are obtained only from the indicated cycles without considering the mechanical losses and the leakages inside the expander. The mechanical losses lead to a lower power output measured on the expander shaft, whereas the leakages enhance the mass flow rate elaborated by the expander without obtaining an increase of the power output. For these reasons, it is expected to obtain worst performance after carrying out experimental tests.

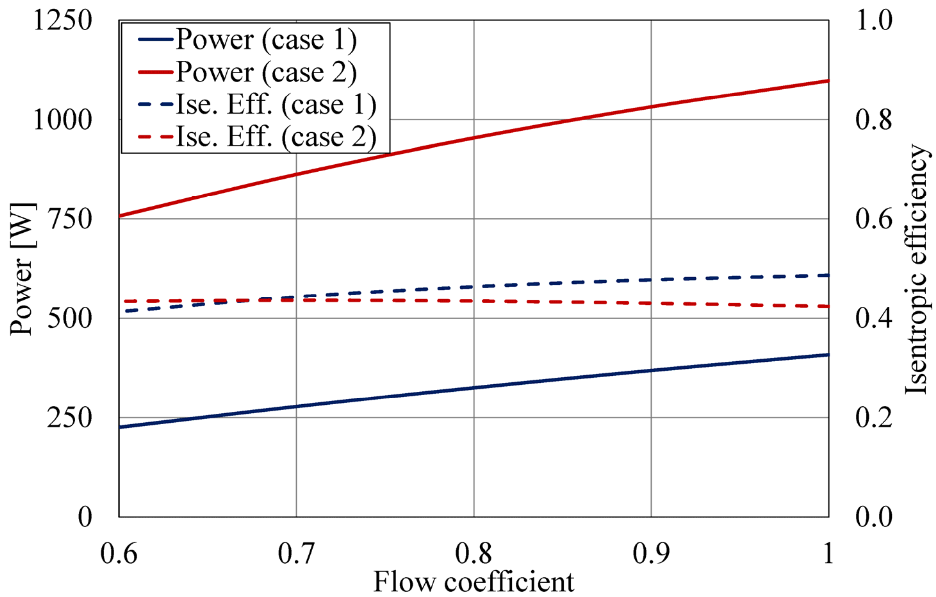

Figure 2.12 - Power and isentropic efficiency trends in the two analyzed cases.

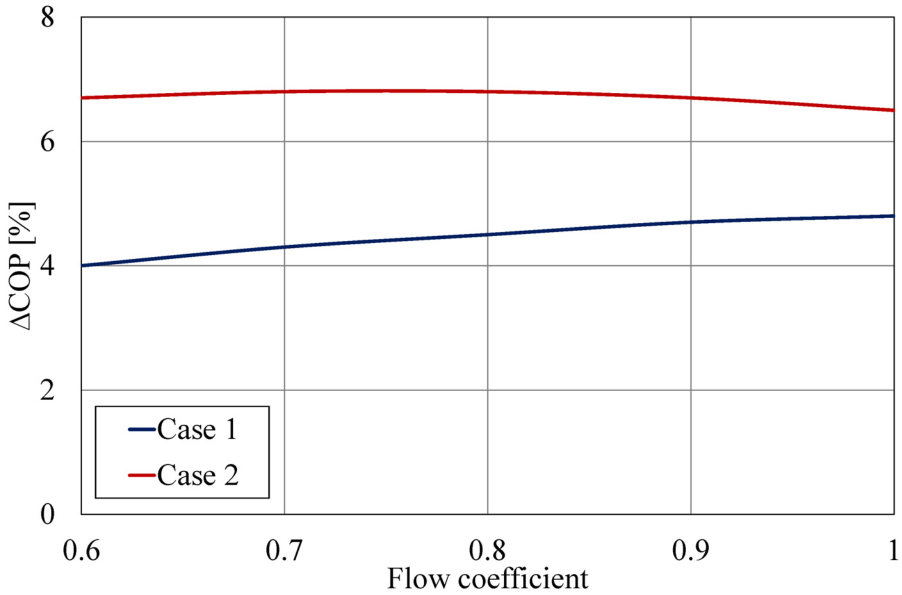

Figure 2.13 - COP improvement in the two analyzed cases.

3 Test rig

The numerical evaluations allowed to identify the main issues of the expander that lead to modify few components to enhance its performance when used in a vapor compression cycle. After making the necessary changes on the design, experimental tests were needed to characterize in detail the expander. In this chapter, the experimental setup on the expander prototype will be presented. In particular, the expander performance was evaluated by measuring the P-V diagrams and the power produced by the machine in different working conditions and at different rotational speed. These measurements allowed to calculate the global parameters of the expander such as volumetric and isentropic efficiencies and its influence on the cycle COP. With the aim to obtain these parameters, a test rig was built (Figure 3.1); it was composed by the expander, the connection rod instrumented with a torque meter and a rotation sensor and the brake/motor section. Moreover, two data acquisition software were developed to acquire and elaborate the signals coming from the sensors.

3.1 Test equipment

All the components are arranged on a portable metallic structure that is positioned on wheels to facilitate its movement and is composed by two decks. The expander is rigidly connected to the brake motor with the axis positioned horizontally and all the devices are anchored on a metal sheet to have a good mechanical resistance.

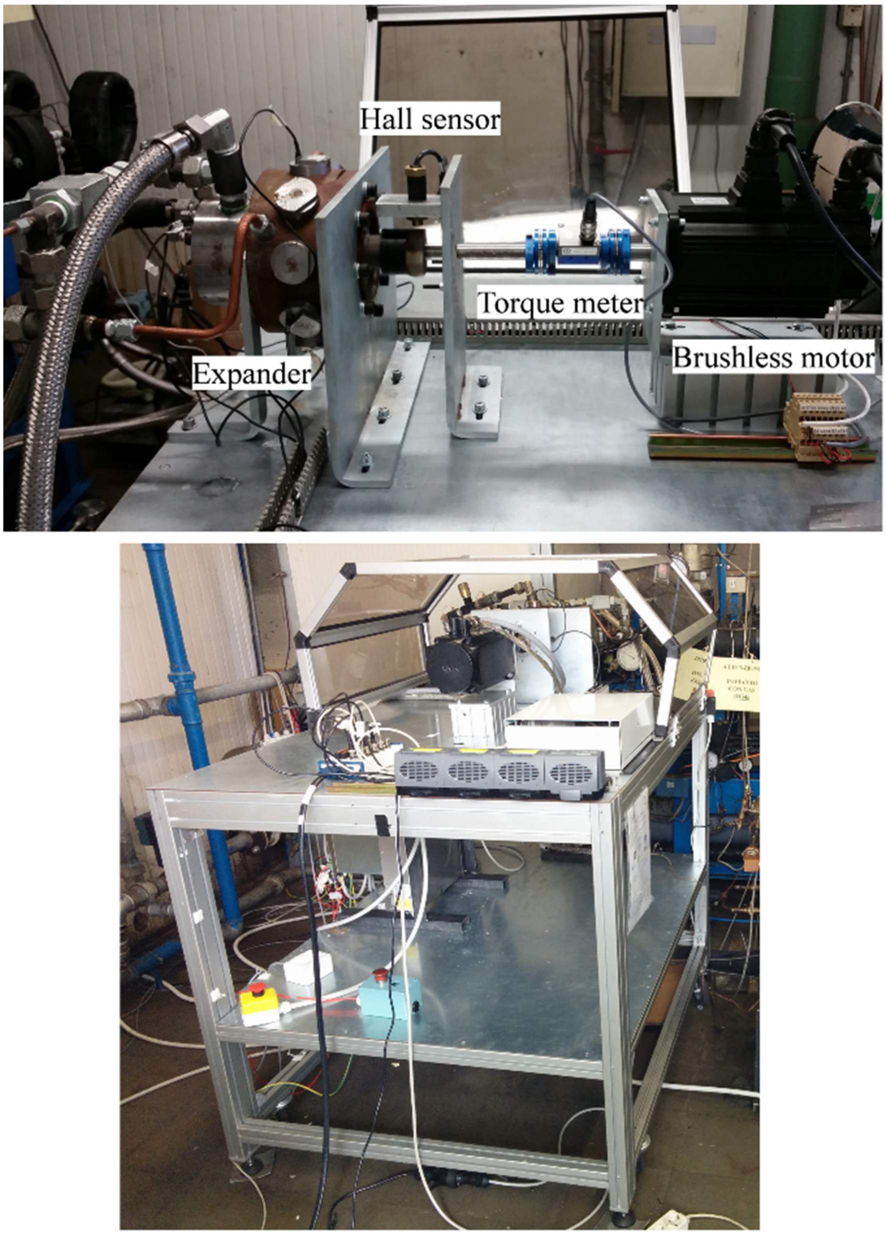

Figure 3.1 - Test rig.

3.1.1 The expander

The expander is connected to the condenser and the evaporator of the heat pump cycle by means of flexible ducts. Moreover, two additional ducts connect the internal part of the expander case to the discharge line. When the expander works, the pressurized fluid goes from the cylinder to the area below the piston through the gap between the piston and the cylinder wall, in spite of the presence of a piston seal. Without the additional ducts, the pressure inside the case would increase up to the average cycle pressure and it would become higher than the in-cylinder pressure (i.e. during the last part of the expansion). As a result, the pressure difference would push up the piston that would lose the contact with the bearing of the shaft leading to the stop of the rotation (Figure 3.2). The use of the additional ducts allows the connection of the internal part of the case to the lower-pressure side through the drain ports present in the original design of the machine in order to maintain the pressure inside the case at the same discharge value. The leakage flow rate is vented through these ducts and then remixed with the mass flow rate coming from the output duct of the machine.

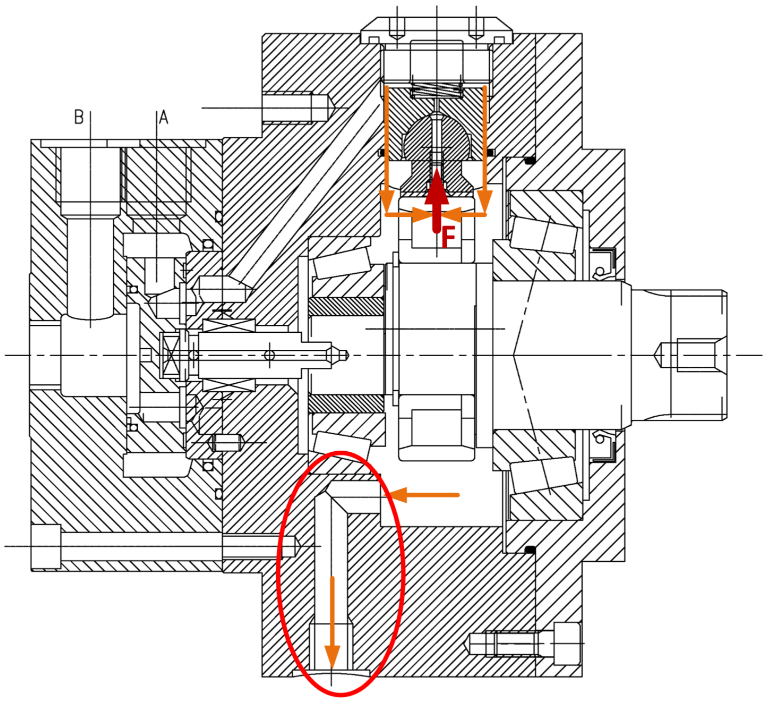

Figure 3.2 - Leakages through the piston and the cylinder wall and the original drain port.

In order to measure the temperature and the pressure at the inlet and outlet of the expander, two dynamic pressure sensors (Kulite XTL-123 series, ±0.1% FSO) and two T-type thermocouples are installed in the ducts upstream the suction phase and downstream the discharge phase on the distributor (Figure 3.3). The dynamic pressure sensors allow to acquire the pressure at high frequency in order to evaluate the suction and discharge pressure trend in each cycle. The choice of the sensors with a right full-scale depends on the heat pump cycle where the expander is tested and, in particular, the working fluid.

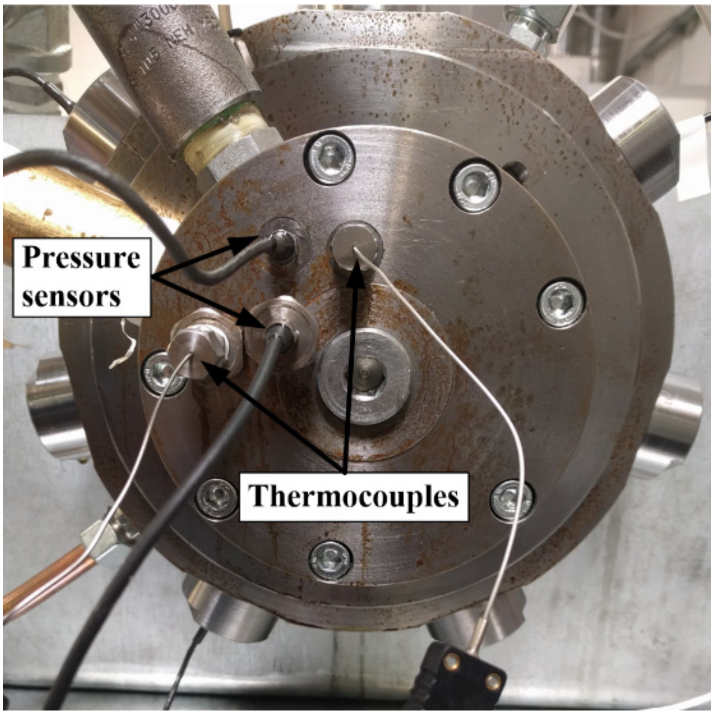

Figure 3.3 - Pressure sensors and thermocouples positioned on the back side of the expander.

In addition, three dynamic pressure sensors are installed above three different cylinders in the cover head in order to measure the time histories of the in-cylinder pressure. Figure 3.4 shows the drawing of the cover heads modified to host the pressure sensors. As the cover head is longer than the sensor, a 2 mm diameter hole was made to connect the sensor to the cylinder. In Figure 3.5, the pressure sensors housed on the three cover heads are showed.

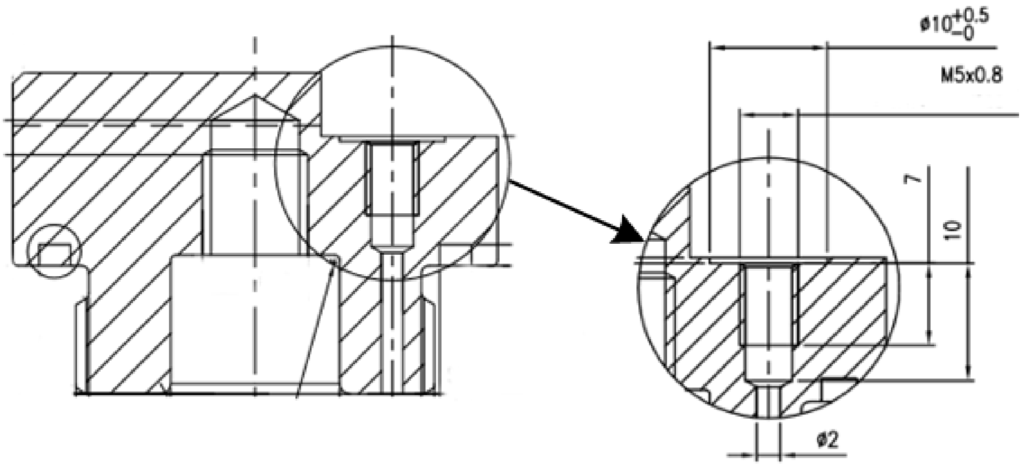

Figure 3.4 - Draw of the cover head with the pressure sensor.

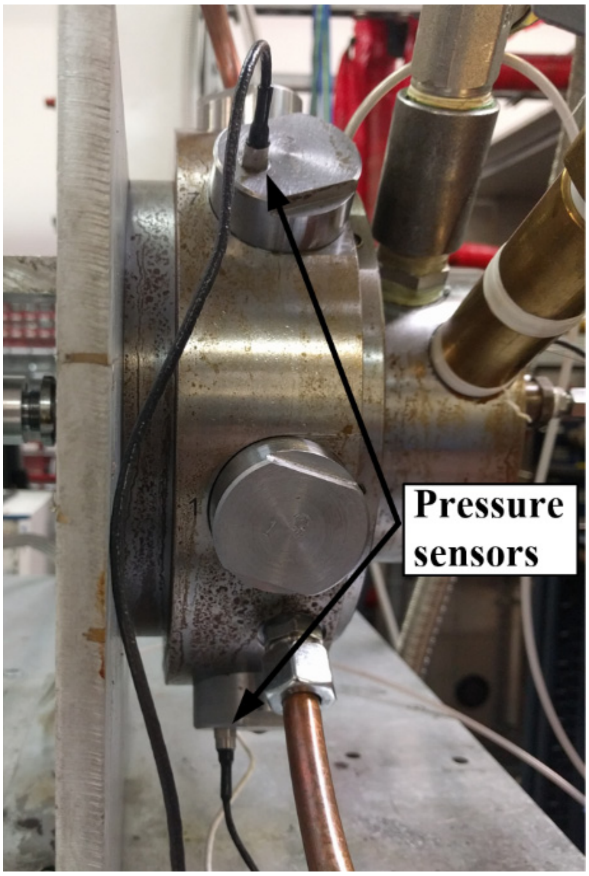

Figure 3.5 - Sensors for in-cylinder pressure measurements positioned on the cover heads.

3.1.2 The instrumented connection rod

The expander is connected to the brake motor by means of an instrumented connection rod and a torque meter. In this section, the shaft angular position and the torque produced by the expander are measured. In particular, a torque meter (Lorenz, nominal torque 10 Nm, ±0.2% FSO) is used; this device, as apart from providing the torque value that allows the calculation of the produced power at a certain rotational speed, is also equipped with an encoder with a 0.5° spacing. Thus, the crank shaft position was measured accurately to determine the piston displacement of the cylinder. In order to have an initial reference in the angular position (crank angle 0°), a hall sensor detects the passage of a groove that has been milled on the rod connecting the expander to the torque meter (Figure 3.6). The combination of these measurement systems allows generating the P-V (i.e. pressure-volume) diagrams of the instrumented cylinders.

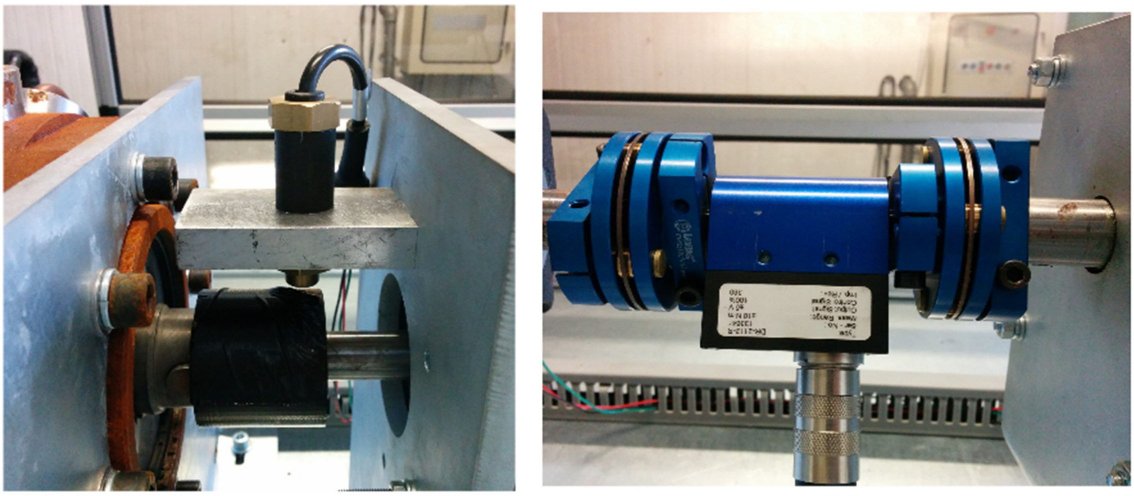

(a) (b)

Figure 3.6 - Hall sensor (a) and torque meter (b).

3.1.3 The brake motor and the servo drive

In order to test the expander at different rotational speeds by maintaining unchanged the working conditions, an electric motor is used. A brushless type motor (AMK, nominal torque 19 Nm) is connected to the torque meter through a flexible coupling. The brushless controls the rotational speed of the expander by means of a servo drive; according to the power produced by the expander, the brushless can be used as a brake or as a motor. More in general, the electric motor is a four-quadrant controller meaning that the speed control is maintained either accelerating or braking in both clockwise and counter-clockwise directions. The brushless directly dissipates the surplus power in the electric grid by making a continuous exchange of electricity between the electric motor and the grid; whether at a certain value of the rotational speed the expander does not produce torque, the electric motor absorbed the electricity from the electric grid.

3.2 Experimental measurement setup

The all signals coming from the sensors are acquired and processed to obtain the desired parameters of the expander. Figure 3.7 shows the experimental setup for the measurements.

It can be seen that two dedicated software were specifically developed to acquire the different types of signals: one is used to acquire the signals at high frequency and generate the P-V diagrams, whereas the other is used to acquire signals at lower frequency and to control the rotational speed of the brushless motor.

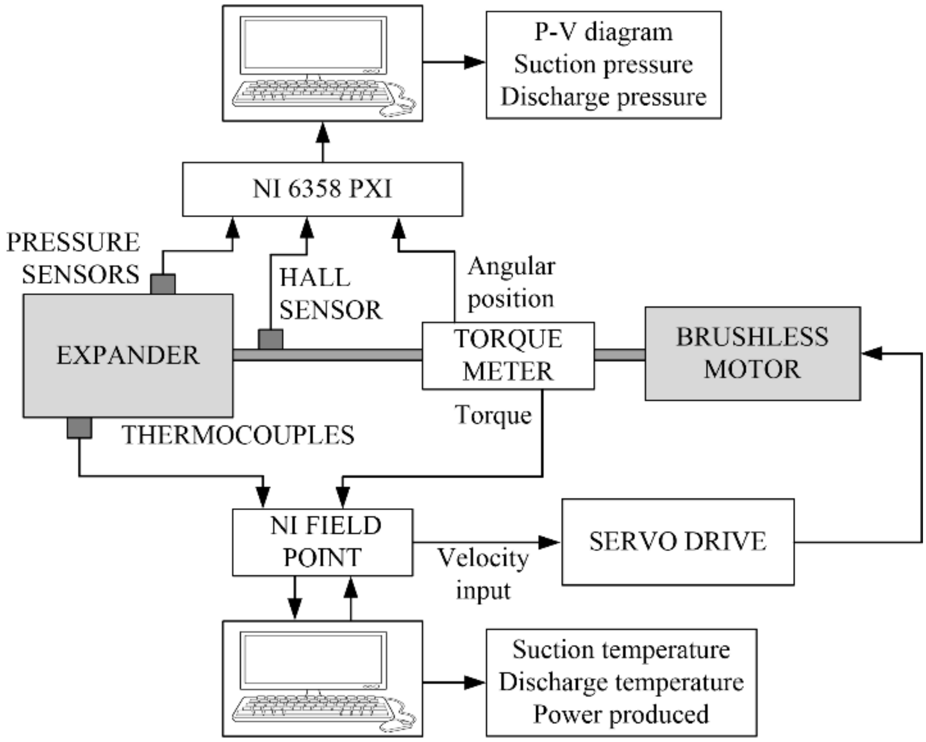

Figure 3.7 - Experimental measurement chain and control system of the test rig.

3.2.1 Generation of the P-V diagrams

All pressures and crank-angles are acquired by using a National Instruments 6358 PXI (Figure 3.8) and, then, processed by a software specifically developed in LabVIEW. The signals are acquired at high frequency (i.e. 100 kHz) in order to rebuild the P-V diagram with high accuracy. In particular, the following data are measured:

- Suction/discharge pressures
- In-cylinder pressures (for three cylinders)
- Crank shaft position
- TDC positions.

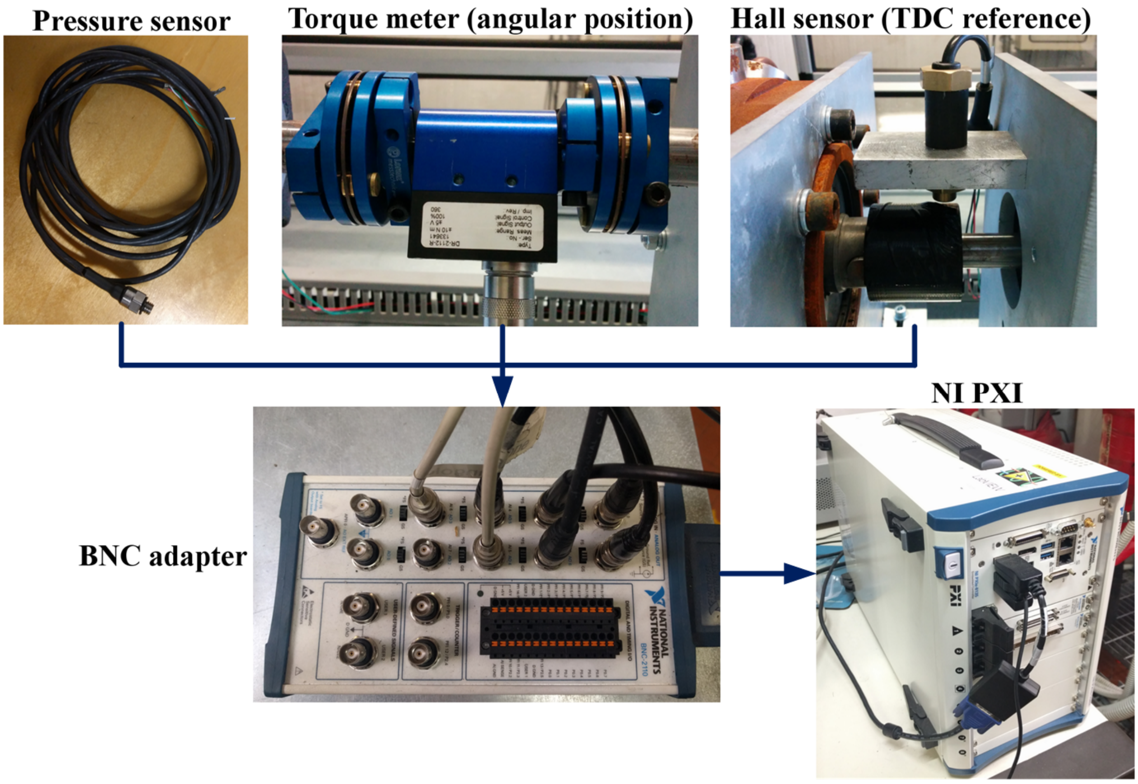

Figure 3.8 - Acquisition system for the generation of the P-V cycle.

The signals of these sensors go to the PXI in form of voltage. The pressure sensors give voltage signals in the range 0-100 mV; the values of the pressures in the correct unit of measure (bar) are obtained using coefficients (i.e. slope and offset) calculated by a previous calibration of the sensors. The encoder inside the torque meter gives a signal in form of square wave from 0 to 5 V. Each peak corresponds to a 0.5° of the crank angular position that means 720 outputs per revolution. By using this information, it is possible to sample the in-cylinder pressure every 0.5°. The acquisition of the pressure signals with this methodology avoids the influence of any change of the rotational speed in one round on the acquired data. Finally, the hall sensor gives an analogue information of the torque meter; a voltage peak corresponds to the passage of the groove present on the expander shaft. In particular, the presence of the groove causes an increase of the distance between the sensor and the shaft that gives an increase of the voltage from 0 to 5 V. By knowing the angular phase shift between the passage of this groove and the position when one piston is at the TDC, these measurements are elaborated to generate the P-V diagrams of the instrumented cylinders, as shown in the scheme in Figure 3.9. Moreover, the P-V diagrams for all three instrumented cylinders are generated by considering that these cylinders are arranged with an angular phase shift of 120°. In order to reduce the influence of the random errors on the measurements, the obtained experimental cycles were averaged among one hundred cycles.

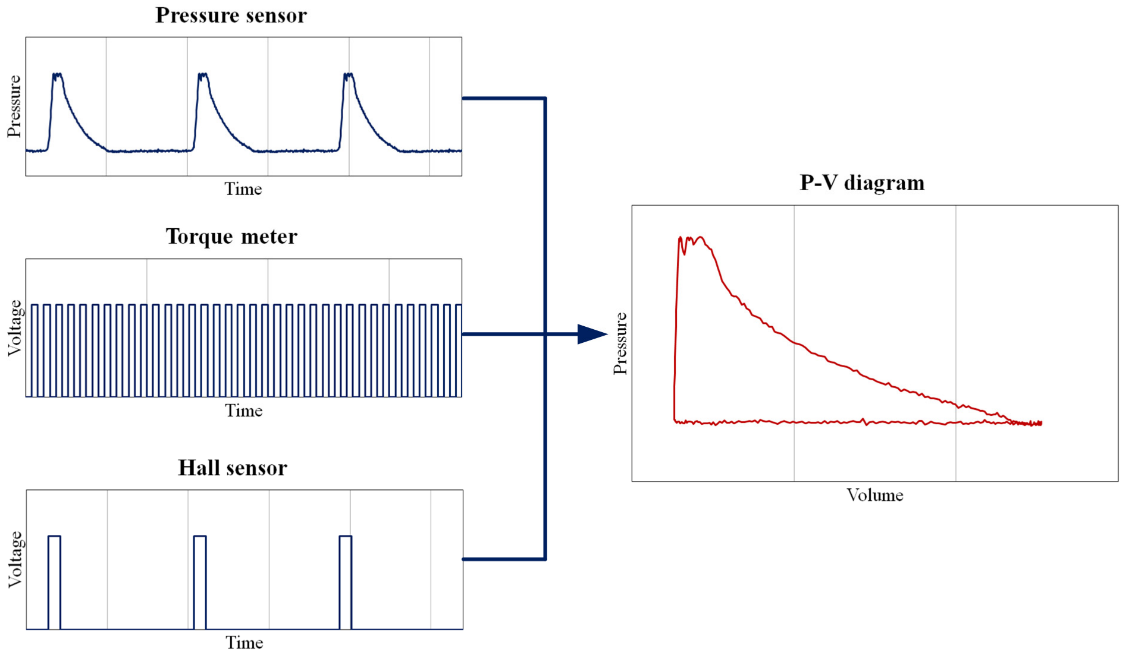

Figure 3.9 - Combination of the signals coming from the pressure sensors, the torque meter and the hall sensor to generate the P-V diagram.

This acquisition method allows a rigorous monitoring of the in-cylinder pressure trends. In fact, it builds the correct P-V diagram also by varying the rotational speed of the expander and the working conditions (i.e. suction/discharge thermodynamic conditions and working fluid).

3.2.2 Static measurements and velocity control

The low-frequency measurements and the control of the brushless are acquired by a National Instrument Field Point (Figure 3.10), whereas a second software developed in LabVIEW is used to process and set the following data:

- Measurement of suction/discharge temperatures;
- Measurement of torque produced by the expander;
- Set of the brushless velocity.

The signals are sampled with a frequency of 1 Hz.

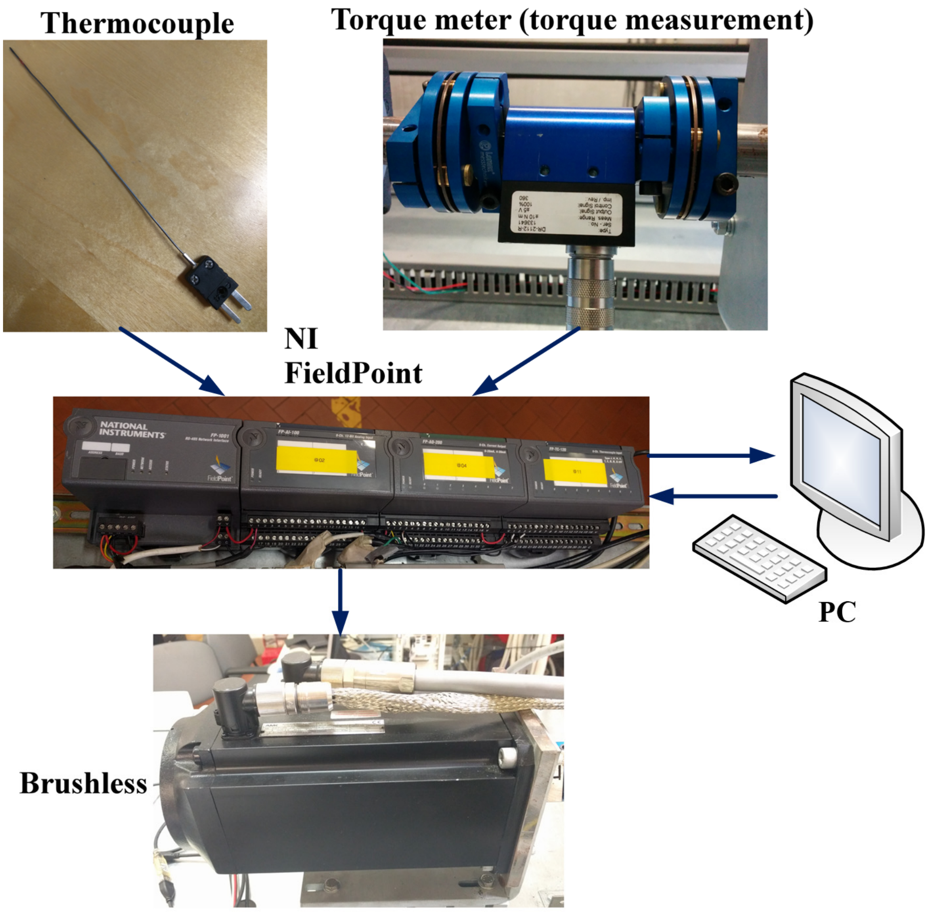

Figure 3.10 - Acquisition system for the low frequency measurements and the brushless control

The T-type thermocouples are connected to the thermocouple module in such a way that the Field Point gives directly the values of the suction and discharge temperature of the expander in °C.

The output of the torque meter for measuring the value of the torque is given in form of voltage and it is converted in Nm by knowing the full-scale of the instrument (i.e. 10 Nm). Its instantaneous value fluctuates greatly due to both the random errors on the measure and the type of the tested machine; in fact, the torque produced by the reciprocating machines, such as the internal combustion engines, fluctuates around a mean value under fixed conditions. For these reasons, the values from the torque meter are averaged among the last 1000 values acquired with a frequency of 100 Hz. In this way, the value of torque obtained is a mean value of the last 10 s. The value read on the software can be positive or negative: if the expander produces a torque at a certain rotational speed, the torque is positive, otherwise it is negative.

Finally, the software allows to control the rotational speed of the expander by setting the velocity of the brushless. A signal in form of current (from 0 to 20 mA) is sent by the software to the current output module on the Field Point that is connected via LAN to the servo drive. Due to the maximum rotational speed of 2000 rpm imposed previously, a variation equal to 1 mA of the signal corresponds to a variation of the rotational speed of 100 rpm.

Therefore, by measuring the torque from the torque meter and by knowing the rotational speed of the expander, which is imposed by the user, it is possible to calculate the real power produced as:

$$W = T \cdot 2\pi \cdot \frac{rpm}{60} \tag{3.1}$$

The two dedicated software allow to carry out accurately the experimental tests of the expander at different rotational speeds and thermodynamic conditions without modifying anything. All the data obtained by means of them, with also the mass flow rate that is measured by a flow meter inside the VCC, lead to a complete characterization of the expander by measuring its performance and by identifying its critical aspects.

4 Experimental results

After assembling the all components and measurement instruments on the test rig with the expander, an extensive experimental activity was performed in order to analyze the behavior of the expander in a vapor compression cycle working with different refrigerants; in particular, the different behaviors of VCC units working with a HFC (i.e. in this case R134a) and CO_2 as refrigerants were evaluated. The performance of the expander was evaluated mainly in terms of isentropic efficiency and COP improvement of the cycle where the expander works. The experimental tests were performed at different thermodynamic conditions and rotational speeds so that to characterize in depth the expander. The measurement of the indicated cycles allows to assess the behavior of the fluid inside the cylinders without considering the mechanical losses and the leakages.

4.1 Experimental tests with R134a

In the first experimental tests, the expander was used in a vapor compression cycle working with R134a. Even though R134a is being phased out, several candidates to its replacement are under development by replacing as far as possible its properties and it might be a significant reference for the tests. Moreover, it has some practical undoubtable advantages like safety, low cost and large availability.

In order to characterize and assess the performance of the machine as expander in a VCC unit, its behavior was evaluated in different thermodynamic conditions. In addition to vary the inlet temperature and pressure (i.e. condenser thermodynamic conditions), tests were carried out also with inlet qualities higher than 0. Even though tests with an inlet quality higher than 0 are not significant for a VCC unit, where the theoretical starting point of the expansion is with saturated liquid (i.e. quality = 0) or subcooled liquid, these tests serve to assess the potential performance related to different properties (i.e. modify of the required volumetric ratio).

4.1.1 R134a heat pump cycle

The expander was tested in substitution of the throttling valve in one of the R134a test rig in Dorin®. As shown in Figure 4.1, the expander was connected in parallel to the main cycle throttling valve, which was generally closed during the tests and was only opened during the start up and shut down procedure (when the expander speed is still low) to avoid pressure peaks in the circuit. In order to regulate the inlet conditions of the fluid, a needle valve was installed upstream to the expander. Two Coriolis mass flow meters (Siemens Sitrans F C Mass 2100, Accuracy: ≤0.15% of mass flow rate) were installed to measure the mass flow rate of the refrigerant in the expander and in the throttling valve branch. A reciprocating compressor by Dorin was used.

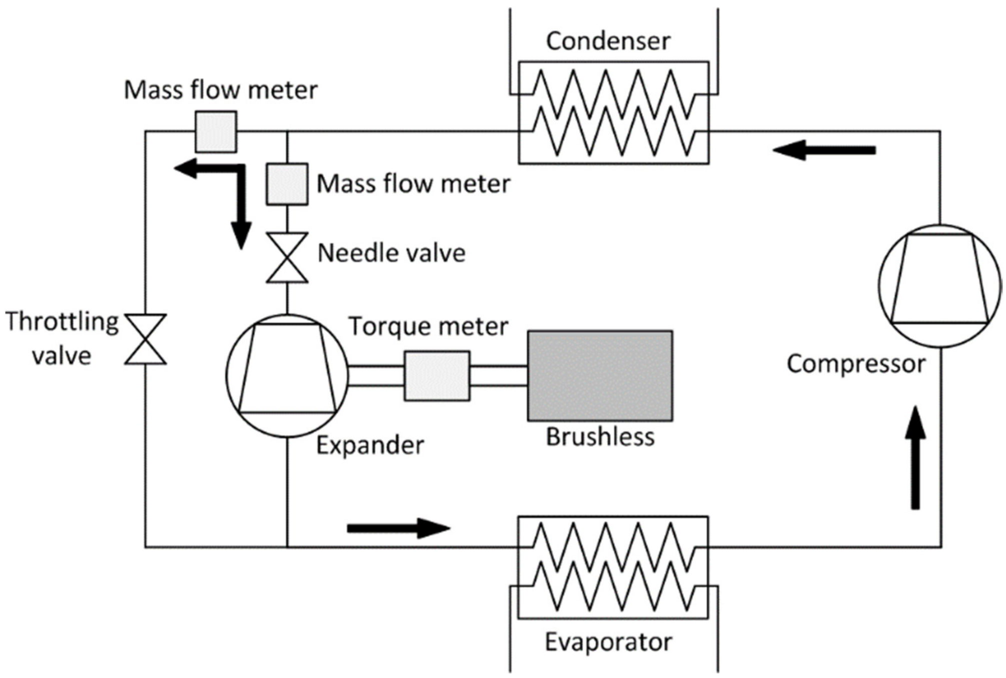

Figure 4.1 - R134a heat pump cycle.

The regulation of the fluid thermodynamic conditions at the expander inlet (pressure and temperature) was made by regulating the mass flow rate of the coolant (water-glycol mixture) in the condenser: the higher the coolant mass flow rate, the lower the inlet fluid pressure. In particular, by increasing the coolant flow rate, the heat exchange in the condenser increases leading to a reduction of the refrigerant temperature and, consequently, pressure. The evaporation pressure was influenced by the pressure drop inside the expander, which depends on the rotational speed and the inlet fluid conditions. The inlet quality was controlled through the needle valve upstream the expander. The condenser working pressure was raised above the nominal test value, then the subcooled liquid coming from the condenser was flashed down to enter the expander at the desired quality and pressure.

The Dorin test rig is shown in Figure 4.2 where it is easy to recognize the Dorin compressor, the mass flow meters and the heat exchangers (i.e. evaporator and condenser).

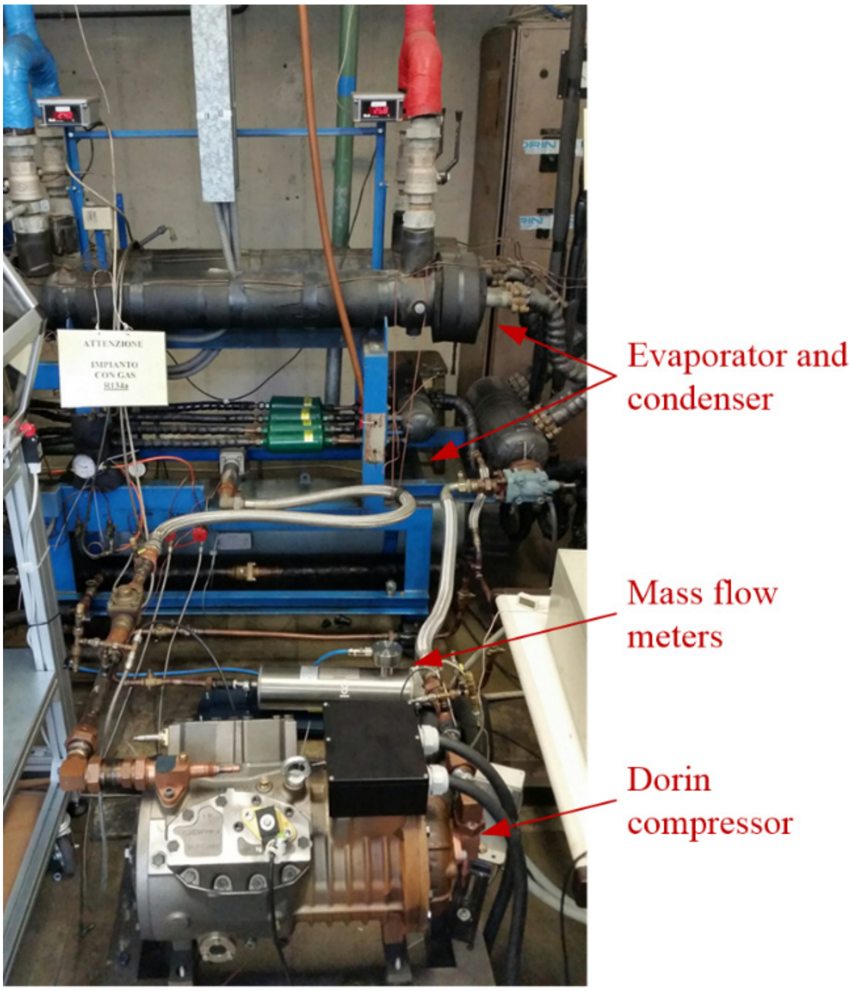

Figure 4.2 - Dorin test rig.

4.1.2 Working conditions with R134a

The tests were carried out with three different nominal working temperatures at the condenser, which are representative of the working charts of commercial heat pumps or refrigeration cycles. The thermodynamic conditions at the evaporator vary depending on the rotational speed and the inlet thermodynamic conditions. The investigated thermodynamic conditions are reported in Table 4.1. The inlet quality of the fluid was varied in the range 0 - 0.8.

Table 4.1 - Experimental thermodynamic conditions with R134a.

Parameter	Test #1	Test #2	Test #3
Suction pressure (bar)	10.2	13.2	16.8
Suction temperature (°C)	40	50	60

In order to measure accurately the thermodynamic conditions at the boundary and inside the expander, the 5 dynamic pressure sensors, as explained previously, were chosen with a proper full scale. In this test rig, due to the higher values reached by the fluid in the tests (i.e. at the condenser side), dynamic pressure sensors with a FSO of 35 bar were used. Table 4.2 lists the instruments and their accuracies.

Table 4.2 - Measurements instruments and their accuracies.

Equipment	Measurement range	Accuracy
Torque meter	0-10 Nm	±0.2% FSO
Pressure transducers	0-35 bar	±0.1% FSO
Thermocouple T-type	-270-370 °C	±0.5 °C
Mass flow meter	0-5600 kg h^{-1}	±0.15% MV
Analog Input –rpm	0-3000 rpm	±5 rpm

4.1.3 Experimental results with R134a

The performance of the expander was evaluated in each working condition at different rotational speeds. At first, the influence of the rotational speed and the working conditions on the performance was evaluated in detail.

Figure 4.3 shows the power output and the torque as function of the rotational speed obtained at different suction temperatures and qualities. At a fixed suction thermodynamic condition, the trends show the typical behavior of volumetric piston expanders, with torque decreasing at increasing rotational speed and power output showing an optimizing value of rpm located at about half of the operating field of the machine. By increasing the rotational speed after the optimizing value, the power output decreases up to become zero. In this condition, the escape velocity of the expander is reached and there is a perfect equilibrium between the power output and the mechanical losses. The trend of the power output is influenced by both the rotational speed and torque (Eq. 3.1); the latter is a function of the volumetric efficiency and the mechanical losses that worsen at higher rotational speeds.

By increasing the suction temperature, the torque and power increase due to the higher pressure at the inlet. In addition, the operating field of the machine widens and the optimizing value of rpm increases. Due to the higher power produced by the expander, the escape velocity is reached at greater values of rotational speed. Better performance is measured also by increasing the inlet quality; at the same suction temperature, the power output reaches higher values. For instance, with a suction temperature of 60 °C the maximum value of the power is about 100 W at 350 rpm with an inlet quality of 0, whereas a maximum power of 240 W at 600 rpm was measured with an inlet quality of 0.56. This behavior is due to the lower required volumetric expansion ratio at higher suction qualities that leads to a higher expansion work, as it will be explained successively.

In order to evaluate the performance of the expander, the trend of the isentropic efficiency in each condition was evaluated (Figure 4.4). It can be seen that with a saturated liquid condition at the inlet, which represents the actual condition in a commercial heat pump, the isentropic efficiency reaches a maximum value of 9% that is low in comparison to the results obtained in literature. By increasing the suction quality, the isentropic efficiency increases showing that the required volumetric ratio of the fluid plays a key role in the expander performance.

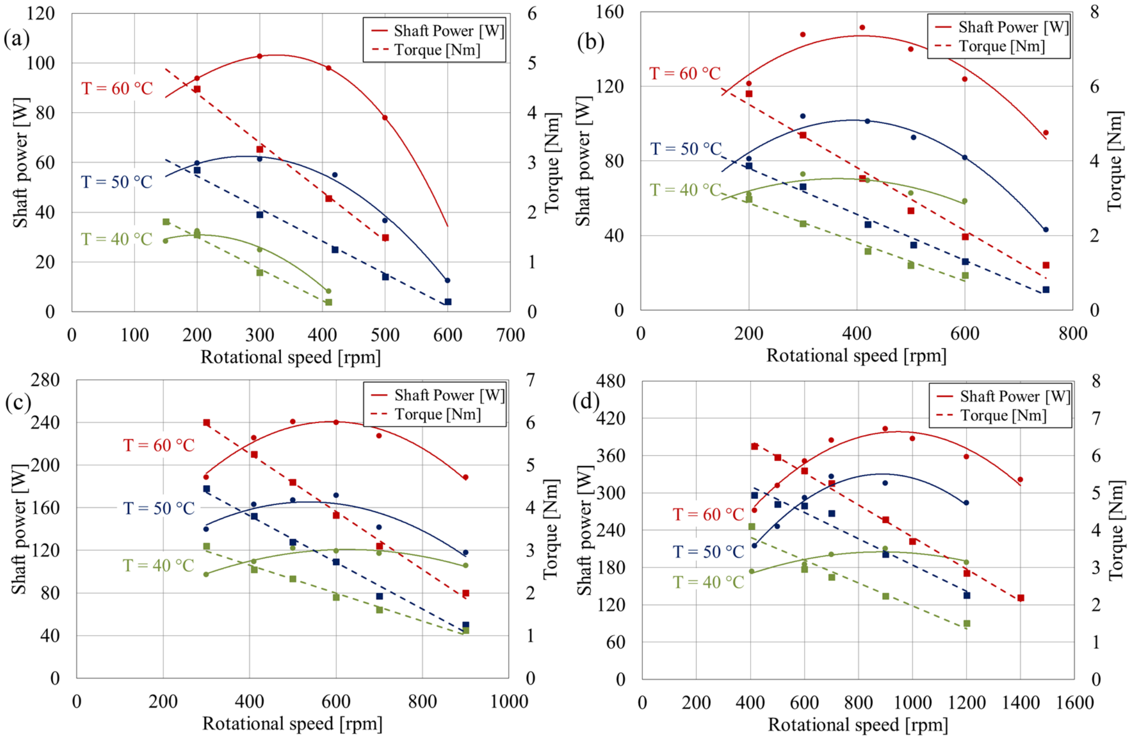

Figure 4.3 - Power shaft and torque at different rotational speed and suction temperatures at inlet qualities of 0 (a), 0.23 (b), 0.56 (c) and 0.8 (d).

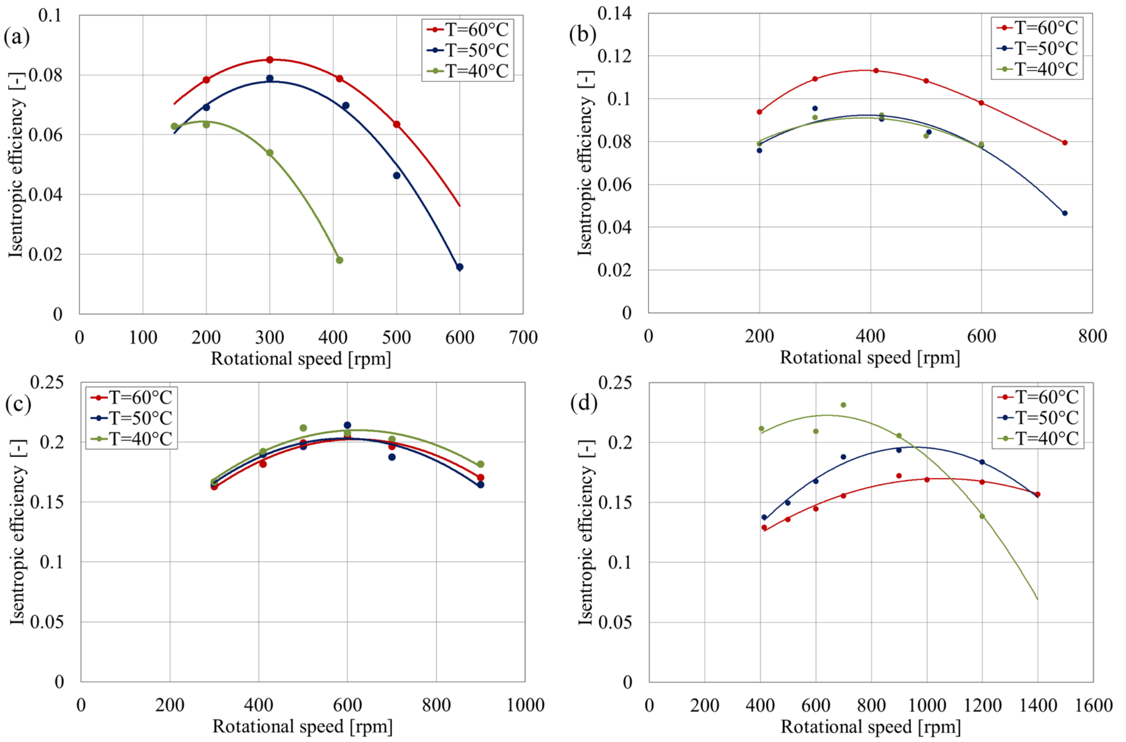

Figure 4.4 - Isentropic efficiency at different rotational speed and suction temperatures at inlet qualities of 0 (a), 0.23 (b), 0.56 (c) and 0.8 (d).

R134a is one of the fluids with larger required volumetric expansion ratio in liquid conditions, which is very difficult to reach in volumetric reciprocating machines. Figure 4.5 shows the theoretical required expansion ratio (R_{Vdes}) needed to obtain an isentropic expansion between the condenser and evaporator fixed pressures at variable inlet qualities. Moreover, it is reported the final output pressures as a consequence of a theoretical pressure drop realized by the expander with the built-in fixed volumetric expansion ratio (R_{Vbuilt}). It is clear that increasing inlet quality leads to lower required R_{Vdes} that gets closer to the built-in expansion ratio of the expander. Therefore, as the inlet quality increases, the expansion realized in the expander leads to greater pressure drops. Even though the actual behavior of the expansion is different from the theoretical isentropic one, this analysis reveals that actually the expander realizes an under expansion leading to lower performance at an inlet quality of 0. The improvement of the performance by increasing the inlet quality is due to the increase of the theoretically exploited pressure drop. Actually, the required volumetric expansion ratio is lower in the part with closed valves because of two reasons:

1) The quality at the beginning of the expansion (i.e. when the suction valve closes) is higher than 0, even though the fluid enters as saturated liquid;
2) Due to the head losses through the inlet duct, the maximum cycle pressure is often lower than the condenser value.

However, the built-in expansion ratio of the expander is always lower than the theoretical required one and the under expansion occurs. The results obtained with higher values of the suction quality demonstrate that an improvement of the performance can be obtained either with an increase of the built-in volumetric ratio or by using fluids with lower required volumetric expansion ratios.

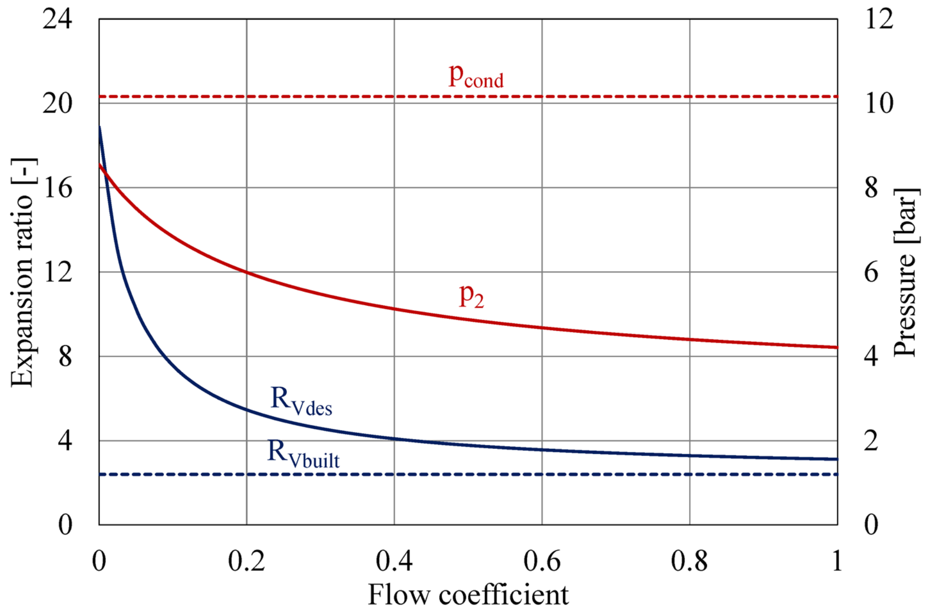

Figure 4.5 - Required volumetric expansion ratio and theoretical pressure drop vs. inlet quality at condenser/evaporator temperatures (40 °C/2.5 °C).

In order to study the expander behavior in detail, it is important to evaluate also the mass flow rate and the volumetric efficiency, as shown in Figure 4.6 that reports their trends as function of the rotational speed with a saturated liquid condition at the suction side. The mass flow rate is almost the same by increasing the rotational speed; its value depends on both the rotational speed that would lead to an increase because of the more displacement per unit time and the leakages that decreases at lower rpms. Because of the negligible variation of the mass flow rate, the volumetric efficiency decreases. It is worth pointing out that by considering the suction volumetric efficiency, which takes into account only the swept volume during the suction phase that deals only 43° of the crank angle (i.e. the swept volume during the suction phase is 6 times lower than the displacement), the values can be significantly higher than one. These values can be justified by (i) the high leakages that are higher at low RPMs, and (ii) the compression of the fluid inside the dead volume during the suction phase, which would increase the available volume. Therefore, these results show the high influence of the leakages on the measurement of the mass flow rate and that the effective elaborated mass flow rate by the expander is much lower than the measured one.

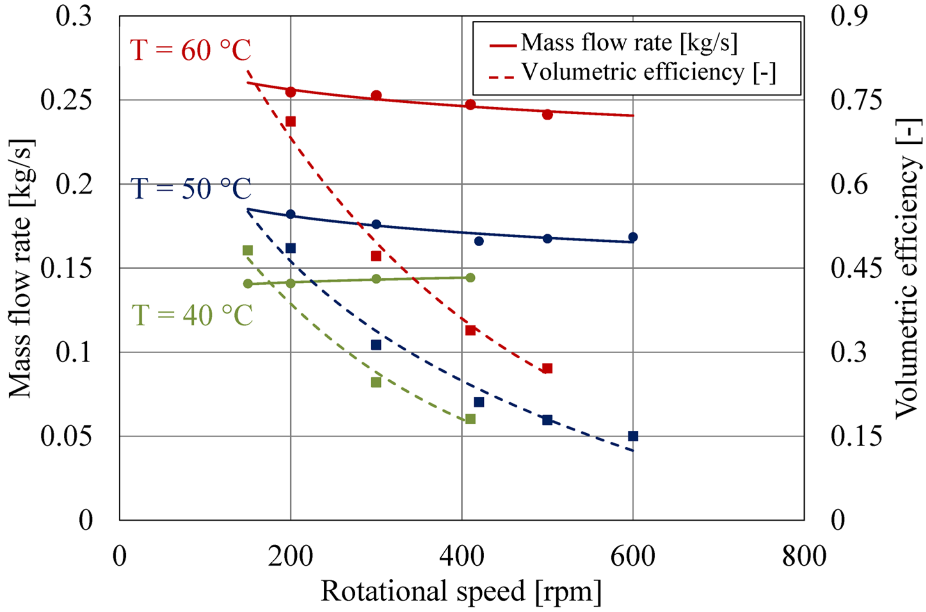

Figure 4.6 - Mass flow rate and volumetric efficiency vs rotational speed at different suction temperatures with a saturated liquid at the inlet.

Another important issue to evaluate for the characterization of the expander performance is related to the mechanical losses that are caused by the friction losses inside the volumetric machine. Figure 4.7 shows the mechanical efficiency as function of the rotational speed with a saturated liquid condition at the suction side. It is measured as the ratio between the measured power on the indicated power obtained by integrating the area of the indicated P-V diagrams and it gives the estimate of the percentage of work lost. Its value is maximum at lower rotational speeds and decreases gradually by increasing the rotational speed. This trend demonstrates that the impact of the mechanical losses on the measured work increases by increasing the rpm. In addition, the mechanical efficiency increases at higher suction temperatures due to the greater power output obtained in these working conditions. Consequently, at fixed rotational speed, the influence of mechanical losses on the performance are reduced by increasing the suction temperature. The low values of the mechanical efficiency (it reaches at maximum 50%) are significant to explain the low performance of the expander. These values are justified by the original hydraulic design of the machine, where the influence of the mechanical losses is much lower than the present case.

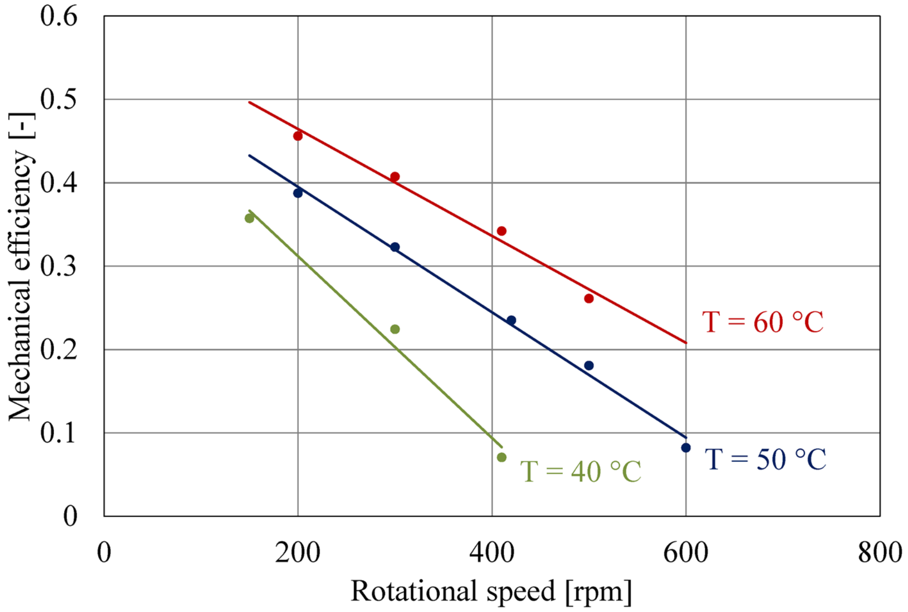

Figure 4.7 - Mechanical efficiency vs rotational speed at different suction temperatures with a saturated liquid at the inlet.

4.1.4 Evaluation of the performance with R134a

The experimental results showed the main critical aspects of the expander. In addition to obtain low performance in terms of power output and isentropic efficiency, the volumetric and mechanical efficiencies are issues that affect the performance. In particular, it is worth noting from Eq. 2.7 that the isentropic efficiency is negatively influenced by the mechanical losses and the leakages, which affect the power output and the mass flow rate respectively. For this reason, the influence of these sources of losses was evaluated by calculating the isentropic efficiency with the indicated power and an estimate of the effective mass flow rate elaborated by the expander. By using the indicated power in substitution of the measured power, the indicated isentropic efficiency (Eq. 2.8) is obtained; in this way, the mechanical losses are not considered. The estimation of the leakages was carried out by comparing the numerical model to the experimental results. It is important to remark that the only parameter to calibrate in the numerical model is the flow coefficient. Therefore, in each working conditions its value was varied until the same area of the numerical and experimental diagrams was obtained. After that, the effective mass flow rate and, consequently, the internal leakages were calculated (Figure 4.8). As explained in the next chapters, the comparison between the numerical and experimental models shows a different trend of the expansion phase; thus, the evaluation of the leakages by comparing the area of the P-V diagrams represents only a rough estimation, but it indicates roughly how they affect the performance. As it was expected, the leakages are greater at higher values of the suction temperature due to the corresponing higher inlet pressures, and at lower rotational speeds.

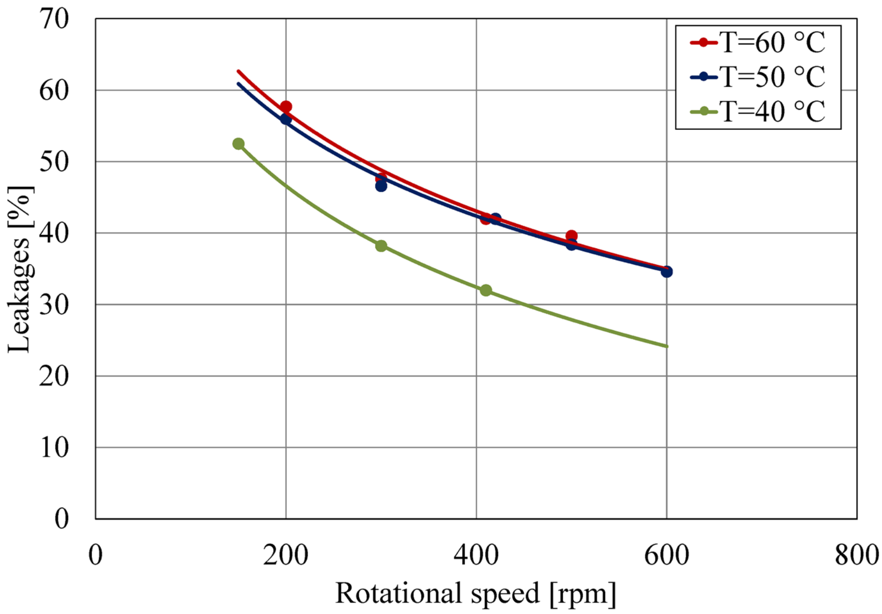

Figure 4.8 - Percentage of leakages in respect to the measured mass flow rate.

Figure 4.9 shows the trends, with a saturated liquid condition at the suction side, of the measured isentropic efficiency (η_{is}), the indicated isentropic efficiency ($\eta_{is,ind}$), the isentropic efficiency by using the measured power and the numerical estimated mass flow rate ($\eta_{is,mass}$) and the isentropic efficiency obtained by neglecting the mechanical losses and the leakages ($\eta_{is,ind,mass}$), as expressed in Eq. 4.1.

$$\eta_{is,ind,mass} = \frac{W_{ind}}{\dot{m}_{num}\Delta h_{is}} \tag{4.1}$$

It can be seen that at lower rotational speed (i.e. 150-200 rpm) the influences of the leakages and the mechanical losses on the isentropic efficiency are similar, as shown by the almost same value of the relative efficiency at these rpms. Conversely, by increasing the rotational speed the influence of the leakages on the isentropic efficiency is reduced, whereas the influence of the mechanical losses increases. The trends show that a strong improvement of the performance can be obtained by reducing the mechanical losses. In fact, the indicated isentropic efficiency reaches a maximum value of about 25% with all the three tested suction temperatures. At higher rotational speed, the leakages are very low and the value of $\eta_{iso,mass}$ is much closed to the measured isentropic efficiency. When considering, at the same time, the indicated power and the effective mass flow rate elaborated by the expander, the relative isentropic efficiency increases significantly. For each working condition, its value reaches a value of 40%, more than 4 times higher than the measured isentropic efficiency.

As last result of the analysis, the COP improvement by using the expander in substitution of the throttling valve in a vapor compression cycle was calculated. In a similar way of the isentropic efficiency, the COP improvement was calculated with the measured power and mass flow rate (ΔCOP), by neglecting the mechanical losses (ΔCOP_{ind}), the leakages (ΔCOP_{mass}) and both of them ($\Delta COP_{ind,mass}$). Figure 4.10 shows their trends, both in heating and cooling mode, obtained with a saturated liquid condition at the suction side at different rotational speed. It is important to remark that in cooling mode the COP improvement is higher because of the increase of the cooling capacity. The results show that with the current expander, the COP improvement is only around 1%, as expected by the low expander performance. However, the COP improvement can reach a value in the range 3-5%, depending on the suction temperature, by neglecting the mechanical losses and a value in the range 5-8% by neglecting also the leakages.

In general, the improvement related to the replacement of the throttling valve with an expander is relatively marginal because of the good thermodynamic performance in heat pumps and refrigeration cycles working with R134a, unless very high isentropic efficiency is achieved, which is typically difficult when dealing with expansion of saturated liquids. By considering a low cost of the expander (i.e. lower than 800 €), it is a common opinion that a COP improvement greater than 3-5% is sufficient to develop the expander/heat pump systems. This analysis demonstrates that, with an improvement of the expander design, which leads to a reduction of the mechanical losses and the leakages, a strong improvement of the performance can be obtained and the COP can be increased up to satisfactory values. On the other hand, the high mechanical losses and leakages are unavoidable due to the original application that must withstand pressures up to 300 bar and works with a fluid with higher viscosity than the working fluid in this study. However, the indicated powers demonstrate the high potential of the expander.

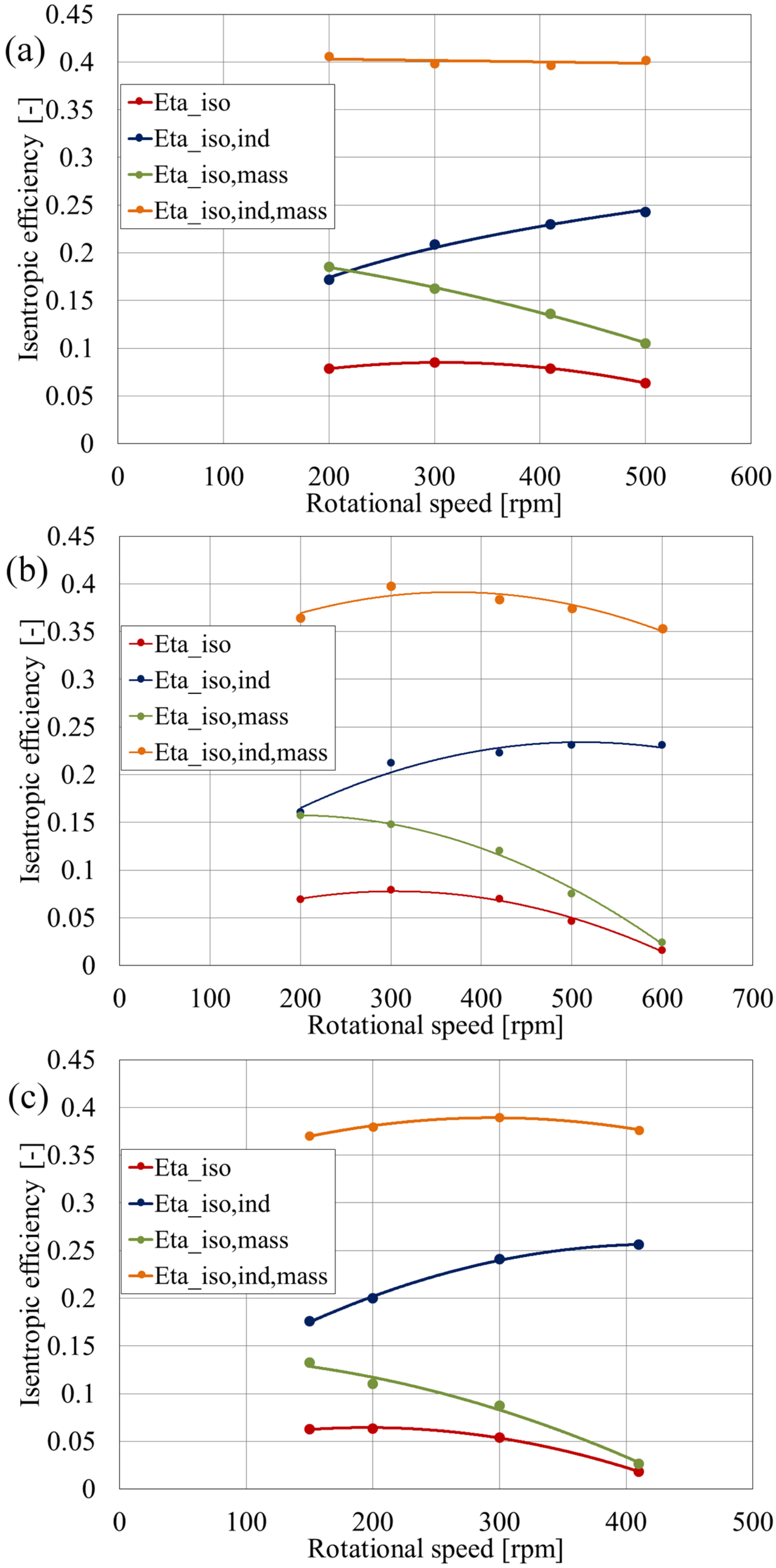

Figure 4.9 - Isentropic efficiencies with measured and numerical values for suction temperatures of 60 °C (a), 50 °C (b) and 40 °C (c).

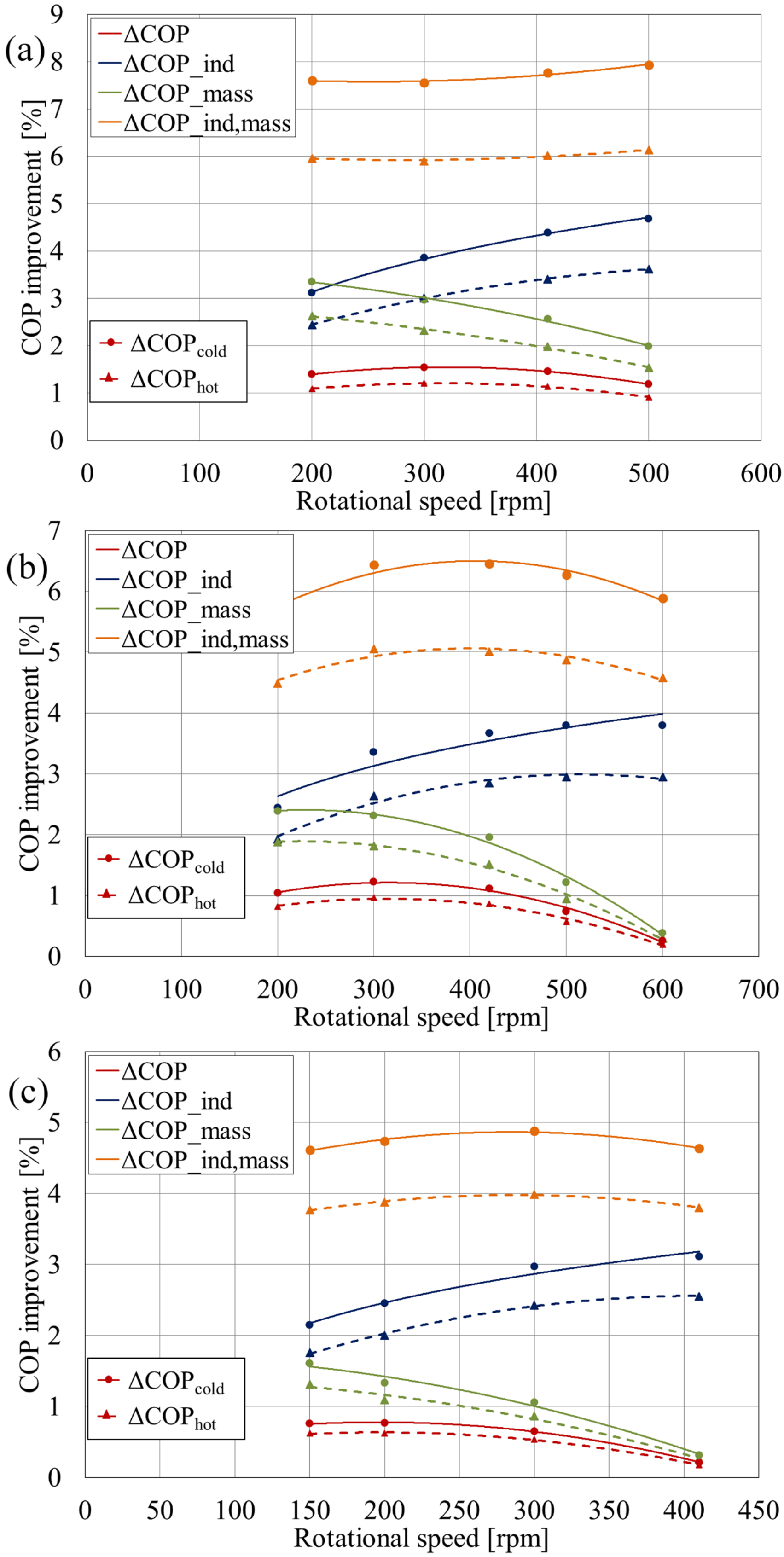

Figure 4.10 - COP improvements with measured and numerical values for suction temperatures of 60 °C (a), 50 °C (b) and 40 °C (c).

4.1.5 Evaluation of the indicated cycles

The results obtained during the tests were also analyzed to assess the influence of inlet temperature, quality and rotational speed on the thermodynamic behavior of the fluid inside the cylinder by the analysis of the indicated P-V diagrams. Figure 4.11 reports the P-V diagram at 500 rpm, a suction temperature of 60 °C and a variable inlet quality. It can be noticed that higher qualities lead to an increase of the peak pressure and a reduction of the discharge pressure. This behavior is mainly due to the decrease of the required volumetric expansion ratio and the increase of the specific volume with high inlet qualities. The decrease of the required volumetric expansion ratio leads to a reduction of the minimum cycle pressure (i.e. discharge pressure). On the other hand, the higher specific volume leads to a reduction of the mass flow rate and, consequently, to lower pressure losses through the valve and the intake duct that cause an increase of the peak pressure. The reduction of the pressure losses leads also to a faster increase of the in-cylinder pressure during the suction phase, as shown by the steeper trend obtained at higher qualities in this phase. Focusing only on the expansion phase, the increase of the inlet quality leads to a steeper curve after the peak pressure, due to the higher manometric expansion ratio consequent to the lower required volumetric expansion ratio. For this reason, the tests with higher inlet qualities show higher performance because of the increase of the expansion work.

Figure 4.12 shows the P-V diagram at variable rotational speed with a saturated liquid condition at 60 °C in the suction side. At a fixed inlet quality, by increasing the rotational speed the peak pressure of the P-V diagram decreases, while the discharge pressure remains almost unchanged. With increasing the expander velocity, the suction hole is opened for less time (even if the crank angle is the same), so less mass enters the cylinder in each cycle, thus leading to a worst volumetric efficiency of the engine, as showed previously in Figure 4.6. In addition, the less time available when the suction valve is opened leads to less steep curves during the suction phase. When considering only the expansion phase at closed valves, the lower mass inside the cylinder leads to a slightly faster decrease of the in-cylinder pressure. However, the curves in Figure 4.12 show that the expansion phase is marginally affected by the rotational speed in the considered speed range.

The decrease of the pressure levels is one of the reason that justifies the trend of the torque in function of the rotational speed (Figure 4.3). In fact, by increasing the rpm, the expander work (i.e. the area of the P-V cycle), which is strictly related to the expander torque without considering the mechanical losses, decreases.

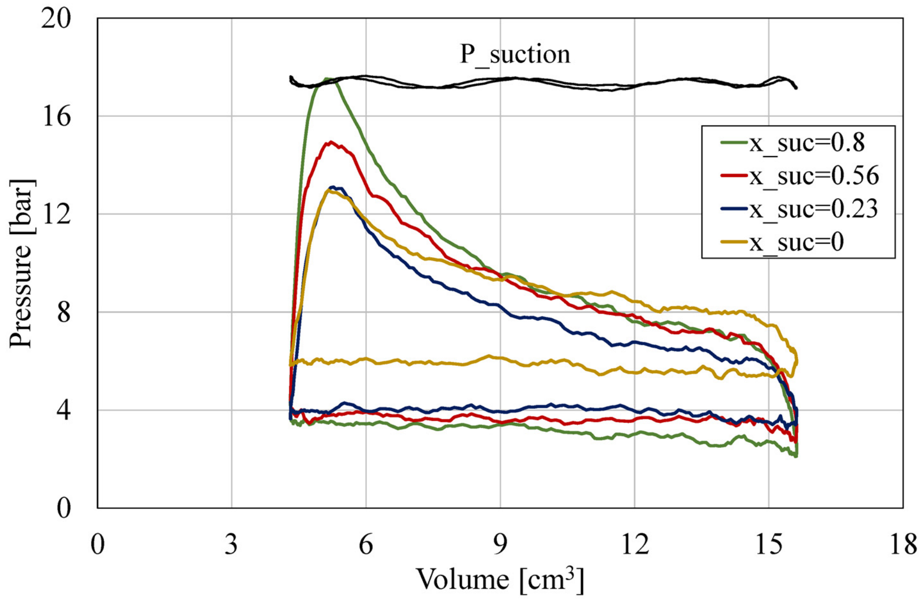

Figure 4.11 - Experimental P-V diagram at 500 rpm for different qualities and a suction temperature of 60 °C.

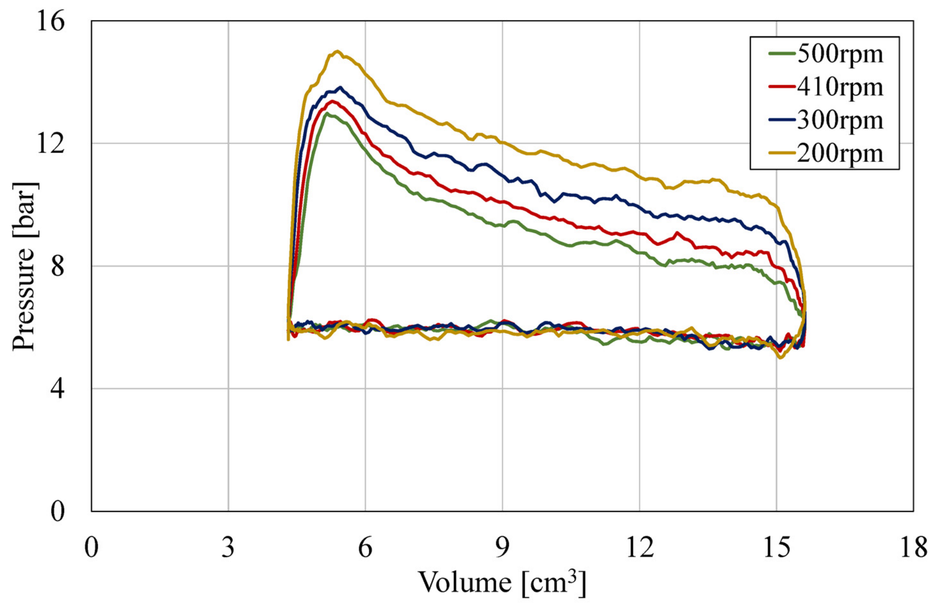

Figure 4.12 - Experimental P-V diagram at different rpm for a saturated liquid and a suction temperature of 60 °C.

In Figure 4.13, the in-cylinder pressure as function of the crank angle for different suction temperature at 400 rpm is depicted. It is apparent that the suction temperature influences the pressure levels only; due to the different suction pressure and the small variation of the expansion ratio, which depends principally on the quality, the discharge pressure changes. Moreover, even though the slope of the in-cylinder pressure during the expansion phase is less influenced by the suction temperature than the quality, the pressure drop, in this phase, is slightly higher by increasing the suction temperature. Consequently, the expansion work increases by increasing the suction temperature leading to higher power output.

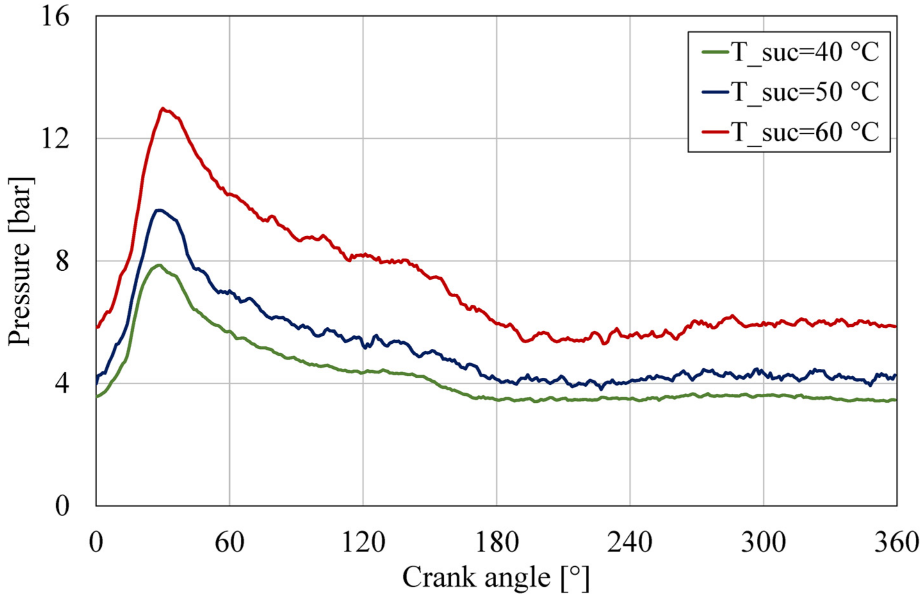

Figure 4.13 - Experimental P-V diagram at different suction temperatures for a saturated liquid and 400 rpm.

It is worth pointing out that, in all the tests at different working conditions, the under expansion is registered, as shown by the pressure at the end of the expansion phase (i.e. when the discharge valve opens) that is always higher than the discharge pressure. Consequently, part of the pressure drop is lost as an isenthalpic expansion without producing expansion work. This behavior of the fluid inside the cylinder is due to the lower volumetric expansion ratio than the required one. A correct design of the volumetric machine, working with a certain refrigerating fluid, is needed so as to exploit the expansion work as much as possible. This issue can be solved by two solutions:

1) The expander might be redesigned in order to increase the volumetric expansion ratio (i.e. when both valves are closed). The main issue that influences this ratio is related to the dead volume, which is principally constituted by the intake duct between the distribution system and the cylinder. A reduction of the dead volume or an increase of the displacement would increase the expansion ratio of the expander.
2) A refrigerant with a lower required volumetric expansion ratio could be tested. Among the refrigerants, R134a has very high required expansion ratio that it is difficult to reach in volumetric machines. By using refrigerants with properties more suitable to the current used expander, the expansion work would increase, as well as the power output of the expander.

In addition to the volumetric ratio, also the mechanical losses and the leakages are critical issues in the use of the expander in substitution of a throttling valve in a vapor compression cycle, as it will be explained in the next chapters in more detail.

4.2 Experimental tests with CO_2

In order to evaluate the influence of the fluid properties on the expander performance, the machine was tested in a vapor compression cycle working with a different fluid from R134a. The experimental results with R134a showed that one of the critical issues that influences negatively the performance of the expander is related to the high required volumetric ratio when a saturated liquid is expanded. Table 4.3 reports the comparison between the required volumetric expansion ratios by using different refrigerants through isentropic expansion processes. It can be seen that, among the HFC refrigerants, other fluids have properties more suitable to use in volumetric expander than the R134a. By expanding the fluid in saturated liquid condition between the same values of the condenser and the evaporator (i.e. from 50 °C to 5 °C), the required expansion ratio of R410A is lower than half of the ratio required by R134a. Consequently, the expansion work produced by the current expander should be strongly higher than the results obtained previously. In addition, the table shows that the volumetric expansion ratios of HFCs are at least three times larger than the CO_2 transcritical cycle that, on the other hand, works with higher pressure levels. For this reason, it is geometrical convenient to test a volumetric expander for CO_2 systems that satisfies small built in volumetric ratio. Moreover, as seen from the wider literature on this application, the interest of using an expander in CO_2 system is justified by the lower COP of the throttling cycle due to the higher pressures. For this reason, the expander was tested also in a refrigeration cycle working with CO_2 in order to evaluate its performance and the behavior of the fluid inside the cylinders. The experimental activity was carried out at the multipurpose test rig in the Department of Industrial Engineering of the University of Florence.

Table 4.3 - Comparison of volumetric expansion ratios between different refrigerants.

Refrigerants	Condensation pressure [bar]	Evaporation pressure [bar]	Volumetric expansion ratio
R134a	13.18	3.49	20.19
R407C	22.16	6.66	12.49
R404A	23.11	7.12	10.34
R410A	30.71	9.36	8.18
CO_2	100	41.77	2.47

4.2.1 CO_2 refrigeration cycle

The test rig with CO_2 was designed in order to allow flexible connections of all of its components, so that many cycle configurations can be reproduced [37]. The main advantage is the possibility to test different components by only substituting them where it is necessary without modify the configuration of the cycle. All the components have be arranged to as to minimize the space and to ensure accessibility of use, as shown in Figure 4.14.

The test rig consists of a refrigerant loop designed to withstand the high pressures needed for operation with CO_2 (up to 140 bar), which is provided with the required thermal and cooling loads by a thermal load management system operating with water as secondary fluid.

Figure 4.14 - Picture of the refrigeration cycle with CO_2.

To test the expander, a traditional vapor compression layout was used (Figure 4.15). After compression (unit provided by DORIN), the fluid flows through an oil separator and enters the gas cooler. According to the most common designs, a gravity separation layout has been adopted to obtain a good compromise between effectiveness and cost. The oil separator consists of a receiver in which the mixture rich in oil is injected on the bottom, and the lighter phase is extracted from the top. The low speed of the descending gas causes most of the oil droplets to fall to the bottom, where the oil is collected by a piping system controlled by electronic valves and levels sensors installed on the compressor. The gas cooler is made by four identical multitube-in-tube heat exchangers, two of them connected in parallel and the remaining in series in order to partially adapt the flow section to the density change during cooling. The cooled refrigerant from gas cooler outlet can flow to both the expansion valve and the expander, in a similar way to the test rig operating with R134a; two needle valves upstream and downstream the expander were arranged to regulate the inlet and outlet conditions. After the expansion, the fluid enters an intermediate pressure receiver (flash tank) that works as gravity separator and, in the studied configuration, has the function to create a large buffer volume so that to allow to separately control both the evaporating and the gas cooling pressures. Finally, the fluid goes to the evaporator consisting of two multitube-in-tube heat exchangers connected in parallel. Contrary to the condenser, in this case the evaporating fluid flows in the minichannels while the water fills the external shell, keeping a counter flow arrangement.

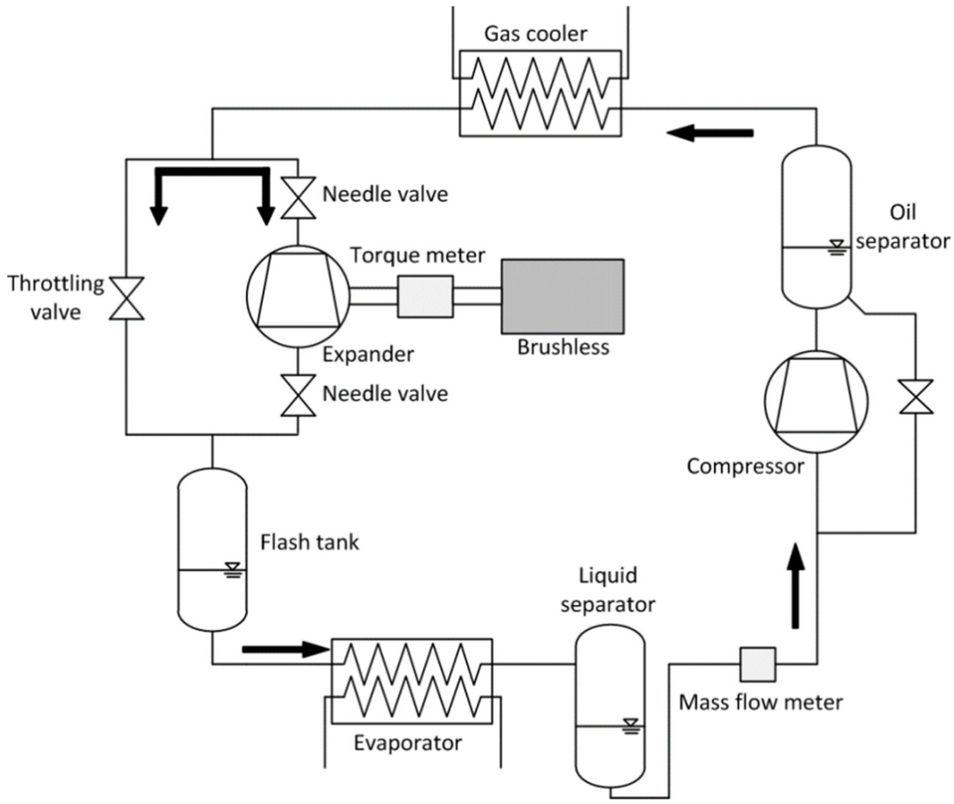

Figure 4.15 - Layout of the test rig with expander working with CO_2.

The facility was designed to allow the automatic acquisition of relevant data from several measurement points. Pressures are sensed by an array of piezoelectric transducers (Wika, ±0.25% FSO) with a FSO from 60 to 160 bar, depending on the measurement points. Temperatures are measured by means of T-type thermocouples. The mass flow rates are measured after the evaporator by a Yokogawa Coriolis meter (model RCCT-34, Accuracy: ≤0.55% of measured mass flow rate). A developed data acquisition software in the LabVIEW environment was used to manage voltage and current signals from the sensors acquired by a multifunction switch Agilent Technologies, which is equipped with an A/D input module featuring 40 channels.

Due to the higher pressure levels reached compared to the R134a system, in this test rig working with CO_2, dynamic pressure sensors with a FSO of 140 bar were arranged on the expander. In Table 4.4, the instruments that were substituted in this test rig in respect to the measurement instruments used to characterize the expander with R134a as working fluid (Table 4.2) are listed.

Table 4.4 - Measurements instruments substituted in the CO_2 test rig from the R134a system.

Equipment	Measurement range	Accuracy
Pressure transducer	0-140 bar	±0.1% FSO
Mass flow meter	0-3000 kg h^{-1}	±0.55% MV

The thermal load to the gas cooler and the evaporator is provided by a water circuit. The cooling system was designed to allow the widest possible temperature ranges of the return water to gas cooler and evaporator without using additional refrigerating machines or burners. The system consists of three water loops, thermally connected by plate heat exchangers (Figure 4.16). This loop is connected to the "hot loop", which exchanges heat with the gas cooler by the heat exchanger HX2. The extra heat is removed by the cooling water loop through the heat exchanger HX1. This loop insists on a 5 m^3 water tank (WT), which is used as a heat sink for the whole system.

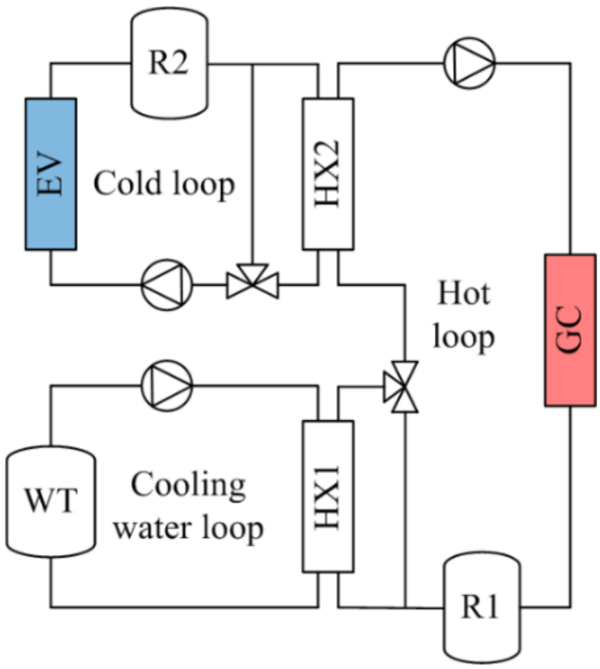

Figure 4.16 - Layout of the thermal load management of the CO_2 system.

4.2.2 Experimental results with CO_2

The first tests of the expander in a CO_2 refrigerating cycle were carried with an inlet temperature and pressure of 30 °C and 75 bar respectively, at different rotational speed. Immediately, it was observed that the expander did not produce torque and, consequently, for each rotational speed the expander was moved by the brushless motor. Compared to the tests with R134a, in this case the mechanical losses dramatically increase and are higher than the indicated power. In Figure 4.17 it can be noticed that both the indicated power and the organic power increase with the rotational speed; while the increase of the indicated power is less steep at higher rpm due to the worsening of the volumetric efficiency, the increase of the organic power, which is caused by the frictional losses, is almost linear with the rpm.

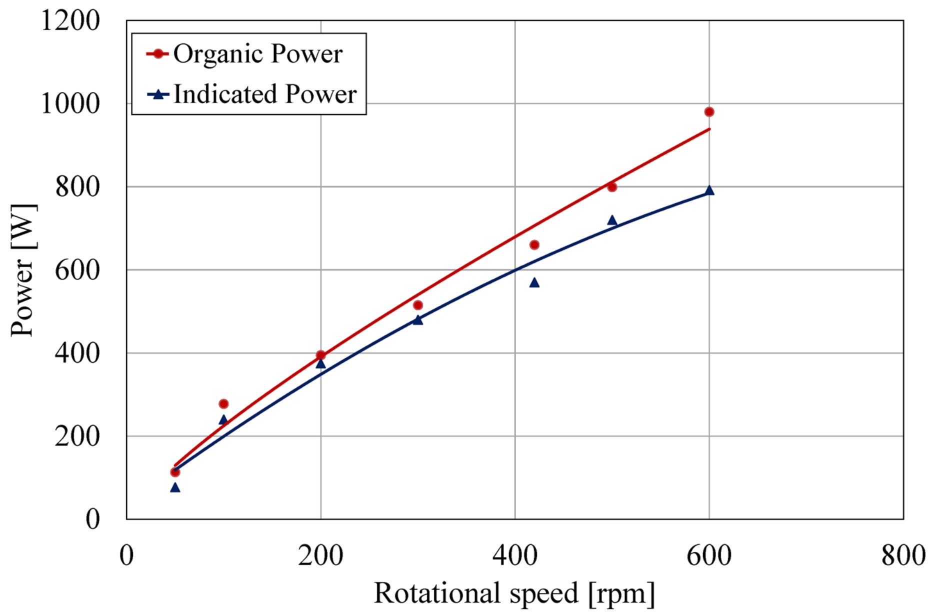

Figure 4.17 - Indicated and organic power with CO_2 at different rotational speed.

However, the indicated cycles show an interesting potential of the expander when used with CO_2, as shown by the “indicated” isentropic efficiency reported in Figure 4.18. Its value increases with the rotational speed, in an analogous way of the indicated power, and reaches a maximum value of 60%.

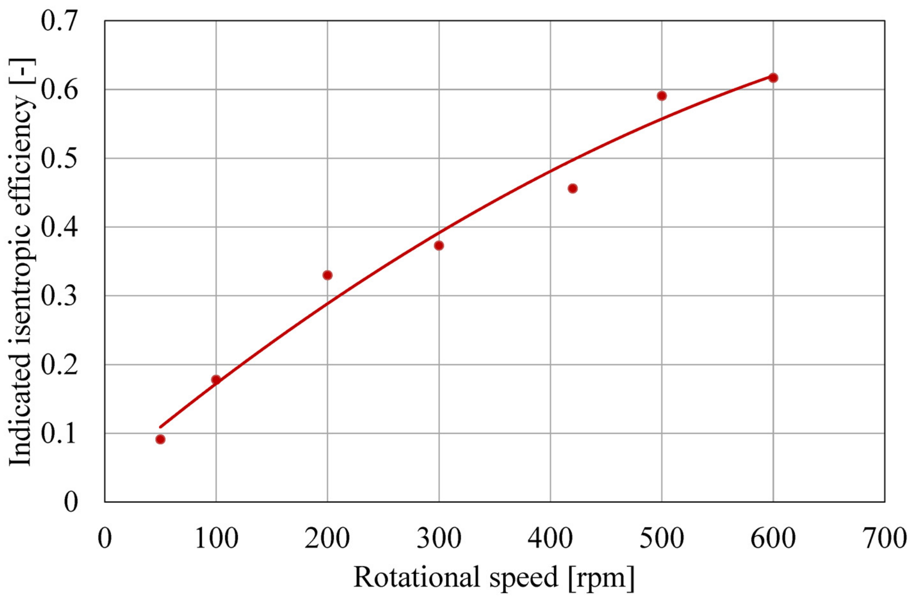

Figure 4.18 - Indicated isentropic efficiency as a function of the rotational speed.

After an assessment of the expander design, it was observed that the main sources of the mechanical losses came from the axial stresses inside the machine. As explained in Chapter 2, the inner part of the expander is linked to the discharge side so that to vent the leakages inside the expander; therefore, the pressure in the inner part of the machine is equal to the discharge pressure that causes an axial force on the shaft that, on the other side, is linked to the ambient pressure (Figure 4.19). For this reason, an axial load on the shaft and the bearings occur towards the shaft outlet. The first tested configuration of the expander was equipped by cylindrical roller bearings, which are not suitable to withstand high axial force on the shaft. The strong increase of the mechanical losses when the expander is used with CO_2 instead of R134a is due to the higher values of the discharge pressure reached during the tests (i.e. from about 5 to 45 bar), which lead to higher axial loads on the shaft and the bearings.

Nevertheless, the high potential demonstrated by the indicated cycles has meant that it was worth carrying out other tests with other bearings on the shaft in order to reduce drastically the mechanical losses and to obtain better performance. Therefore, the inner part of the expander was slightly modified to allow the housing of tapered roller bearings as replacement of the cylindrical roller bearings in order to withstand high axial loads on the shaft. Thus, it was possible to carry out further experimental tests on the same CO_2

refrigerating cycle by using the modified expander with the substituted bearings.

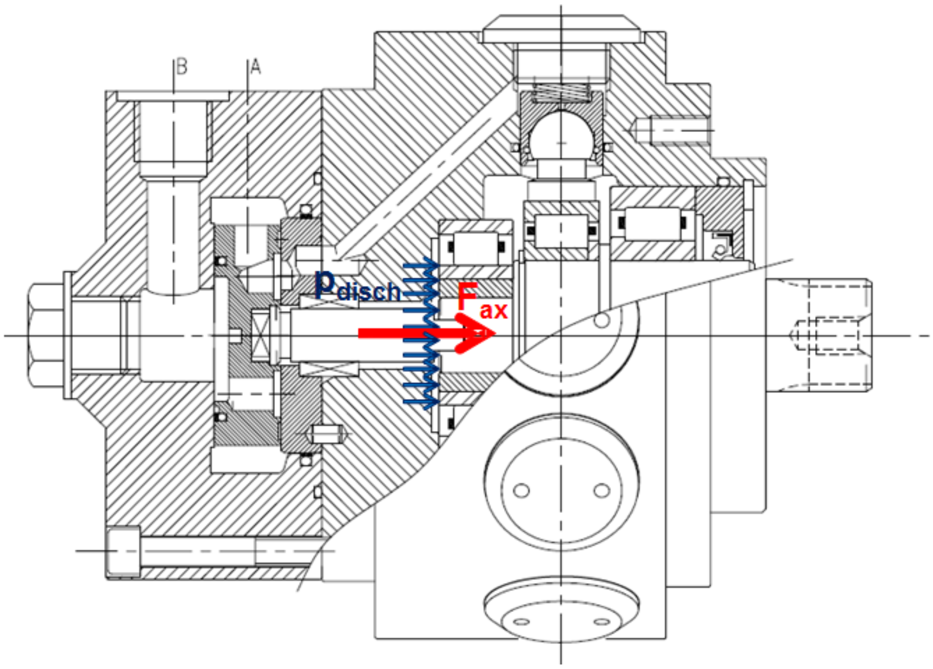

Figure 4.19 - Axial load on the first configuration of the expander.

4.2.3 Experimental tests with the modified expander

The performance of the expander, after replacing the bearings, were evaluated in supercritical conditions in the range between 300 and 1000 rpm. The speed range was chosen as a result of preliminary tests that showed a maximum power around 600-700 rpm. In addition, the preliminary tests showed that over 1000 rpm the expander did not produce any torque. Furthermore, by considering that the expander will be connected to an electric generator, rotational speeds below 300 rpm were dimed to be too low for having a good efficiency of the electric machine. The experimental conditions are listed in Table 4.5.

Table 4.5 - Experimental thermodynamic conditions with CO_2.

Parameter	Value
Gas cooler pressure (bar)	81.8
Gas cooler temperature (°C)	34.2
Evaporation pressure (bar)	49.5-51

At a first glance, it was observed the improvement of the performance by replacing the cylindrical roller bearings with the tapered ones. In fact, in the tested speed range, the power output is always positive due to the reduction of the frictional losses. Figure 4.20 shows the trend of the power output, the indicated power and the organic power at different rotational speed. The power produced by the expander reaches the maximum value of 316 W at 700 rpm. By comparing the results obtained with both versions of the expander, the modification of the bearings led to a reduction of the frictional losses up to almost 400 W. This is a very important result, since it shows that the substitution of the bearings is moving towards the right direction of increasing expander's efficiency. By increasing the rotational speed over the optimizing value, the power output decreases due to both the worsening of the volumetric efficiency and the increase of the frictional losses. Over a rotational speed of 1000 rpm, the organic power exceeds the indicated one and the torque produced by the expander is negative (i.e. the brushless acts as motor).

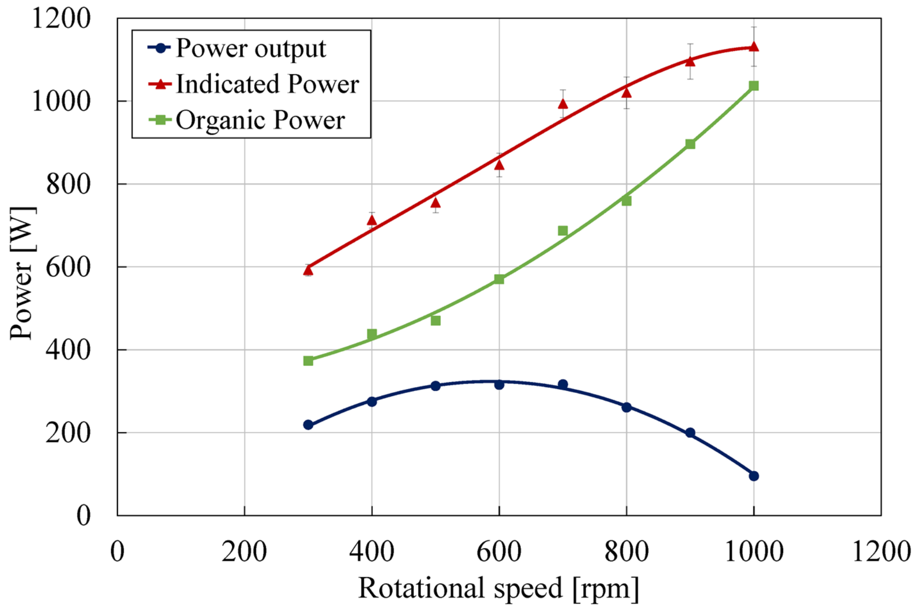

Figure 4.20 - Measured, indicated and organic power versus RPMs.

Due to the higher values of the measured power obtained in these tests compared to the values obtained with R134a, the mechanical efficiency is greater than the value with the tests with R134a at each rotational speed (Figure 4.21). However, the trend shows that, in spite of the arrangement of the tapered roller bearings on the shaft, the impact of the mechanical losses on the performance with CO_2 are still high, especially at high rotational speed.

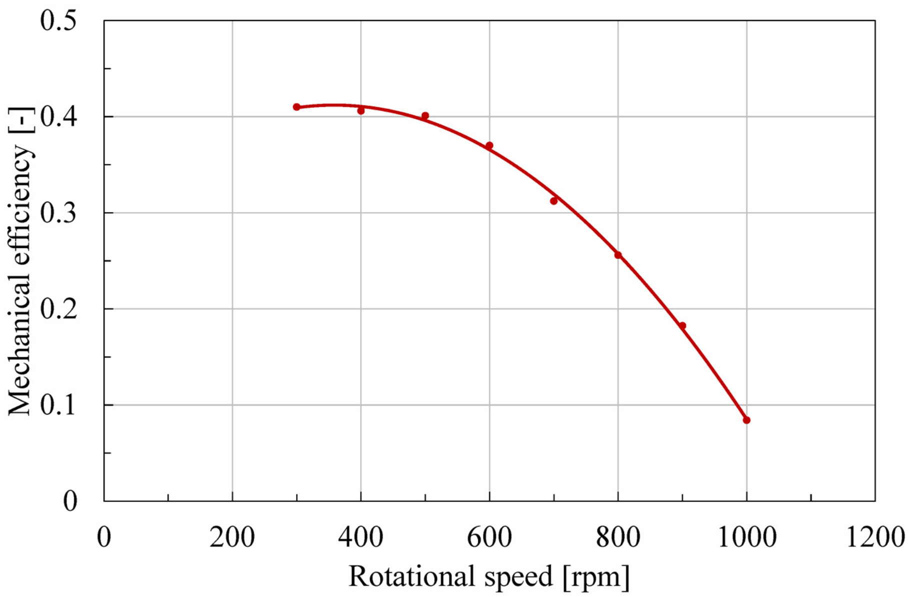

Figure 4.21 - Mechanical efficiency versus rpm.

Figure 4.22 shows the mass flow rate and the volumetric efficiency as function of rotational speed. The trends are very similar to the trends obtained by the tests with R134a. The mass flow rate increases slightly at higher rotational speed because of the more displacement per unit time and, consequently, the volumetric efficiency decreases. The decrease of the volumetric efficiency at higher rotational speed is justified mainly by the reduction of the time available for the suction phase. In addition, also in this case, by considering the suction volumetric efficiency, the values would be higher than one mainly due to the high leakages that have still a strong impact.

In order to evaluate the feasibility of this solution working with CO_2, the isentropic efficiency was evaluated at different rotational speeds with the measured power and the indicated power (Figure 4.23); the value of the indicated isentropic efficiency, as seen previously by the indicated power, shows that there is still room for improvement. The difference between these efficiencies is due to the high mechanical losses. Moreover, the expected isentropic efficiency was calculated by considering a mechanical efficiency of 0.65 that represents a reasonable value according to other studies on a radial piston machine. The expander isentropic efficiency achieves a maximum value of 19%, whereas the isentropic indicated efficiency and the expected isentropic efficiency reach levels of

66% and 41% respectively, showing the promising potential of this solution. It is worth noting that the isentropic efficiency is negatively influenced also by the leakages, so it can be further improved by the reduction of the leakages.

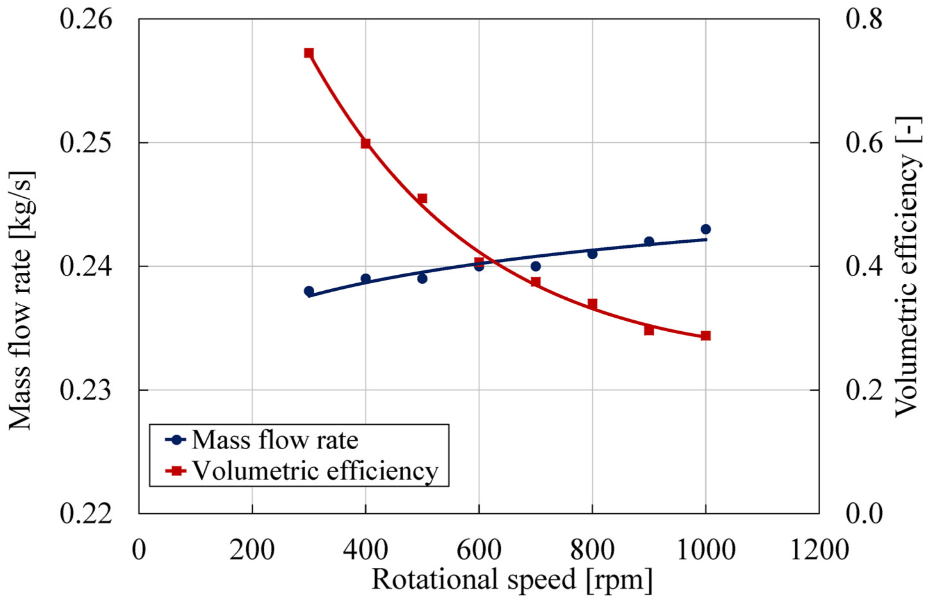

Figure 4.22 - Mass flow rate and volumetric efficiency versus RPMs.

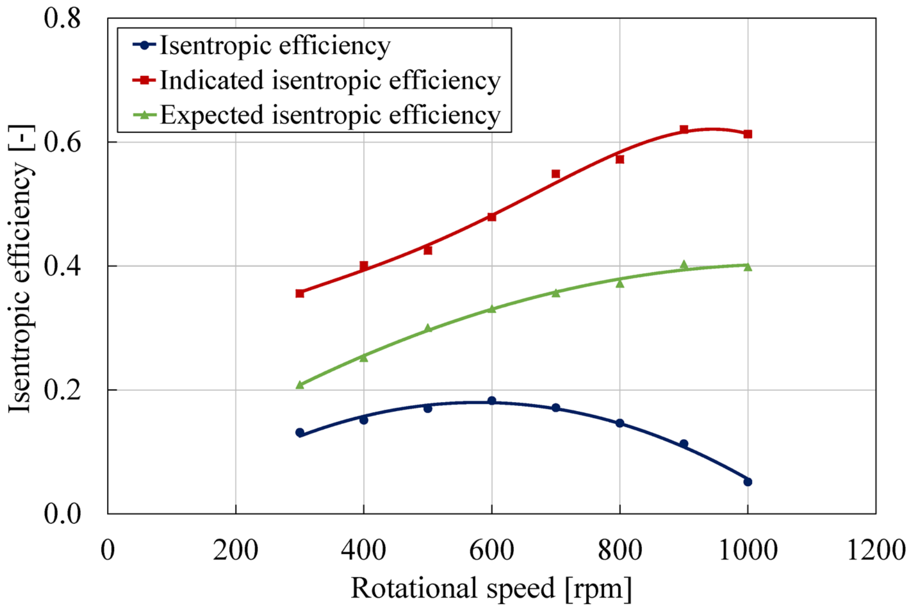

Figure 4.23 - Measured, expected and indicated isentropic efficiencies versus RPMs.

Finally, the COP improvement potential of the refrigeration cycle with the adoption of the expander replacing the throttling valve can be calculated. Figure 4.24 shows the trends of the COP improvements obtained with the measured, the expected and the indicated powers. Actually, the COP improvement referred to the measured isentropic efficiency shows a maximum of 7.4%. The potential improvement of COP with the above mentioned reasonable reduction of friction would be greater and achieve maximum values of 20.5% and 34.5% respectively for the expected and the indicated power.

These values are much higher than the results obtained when working with R134a. The improvement of the COP is stronger when the expander is used in a CO_2 refrigerating cycle for two main reasons:

- The power produced by the expander is higher due to the greater values of the suction pressure;
- The COP of the simple throttle cycle is lower for CO2 systems in respect to the HFC ones.

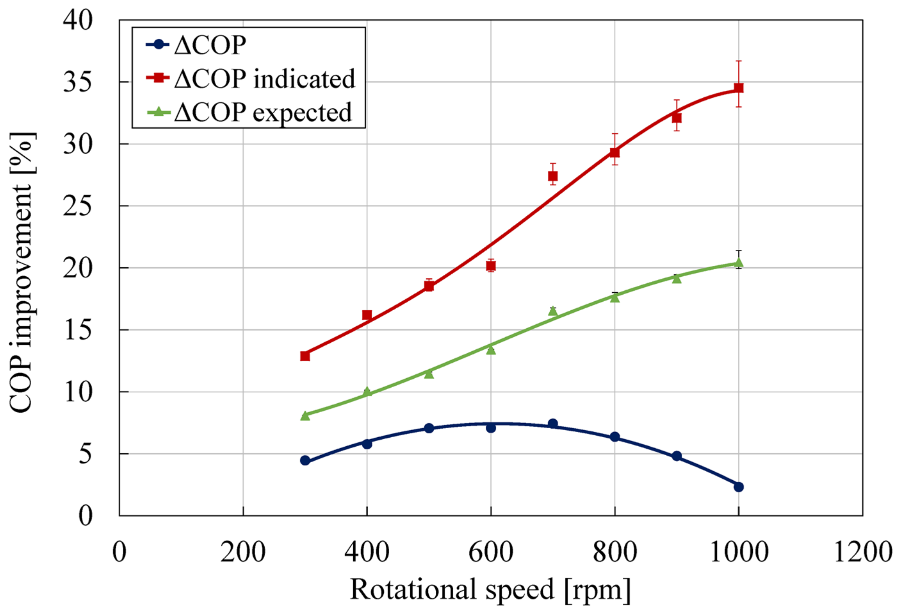

Figure 4.24 - System COP improvement with expander.

4.2.4 Indicated cycles with CO_2

The very interesting result of efficiency improvement can be explained with the indicated cycles obtained during the tests. Figure 4.25 shows the difference between the indicated cycles, averaged in the three instrumented cylinders, obtained at 300 rpm and 900 rpm, so that to analyze the influence of the rotational speed on the thermodynamic cycle. During the suction phase, the in-cylinder pressure increases with a different slope. When the expander rotates faster, the same crank angle is swept in less time and the peak pressure is obtained at higher displacement. However, the peak pressure inside the cylinders equals the suction pressure in all tests, even at high rpm. This behavior shows the better filling of the expander obtained when using CO_2 that is one of the main reason that leads to the improvement of the expander performance compared to the tests with R134a. On the other hand, the increase of the rotational speed leads to the shifting of the matching between the expander and the compressor to slightly higher mass flow rate and lower pressure ratios. Therefore, the discharge pressure and, consequently, the in-cylinder pressures reached during the discharge phase increase. In addition, at the end of the expansion with a rotational speed of 300 rpm only a small part of the expansion is lost due to the under expansion. At high rpm, an over expansion below the discharge pressure is registered. The different slope of the expansion phase is due to the worst filling of the cylinder at high rpm that reduces the in-cylinder mass during the expansion phase. For this reason, the fluid density, as well as the in-cylinder pressure, decreases more rapidly at 900 rpm compared to 300 rpm.

The behavior of the fluid inside the cylinder is completely different when the expander works with CO_2 or R134a especially in the expansion phase. In fact, the lower volumetric ratio required by the CO_2 when expanding from the suction to the discharge pressure leads to a greater pressure drop during the expansion phase and the expansion work has a higher impact on the power produced. It follows that the expansion work lost at the discharge valve opening before the TDC is very small at lower rotational speeds, whereas it is null at higher rpm, where the over expansion occurs.

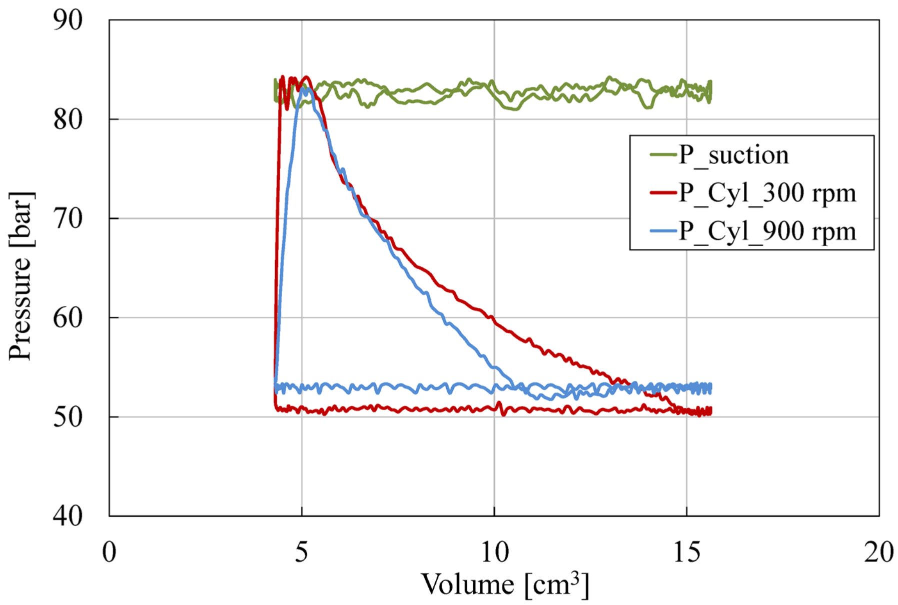

Figure 4.25 - P-V cycles with the CO_2 as working fluid.

In conclusion, the thermodynamic cycle shows a higher potential of the expander when used in a vapor compression cycle as replacement of the throttling valve, as shown by the indicated powers. Thanks to the lower required volumetric ratio of the CO_2, the performance is strongly greater when the expander works in a CO_2 system compared to the HFC cycles. However, all the tests demonstrate that the performance of the expander can be further improved by reducing the leakages and the mechanical losses, which have a strong influence on the expander efficiencies. An improvement of the expander design is needed to reduce these losses. As seen in the next chapter, a detailed evaluation of these sources of loss is necessary to evaluate the critical aspect of the original version of the machine.

5 Assessment of the expander design

The tests performed with both R134a and CO_2 as working fluid showed an interesting potential of the expader when used in a vapor compression cycle in substitution of a throttling valve. The results obtained from the indicated cycles demonstrated that the indicated isentropic efficiency reaches very interesting values leading to a considerable COP improvement of the systems where the expander runs. The efficiency improvement is higher when the expander works with CO_2 instead of R134a because of the lower COP of the simple throttle cycle and the better behavior of the fluid inside the cylinder. However, the measured useful shaft power output of the expander highlighted that the performance is negatively affected by the following issues:

- the required volumetric expansion ratio of the fluids that, in case of R134a, is higher than the built-in volumetric ratio and, consequently, allowed low expansion work;
- the leakages through the components inside the expander that reduce the expander efficiency;
- the unavoidable mechanical losses inside the expander that decrease the power produced by the machine.

Whereas the first issue influences the behavior if the fluid inside the cylinder, the others affect the performance by increasing the elaborated mass flow rate and reducing the power produced by the expander. These loss sources are related to the original application of the tested machine, which must work with a different type of fluid (i.e. oil instead of refrigerants) that has different properties, especially greater viscosity, and reaches high values of pressure (i.e. up to 300 bar). In order to obtain better performance of the expander, all these issues have to be considered. Therefore, a detailed analysis of each aspect was performed to assess the influence of the expander design on its performance.

5.1 Assessment of the built-in volumetric ratio

As seen in the previous chapter, R134a is one of the fluids that requires larger volumetric expansion ratios to obtain an isentropic expansion between the condenser and the evaporator pressures when starting from the saturated liquid state at the condenser outlet. Figure 5.1 shows the theoretical required volumetric expansion ratio as a function of the saturation temperatures T_{cond} and T_{eva}. Its value is always much higher than the built-in volumetric expansion that is equal to 2.4. When the expander works with a different fluid, such as R410A, the required volumetric ratio is reduced and is closer to the built-in value. However, the indicated cycles obtained with R134a showed that the behavior of the fluid inside the cylinder leads to reasonable values of indicated efficiencies. In fact, the values reported in Figure 5.1a are much higher than the real values required by the fluid inside the cylinder at the beginning of the expansion due to the pressure losses through the inlet duct and the finite opening time of the suction valve; for these reasons, the fluid quality when the suction valve closes is higher than 0 leading to lower required volumetric ratios. Nevertheless, the in-cylinder pressure at the end of the expansion phase is higher than the discharge pressure showing that the under expansion is registered and part of the pressure drop is lost as an isenthalpic expansion. For this reason, an improvement of the expander design that leads to an increase of the built-in volumetric ratio can be considered in order to obtain better expander performance.

The increase of the expansion volumetric ratio can be done by three modification of the expander redesign:

- the displacement volume can be increased by enhancing the bore and the stroke of the piston. These modifications cause an increase of the mass flow rate elaborated by the machine that could be too high for the considered refrigerating/heating systems;

- the dead volume can be reduced mainly by decreasing the dimension of the intake duct, above all its diameter. However, the reduction of the diameter would lead to an increase of the pressure losses during the suction/discharge phase that causes a worsening of the volumetric efficiency, a reduction of the peak in-cylinder pressure and an increase of the in-cylinder pressure during the discharge phase;
- the valve timing can be modified. The suction valve can be closed before the actual value in order to begin the expansion phase at a lower cylinder volume; also in this case, the volumetric efficiency would worsen due to the lower time available to the suction phase. In addition, the discharge valve can open later than the actual value leading, on the other hand, to a worst exploitation of the free discharge before the BDC.

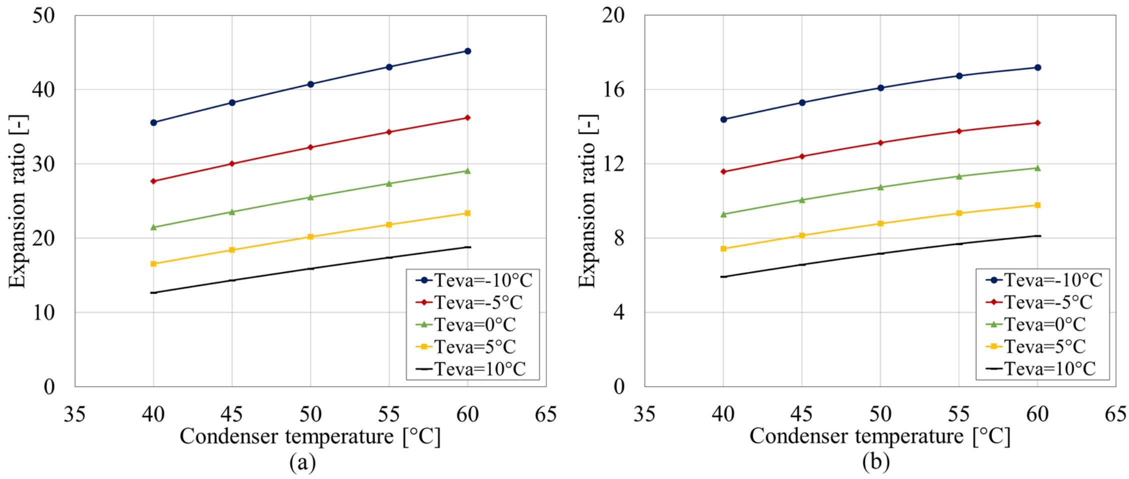

Figure 5.1 - Theoretical required volumetric expansion ratio vs. condensation and evaporation temperatures for R134a (a) and R410A (b).

Therefore, a proper design can be done by evaluating compromises between the different issues of the expander; in particular, the reduction of the dead volume would cause an increase of the pressure losses during the suction/discharge phases. In addition, it must be remarked that by using the expander with CO_2, the fluid behavior is more efficient, as shown by the over expansion that is registered at high rotational speed. Consequently, the proper volumetric ratio has to be chosen depending on the working fluid. The redesign of the volumetric ratio of the actual expander is fundamental when it works with HFC refrigerants, especially R134a, whereas the actual cylinder design is suitable with CO_2.

5.2 Assessment of the leakages

In general, the reciprocating machines are characterized by leakages inside them due to the relative movement between the components. The presence of these losses means that the mass flow rate elaborated by the cylinder is lower than the measured one elaborated by the whole cycle. For this reason, part of the mass flow rate bypasses the cylinder without producing work leading to a reduction of the expander efficiency.

In the tested expander, the leakages are present in both the distributor and the cylinder. In particular, there are the following paths for the leakages (Figure 5.2):

- through the rotating plate and the case in the distributor. In spite of the presence of the seal between these components, the pressurized fluid coming from the suction side goes directly to the discharge side, at the lower pressure, without passing through the hole in the rotating plate;
- through the rotating and the stationary plates. In this case, the seal is assured by the grooves present on the side of stationary plate in contact with the rotating one. Nevertheless, after passing through the suction hole in the rotating plate, the fluid could go directly to the discharge holes and, successively, to the low pressure side;
- through the piston and the cylinder wall. Even though there is a seal between the piston and the cylinder, part of the fluid inside the cylinder goes to the inner part of the machine, which is linked to the discharge side, as explained in Chapter 2.

In order to evaluate the main source of the leakages between the paths in the distributor and the cylinder, the two following tests were performed in the same working conditions with a null rotational speed of the expander in the R134a heat pump cycle:

1) test with all ducts opened: in this case, the mass flow rate measured in the cycle took into account the all leakages inside the expander;
2) test with the discharge duct closed so that only the internal part of the expander

is linked to the discharge side; for this reason, only the leakages through the cylinder wall and the piston were measured.

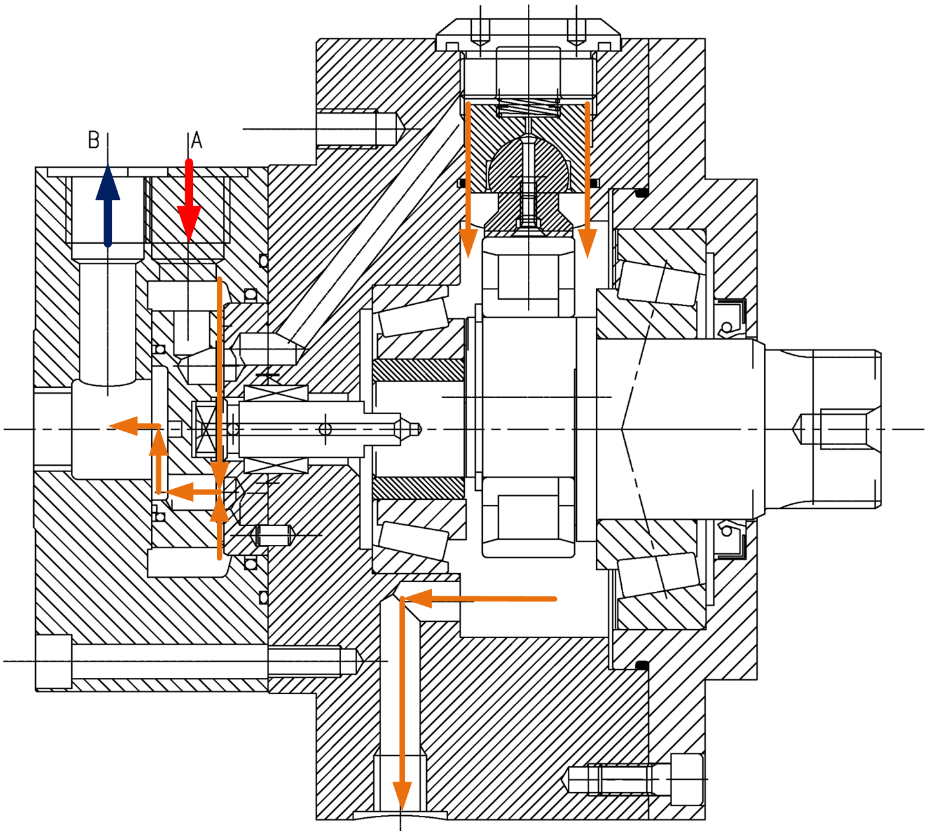

Figure 5.2 - Leakages inside the expander.

The results of these tests are listed in Table 5.1. The boundary conditions are almost the same in order to compare the results. The values demonstrate that the leakages through the cylinder wall are almost the 12% of the total. Therefore, the main issue that influences at most the leakages is related to the paths between the rotating plate and the expander case on one side, and the stationary plate on the other side. The main issue of the current seal is the need of a relatively high preload to be effective against leakages with liquid/vapor refrigerants. Unfortunately, the presence of this seal leads to a significant friction loss; the higher the preload, the lower the leakages and the greater the friction losses. The proper value of the preload has to be given as a compromise between fluid-dynamic and mechanical losses.

Table 5.1 - Comparison between the tests to measure the sources of leakages.

Tests	Condensation pressure [bar]	Evaporation pressure [bar]	Mass flow rate [kg/s]
Discharge duct opened	18.72	1.82	196.7
Discharge duct closed	18.56	1.79	23.7

The strong influence of the leakages on the expander performance was shown by the results obtained from the tests with the R134a. By considering the effective mass flow rate elaborated by the cylinders (i.e. without leakages), the isentropic efficiency could increase more than twice at lower rotational speed (i.e. 150-200 rpm); its increment is less marked by increasing the rotational speed. Therefore, the reduction of the leakages would lead to a considerable increase of both the expander efficiency and the COP improvement of the cycle where the expander works. Unfortunately, with the current O-rings, the leakages can be reduced only by increasing the preload that, at the same time, leads to an increase of the friction losses.

5.3 Assessment of the mechanical losses

As shown by the comparison between the measured and the indicated power, the mechanical losses due to the friction between the different components inside the expander have a great influence on the performance by reducing its overall efficiency. Mainly, friction occurs on the following parts of the proposed expander (Figure 5.3):

1) Contact between the backside of the rotating plate and the case of the expander.
2) Contact between the front side of the rotating plate and the stationary plate.
3) Contact between the piston and the cylinder wall.
4) Contact between the bottom hemispherical piston surface and the connecting rod.
5) Tapered bearings (between the shaft ant the case).
6) Cylindrical bearing (between the shaft and the piston).
7) Shaft frontal seal.

Several tests were carried out in order to characterize the friction losses of the expander. The tests were conducted without the working fluid, with the expander moved by the electrical motor at different rotational speeds. In order to evaluate the impact of each of the above mentioned friction sources, the single components were progressively removed in order to evaluate their impact. The following cases where investigated in the tests:

1. fully assembled expander with all components;
2. expander without rotating plate;
3. expander without pistons;
4. expander without pistons and rotating plate;
5. expander without pistons, rotating plate and frontal seals.

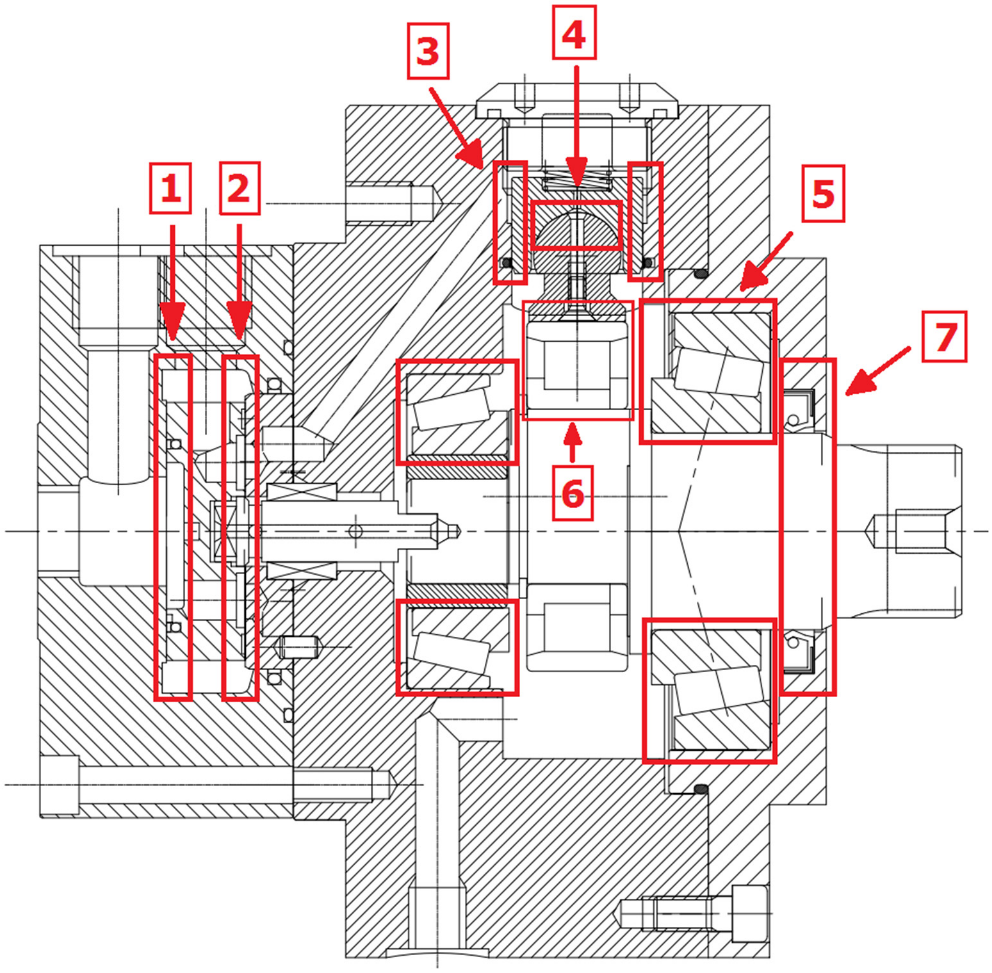

Figure 5.3 - Sources of mechanical losses.

Figure 5.4 shows the values of friction power obtained in the tests. At a first glance, it can be noticed that the power lost due to the frictions by rotating the fully assembled expander at atmospheric conditions is very high in comparison to the indicated power measured in the experimental test. For instance, at 600 rpm the friction power is more than 300 W, whereas, generally, the indicated powers are less than 1 kW, especially in the case of R134a tests. These results demonstrate that the mechanical losses have a great negative influence on the performance. In addition, their values increase with the rotational speed because of the dependence of the friction on the velocity. Obviously, by removing the single components inside the expander, the mechanical losses decrease.

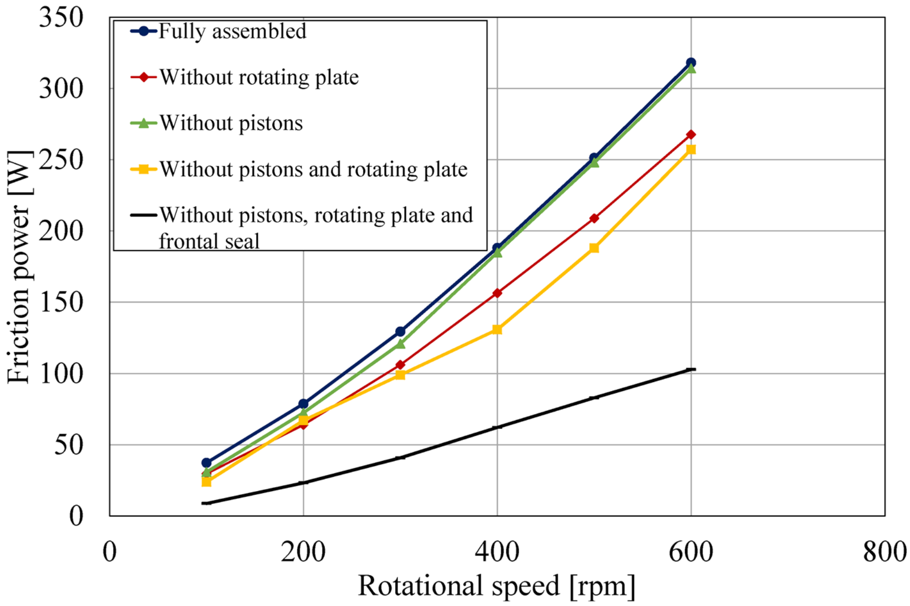

Figure 5.4 - Friction power vs rotational speed.

Figure 5.5 shows the contribution of each component to the friction torque at different rotational speed, as a result of the elaboration of the previous tests. As it is evident, the bearings and the frontal seal are the components mostly affecting the total friction torque. Further, while the contribution of the pistons and the rotating plate to the total friction under atmospheric pressure decreases with the rotational speed, the influence of the bearings and of the frontal seal on total friction torque increases with rpms. The frontal seal is necessary to assure a perfect seal from the inner part of the expander, which is at the discharge pressure, and the ambient. On the other hand, the high preload needed during the assembly of both the frontal seal and the bearings of the expander inevitably leads to significant mechanical losses. In addition, it must be remembered that when the expander works in a vapor compression cycle with a refrigerant, the pressure inside the case causes an axial force on the shaft, which further increases the load on the frontal seal and the bearings and, consequently, the friction losses.

In conclusion, the above-described tests showed that even in absence of a pressurized fluid inside the expander the mechanical losses have a high impact on the expander performance and efficiency. As mentioned in the previous chapters, these results are justified by the original hydraulic design of the machine, which has to withstand pressures up to 300 bar that are much higher than the values of the fluid pressure reached in a heat pump cycle. Therefore, a redesign of the machine is necessary in order to use the most appropriated components to the proposed application. For instance, the size of the shaft and, consequently, the bearings could be reduced so that to reduce the friction losses on these components.

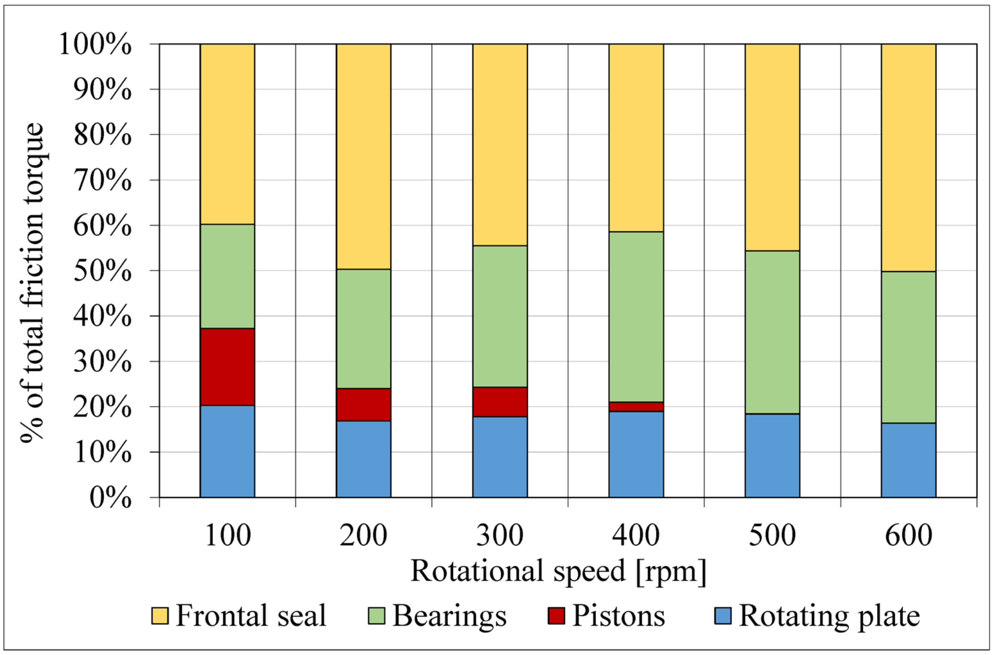

Figure 5.5 - Relative influence of each component on friction losses.

5.4 Redesign of the expander

The negative impact of the in-built volumetric ratio, the leakages and the mechanical losses on the expander performance led to the necessity of a redesign of the expander. For this reason, a new version of the expander was designed and manufactured by maintaining the original concept of the machine. As shown in Figure 5.6, the overall architecture of the expander was retained, whereas the changes concern the size of the components and the type of bearings. Above all, the redesign focused on the reduction of the mechanical losses and the increase of the volumetric ratio to make the expander more suitable for use with HFCs.

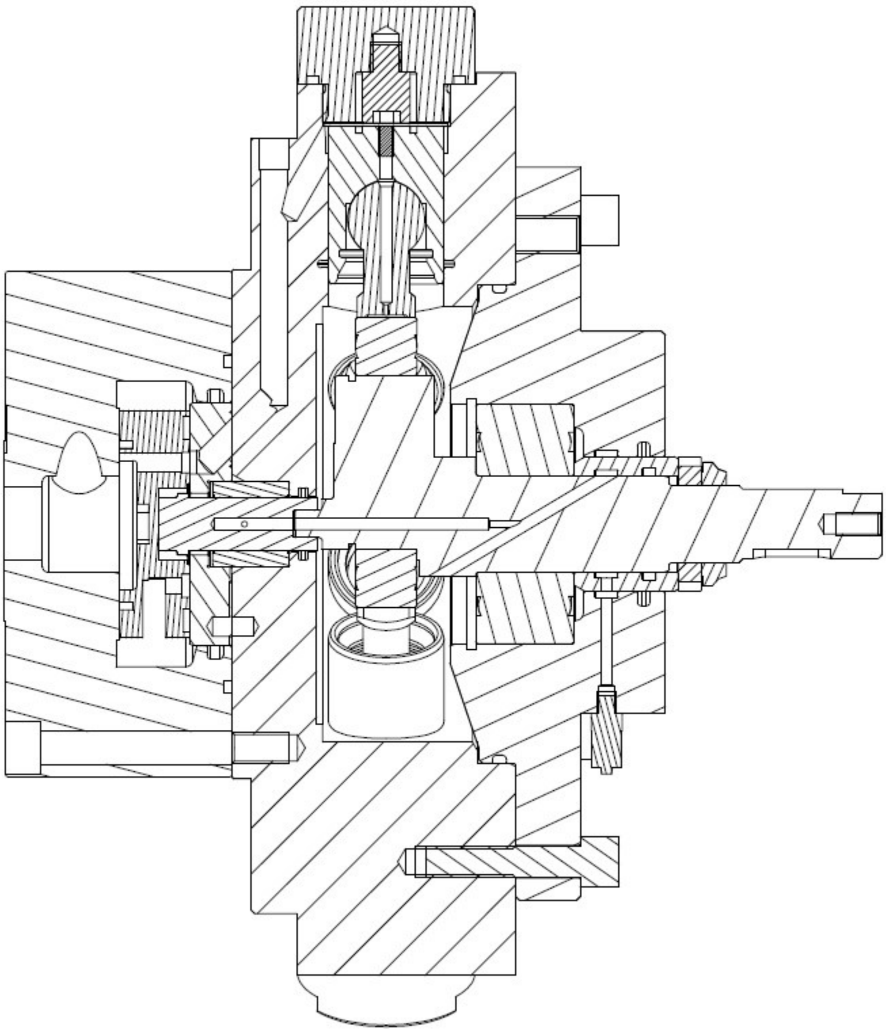

Figure 5.6 - Redesign of the expander.

The eccentricity of the shaft was increased in order to enhance the stroke of the piston and the volumetric expansion ratio. This change led to the need to increase the radial dimension of the case and, consequently, the length of the intake duct that constitutes part of the dead volume. As a compromise, the stroke was increased from 16 to 32 mm so that the displacement of each cylinder was doubled. Moreover, in order to limit the increase of the radial dimension, the number of the pistons was reduced from 9 to 7. The obtained displacement of the expander was enhanced from 102 to 150 cm^3, whereas the expansion ratio was increased more than twice, also considering that the size of the case was reduced axially, as it will be explained later.

In addition to the improvement of the thermodynamic behavior of the cylinders, these changes led also to the reduction of the mechanical losses. In particular, the reduction of the number of pistons has meant that a reduced number of interacting surface are present in the expander and the friction losses due to the contact between the pistons and the cylinder walls were decreased.

Moreover, it must be considered that the shaft and the bearings in the original version of the machine were sized to stand loads up to 300 bar. Considering the pressure of the current application, the size of these components could be reduced to stand load to 80 bar. The reduction of the loads led to another interesting simplification of the design: in addition to the bearing on the eccentric shaft, only a double row angular contact ball bearing was used at the right end of the axis to stand both axial and radial loads. Due to the removal of a tapered bearing, the axial size of the shaft could be reduced. The reduction of the size of the shaft and the replacing of the bearings should lead to a sensible decrease of the mechanical losses. Finally, by considering that the diameter of the shaft at the outlet of the expander was decreased from 40 mm to 18 mm, the diameter of the frontal seal was reduced, thus leading to further lower frictional losses.

As regard the distributor, even though the timing was maintained the same as the previously version, the rotating plate and the case was modified in order to invert the inlet with the outlet. In this way, whereas in the previous version the fluid passed through the holes in the plates radially, in the modified design the fluid enters the plates axially so that to reduce the concentrated pressure losses during the suction phase, that causes a reduction of the peak pressure inside the cylinder and of the expander efficiency. It follows that the pressure losses increase during the discharge phase that are much smaller in comparison to the pressure losses in the suction phase, as seen by the experimental results. Figure 5.7 shows the comparison between the previous version of the expander and that after the redesign.

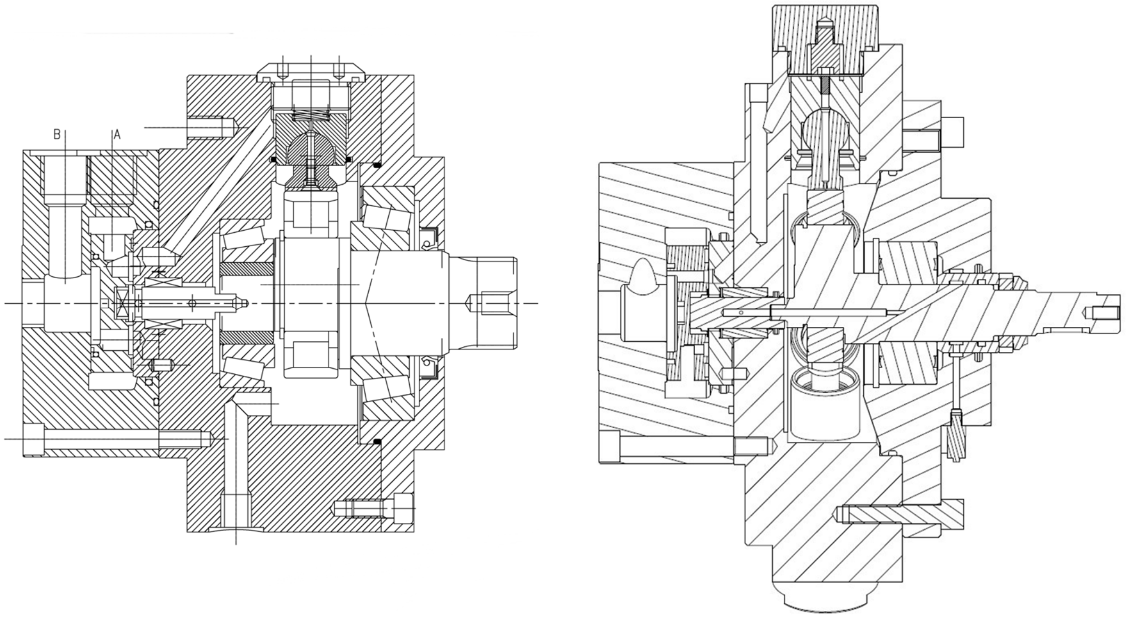

Figure 5.7 - Comparison between the previous version of the expander (left) and that after the redesign (right).

A last important issue in the redesign of the expander is related to the lubrication. In the previous version, the lubrication of the components inside the expander was assured by putting an amount of oil in the bottom drain chamber to be spread by the eccentric rotating shaft and by injecting a small amount of oil in the fluid before the expander. With this method, when the fluid enters the expander, it is unknown the amount of oil in each component. Therefore, in the modified expander it was expected to inject in two different parts of the machine. In particular, a duct in the shaft from the outlet of the expander to the internal part of the case is present to lubricate the bearings and the pistons (Figure 5.8a). Moreover, it was expected to lubricate the plates through a duct from the external part of the case to the distributor (Figure 5.8b), in order to reduce both the friction losses between the rotating and the stationary plates and the leakages through these components.

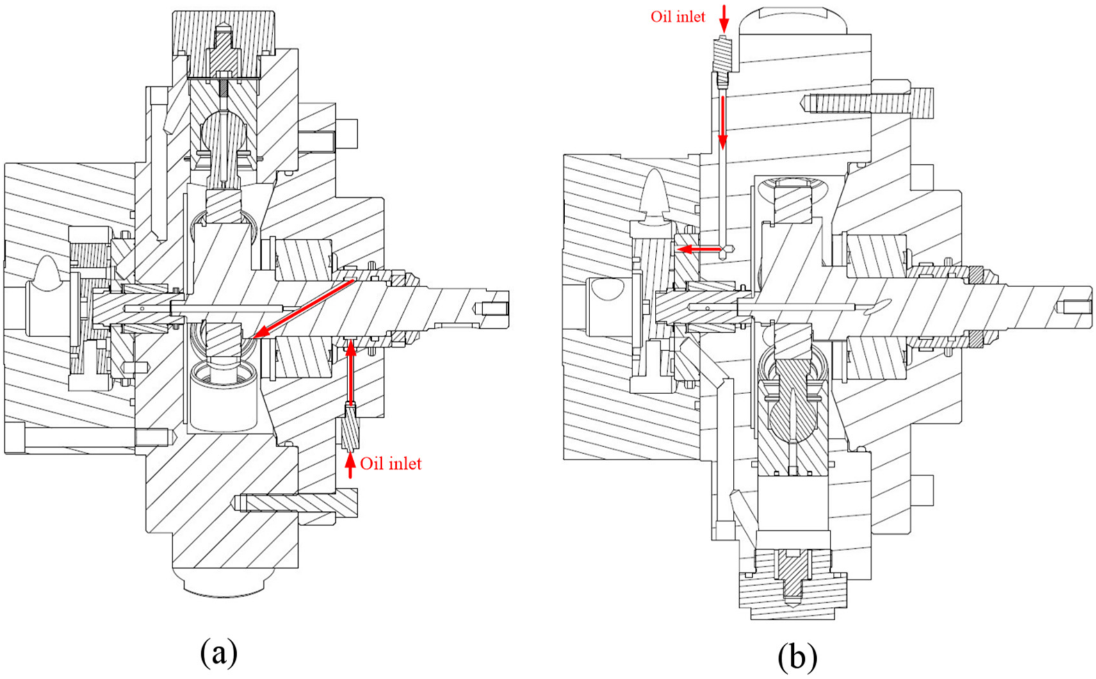

Figure 5.8 - Axial section of the expander with the oil inlets for bearings and piston lubrication (a) and for the the distributor lubrication (b).

These modifications should improve the performance by improving both the thermodynamic performance, due to the enhancement of the expansion ratio, and the mechanical losses. This improvement will be verified by testing the modified expander in a dedicated cycle.

6 Dedicated test rig for testing the modified expander

In order to evaluate the effective improvement of the expander performance after the redesign, a dedicated test rig was developed with the aim to create the desired boundary conditions of the expander. This test rig was designed to improve some critical aspects of the previous tested cycles due to both the difficulty to reach the stability and the high size of the plant. Because of the issue of working with CO_2 related to the high pressure levels that increase drastically the mechanical losses, the interest was focused on testing HFC refrigerants with, on the other hand, a lower required expansion ratio than the R134a. For this reason, the R404A and R410A were tested as working fluids inside the cycle so that to work with a more suitable fluid for the expander, as shown in Table 4.3.

6.1 Hot-gas bypass cycle

In addition to measure the expander performance, the test carried out on the vapor compression cycle with R134a and CO_2 showed problems related to the test rig where the expander works. The main issue concerns the difficulty and the slowness to reach stable conditions of the cycle so that to measure accurately the thermodynamic conditions and the expander performance. Generally, this issue is due to the size of the cycle and the need to regulate the loads on both the condenser and the evaporator. Moreover, the previous tested cycles were too big and included too many components for testing only the proposed expander. For these reasons, a dedicated test rig was designed and developed in order to test only the expander leading to the following advantages:

- Higher velocity and easier to reach the cycle stability
- Smaller size of the cycle
- Smaller number of components
- Lower manufacturing costs

6.1.1 Basic thermodynamic cycle

The developed cycle is a hot-gas bypass loads stand, as shown in Figure 6.1. After the compression from the state point 1 to 2 by the compressor, some fraction of the refrigerant is throttle through a bypass valve to the state point 5 by obtaining a superheated vapor at lower pressure. The remaining refrigerant is condensed to reach the condition of saturated (or subcooled) liquid at the state point 3, and then reduced its pressure by passing through a throttling valve. Finally, the cold two-phase refrigerant is mixed with the hot gas coming from the bypass in order to reach the right thermodynamic conditions at the inlet of the compressor. Figure 6.2 depicts the pressure-enthalpy diagram of the hot-gas bypass cycle.

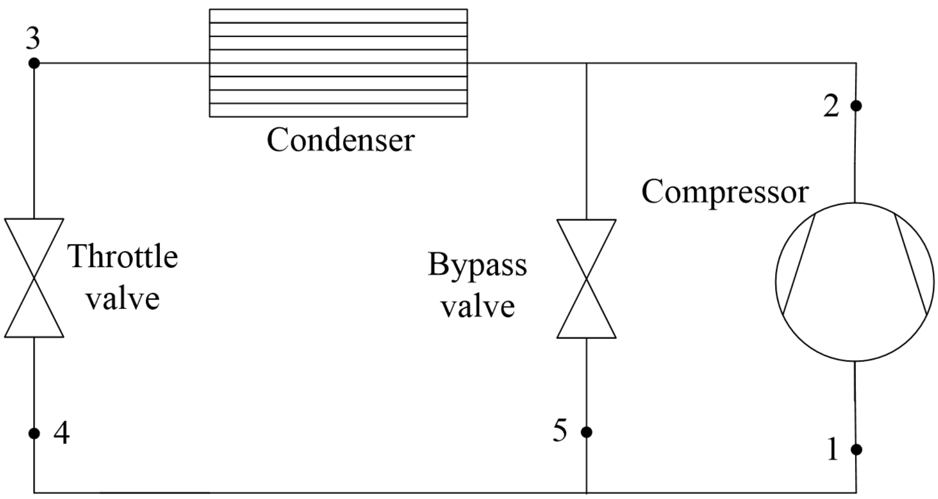

Figure 6.1 - Schematic of the hot gas bypass cycle.

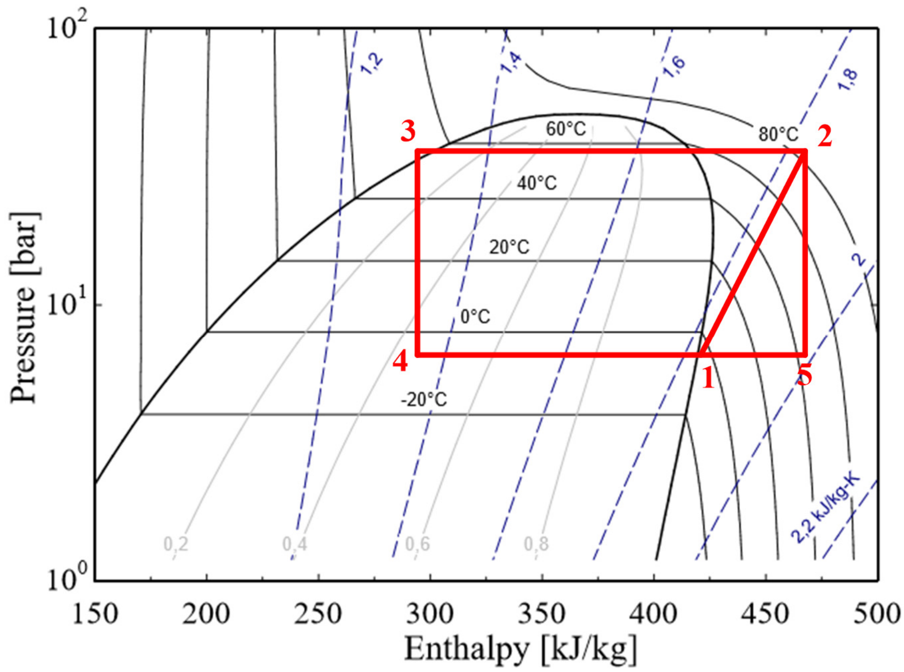

Figure 6.2 - Pressure-enthalpy diagram of the hot-gas bypass cycle.

This type of cycle has been used by other researchers in order to test the performance of the compressor. In addition to the advantages listed previously, by using this cycle a smaller thermal load is requested by the condenser due to the lack of the evaporator load; in fact, the thermal load is equal to the compressor power.

The first description and theoretical analysis on this type of cycle was done by McGovern [38], which demonstrates that it is feasible in principle. Bell et al. [39] tested a hermetic scroll compressor for refrigerant R410A with oil injection in a hot-gas bypass load stand showing that an increase of the overall isentropic efficiency is obtained by injecting oil. Gessler et al. [40] presented a thermodynamic model of a hot gas bypass used to evaluate centrifugal compressor performance. The comparison with the experimental results showed that the model achieves a good agreement within 2.5%. A thermodynamic model analysis of this type of cycle was developed also by Bradshaw [41] to calculate the state points and the relevant performance metrics and to identify some best practices.

Because of the numerous advantages of using this cycle, this idea was used to test the expander that replaces the throttling valve.

6.1.2 Development of the cycle with expander

In the application presented in this work, a hot-gas bypass cycle was designed and developed for testing the expander (Figure 6.3). In a similar way to the tested vapor compression cycles, the expander was arranged in parallel to the throttling valve. In order to design the test rig and provide the diameter size of the piping, a simple thermodynamic analysis was carried out in reference to the diagram in Figure 6.2 by considering that the expansion phase (3-4) was done only by the expander.

From an initial thermodynamic condition (i.e. at the state point 1), the refrigerant is compressed to reach the condition at the state point 2 depending on the compressor isentropic efficiency (i.e. in this case, it is assumed equal to 0.7). Successively, the part of refrigerant that goes to the expander is condensed up to reach the saturated liquid condition, whereas the remaining part reduces its pressure by an isenthalpic expansion of a superheated vapor. At the points of mixing and splitting of the refrigerant (i.e. 1 and 2), the resolution of the continuity and energy equations (Eqs. 6.1-6.2) allows the determination of the mass flow rate in each part of the cycle. It must be considered that, at these state points the heat and work transfers are null.

$$\sum_{inlets} \dot{m}_i - \sum_{outlets} \dot{m}_i = 0 \tag{6.1}$$

$$Q - W + \sum_{inlets} (\dot{m}h)_i - \sum_{outlets} (\dot{m}h)_i = 0 \tag{6.2}$$

It was estimated that the mass elaborated by the compressor is higher than about three times the mass flow rate of the expander, in each thermodynamic working condition. In addition, by considering the same mass flow rate elaborated by the expander during the tests with R134a, the all values of mass flow in the different parts of the plants were calculated in order to determine the size of the components and the piping. By working with R404A in an intermediate working condition through the expander, from 50 °C to 0°C, the power required by the compressor, and consequently the condenser, is almost 25 kW, whereas with R410A the power increases up to 35 kW.

This analysis, as it was reasonable, shows the main drawback of using the hot-gas bypass cycle for testing the expander. Compared to the traditional vapor compression cycle, it is necessary to use an oversized compressor because of the higher mass flow rate elaborated by the compressor than the expander. In particular, a compressor with a required power higher than almost three times in respect to the VCC unit has to be used. Nevertheless, the numerous advantages explained previously mean that the use of the hot gas bypass cycle for testing the expander is convenient due to both the ease of reaching the stability and the less number of components.

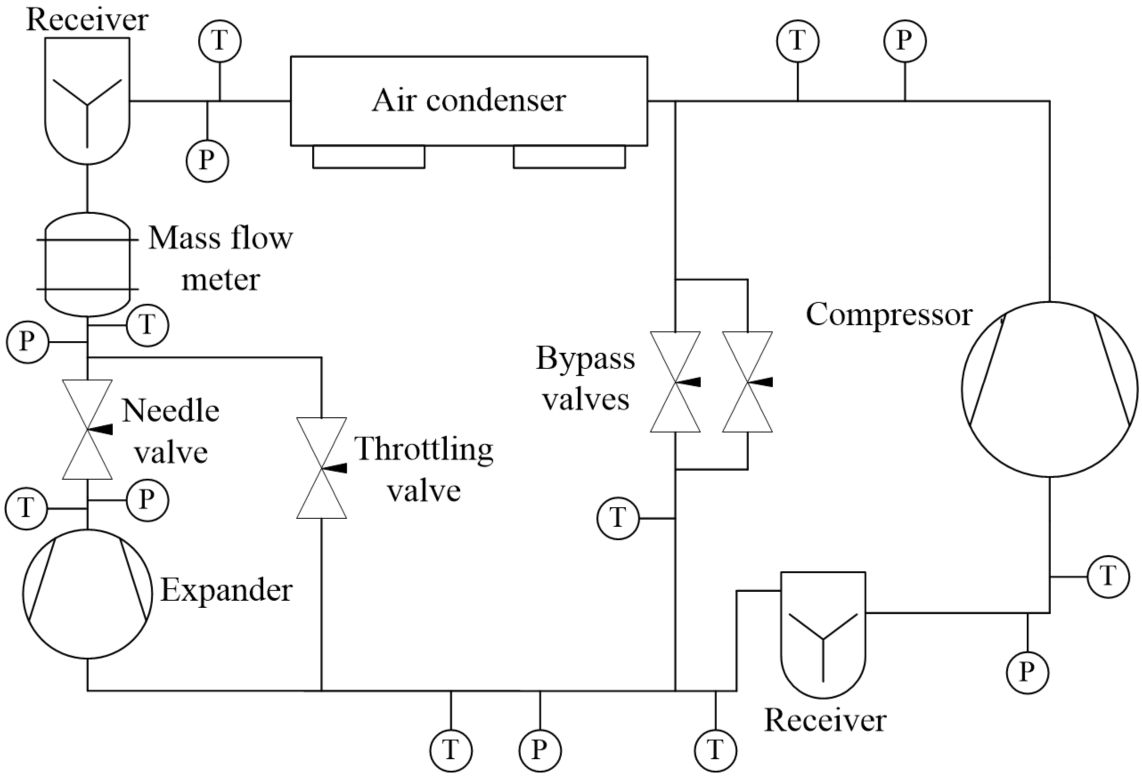

Figure 6.3 - Hot-gas bypass cycle with expander.

In the cycle developed in this work, as shown in Figure 6.3, the compressed refrigerant is condensed by an air condenser that is constituted by fans, whose rotational speed influences the higher pressure and temperature of the cycle; the higher their speed, the lower the pressure and temperature in the condenser. After the condenser, the liquid refrigerant enters a liquid separator in order to obtain liquid at the expander inlet. When the throttling valve is closed, the liquid refrigerant enters the expander after passes through a needle valve that is used to regulate the working conditions at the expander inlet. The remaining compressed part of refrigerant reduces its pressure through two bypass valves that are used for both a coarse and a fine lamination. The mixed flow enters the vapor separator in order to obtain a refrigerant in vapor conditions at the inlet of the compressor. The picture of the test rig is shown in Figure 6.4. It can be seen the smaller size of the plant in respect to the previous tested VCC units and that the components are arranged on a portable structure on wheels to facilitate its movement.

Figure 6.4 - Picture of the test rig.

Copper pipes have been used to connect the components of the test rig. The compressor and the air condenser are provided from Dorin® and can withstand values of pressure up to 30 bar. In order to prevent damages of these components and the risk of accidents, a relief valve is installed in the liquid receiver at higher pressure, which opens when the pressure exceeds a value of 30 bar. In addition, a pressure switch is installed at the outlet of the condenser in order to turn off the compressor when the pressure at this point exceeds a value of 27 bar. For these reasons, the developed cycle could be used with R404A without significant problems and with R410A at low condenser temperatures (i.e. slightly higher than 40 °C). Finally, the rotational speed of the compressor can be modified from 30 to 70 Hz by means of an inverter connected to it.

6.1.3 Acquisition system

The cycle is provided by instruments to measure the thermodynamic conditions in each point and to calculate the performance of the expander. In particular, variables to be measured are pressures, temperatures and the mass flow rate elaborated by the expander.

The measurement instruments are those already used in the CO_2 vapor compression cycle (Table 6.1). Pressures are measured by piezoelectric transducers (Wika, ±0.25% FSO, FSO 60 bar) located in a specific panel arranged on the structure of the test rig. The transducers are connected to the circuits by means of Stauff SGS installed on the piping at the point indicated in Figure 6.3, which include an automatic ball check that closes when the hose is removed so that to connect and disconnect the transducers avoiding gas losses. Temperatures are measured by means of T-type thermocouples. The mass flow rate through the condenser and the expander is sensed by a Yokogawa Coriolis meter (model RCCT-34, Accuracy: ≤0.55% of measured mass flow rate) arranged after the condenser in order to measure a flow in a liquid condition.

Voltage signals from the pressure transducers (in the range 0-10 V) and thermocouples and current from mass flow meter (in the range 4-20 mA) are acquired by a NI Field Point located in the panel where the pressure transducers are arranged. Whereas the thermocouples are connected to the thermocouple module that gives directly the values of the temperature in °C, the pressure transducers and the mass flow meter are connected to an input module that acquires signals both in voltage and current. A dedicated software in the LabVIEW environment was developed to process the acquired data and obtain the desired measurements. By means of tables including the fluid properties, it is possible to obtain and visualize the P-h diagram of the whole cycle both with and without the use of the expander, as shown in Figure 6.5.

Table 6.1 - Measurements instruments and their accuracies.

Equipment	Measurement range	Accuracy
Pressure transducers	0-60 bar	±0.25% FSO
Thermocouple T-type	-270-370 °C	±0.5 °C
Mass flow meter	0-3000 kg h^{-1}	±0.55% MV

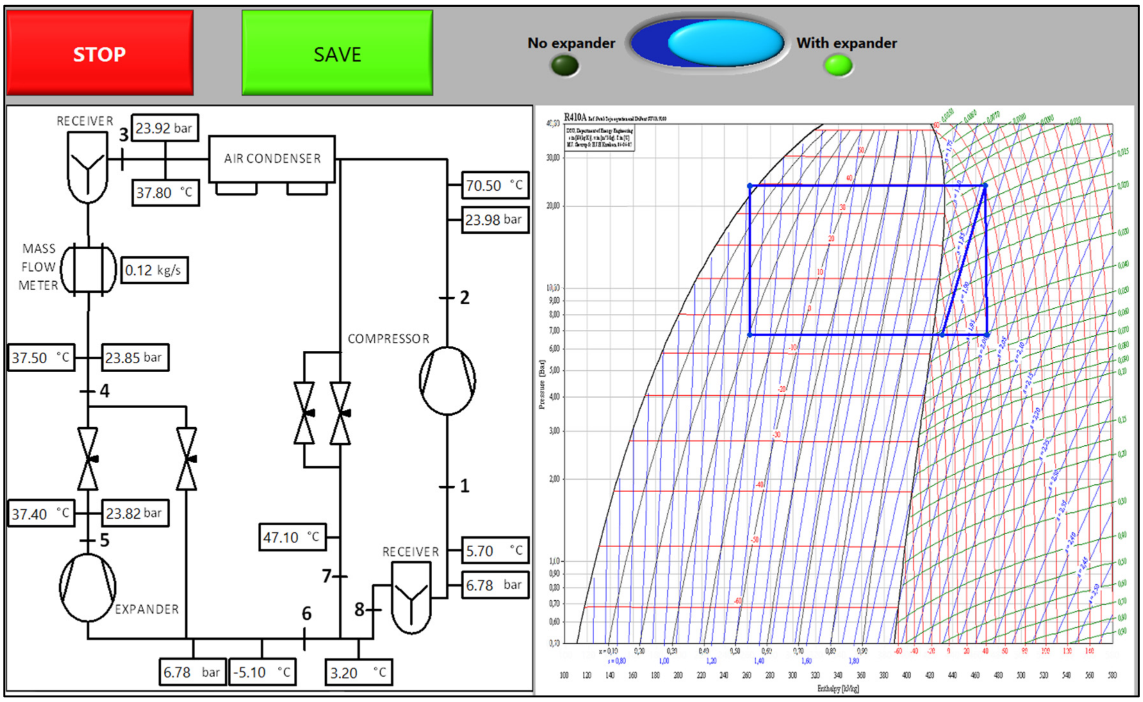

Figure 6.5 - Front panel of the developed LabVIEW software.

6.2 Experimental results

By means of the developed hot-gas bypass cycle, the modified expander was tested experimentally in order to evaluate the effective improvement of the performance. The tests were carried out with both R404A and R410A. The thermodynamic conditions are listed in Table 6.2. The pressure levels reached during the tests were kept relatively low so that the elaborated mass flow rate elaborated by the expander does not exceed the design values; otherwise, at higher pressure levels the mass flow rate increases and the condenser can not condense completely the fluid leading to obtain a fluid with a quality higher than 0 at the inlet of the expander.

Table 6.2 - Experimental thermodynamic conditions with R404A and R410A.

Parameter	R404A	R410A
Suction temperature (°C)	40	36
Suction pressure (bar)	18.3	22
Discharge temperature (°C)	2	8
Discharge pressure (bar)	6.5	10.25

These first tests show the improvement obtained after the redesign of the expander and by using a fluid with a lower required volumetric expansion ratio. Figure 6.6 and Figure 6.7 report the isentropic efficiency and the indicated isentropic efficiency obtained with R404A and R410A respectively. The peak values of the isentropic efficiency measured at the shaft that reaches and exceeds 20% during the experimental tests demonstrate that a strong improvement is reached in comparison to the tests with the previous tested HFC refrigerant (i.e. R134a), where the efficiency reached at maximum 9%. However, the indicated isentropic efficiency, which reaches values over 40%, shows that the mechanical losses still have a great impact on the performance and further improvement can be obtained. On the other hand, the values of the indicated isentropic efficiency show the good thermodynamic behavior of the fluid inside the cylinders.

It must be considered that the isentropic efficiency depends strongly on the thermodynamic conditions at the inlet and outlet of the expander. In particular, higher pressure levels lead to greater performance. For this reason, it is reasonable to think that the performance of the expander should improve when used in a VCC unit at a higher pressure difference between the condenser and the evaporator, especially working with R410A.

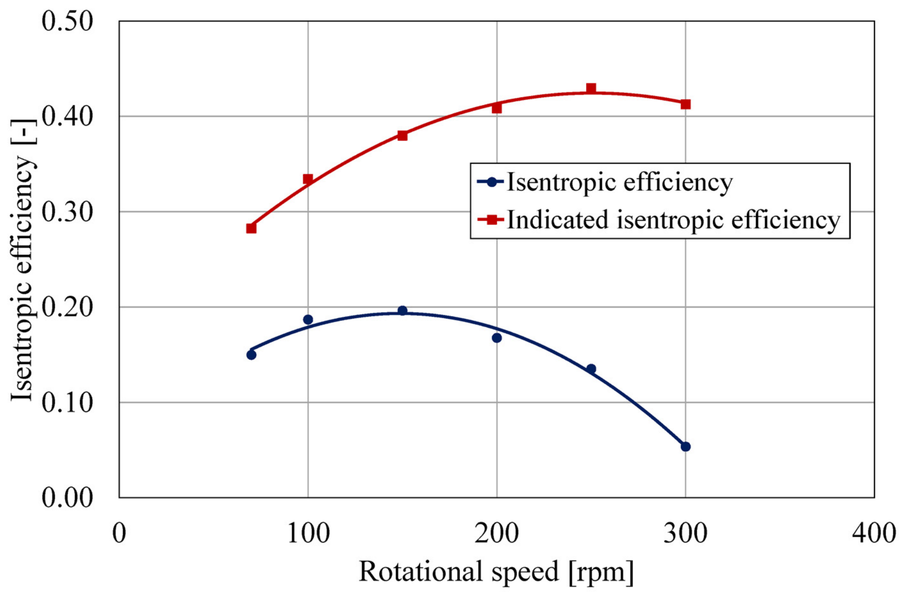

Figure 6.6 - Measured and indicated isentropic efficiencies as function of rotational speed with R404A.

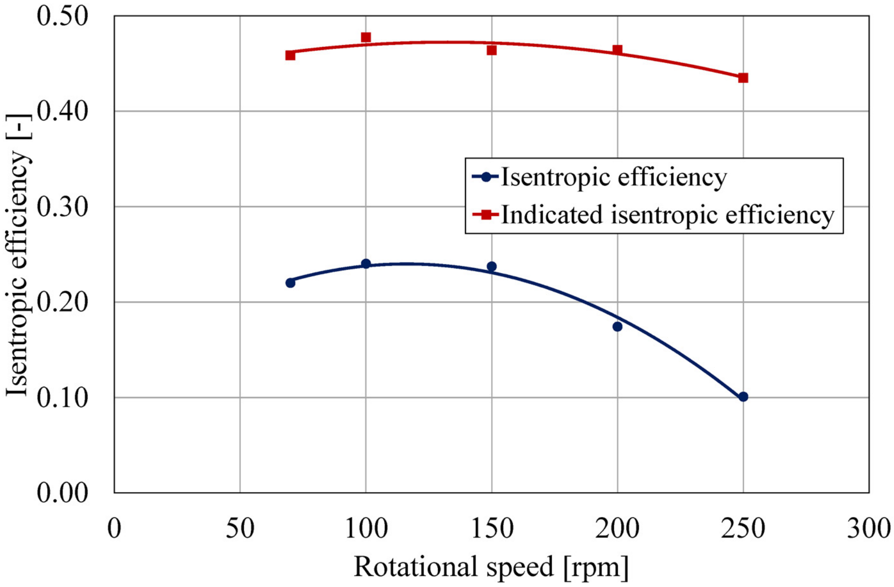

Figure 6.7 - Measured and indicated isentropic efficiencies as function of rotational speed with R410A.

7 Improved numerical model of the two-phase expansion

In the last part of the work, the experimental results were compared to the numerical results obtained from the 0D quasi-steady model, explained in Chapter 2, so that to assess the reliability of the approach and evaluate the critical issues. The P-V diagrams were compared in order to verify the matching between the values of the in-cylinder pressure at each crank angular position. The analyses were carried out on the tests with R134a in order to evaluate the behavior with different workings in terms of suction temperature, pressure and quality.

7.1 Comparison between experimental results and the 0D numerical model

By imposing the boundary conditions equal to the working conditions in the experimental tests, the only parameter to calibrate in the numerical model was the flow coefficient of the valves; this value depends on the inlet fluid conditions and rotational speed and it was unknown before the experimental tests. This calibration was done in order to obtain the matching between the indicated cycles. By reducing the value of the flow coefficient, the peak of the in-cylinder pressure decreases and the slope of the curve in the suction phase is lower because of the increase of the pressure losses. The comparison shows that by calibrating the model to match the in-cylinder pressures in the suction and discharge phases, the measured pressures in the expansion phase are lower than the numerical values. As an example, Figure 7.1 shows the comparison between the measured and estimated P-V diagrams with a saturated liquid of R134a at 60 °C in the suction side, at 500 rpm expander velocity. A general good agreement was found, but the predicted and the measured pressure trends in the expansion phase are very different. The difference is higher at the beginning of the expansion phase. Conversely, the suction and discharge phases modeled by the 0D numerical model follow the same trends of the experimental cycles. It was observed that in the different comparisons carried out at different working conditions, the flow coefficients of the valves assumed values in the range 0.4-0.45 when a saturated liquid enters the expander, whereas their values increase slightly with the suction quality; these values justify the high pressure losses during the suction phase, especially when the fluid enters as saturated liquid.

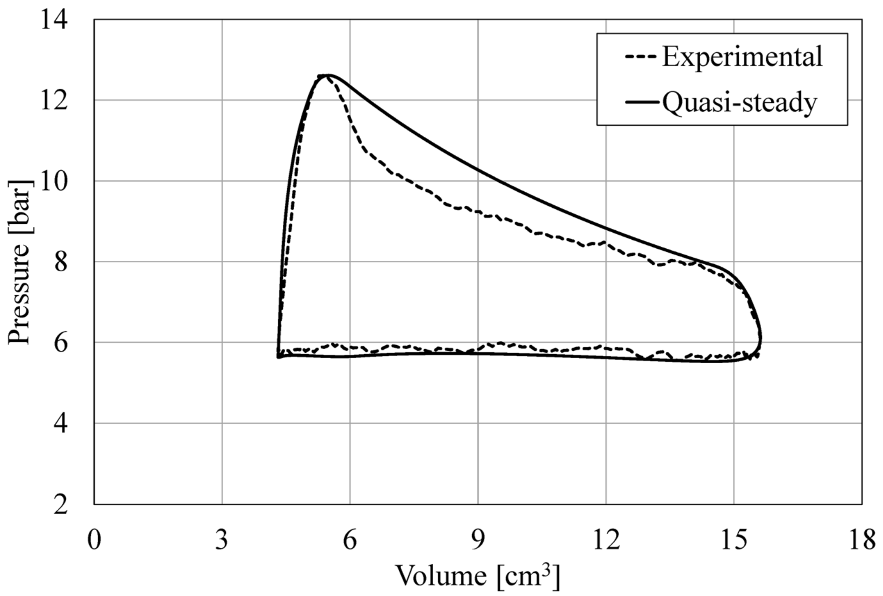

Figure 7.1 - Comparison between the experimental and the numerical P-V diagrams at a suction temperature of 60 °C, saturated liquid and 500 rpm.

This comparison shows that the expansion of a two-phase fluid can not be modeled by an isentropic model, but a more complex description of the phenomena occurring during this phase is needed.

In order to better understand the behavior of the fluid during the expansion phase and develop a correct numerical model to predict the trend of the in-cylinder pressure an analysis of the literature on this topic was carried out.

7.2 State of the art on the two-phase expansion

In general, two-phase expansion devices are a practicable solution also in other applications for improving the energy efficiency. In addition to the recovery energy by replacing the throttling valve in vapor compression cycles, this type of expander may be a key component in trilateral cycle systems [42]. These systems are used to recover the waste energy of an energy system. Figure 7.2 shows a scheme of a trilateral cycle in the T-s diagram. In the two-phase expander, the liquid (i.e. water) at high pressure and temperature, due to the heat transfer with the heat carrier, expands into the wet vapor region by producing work.

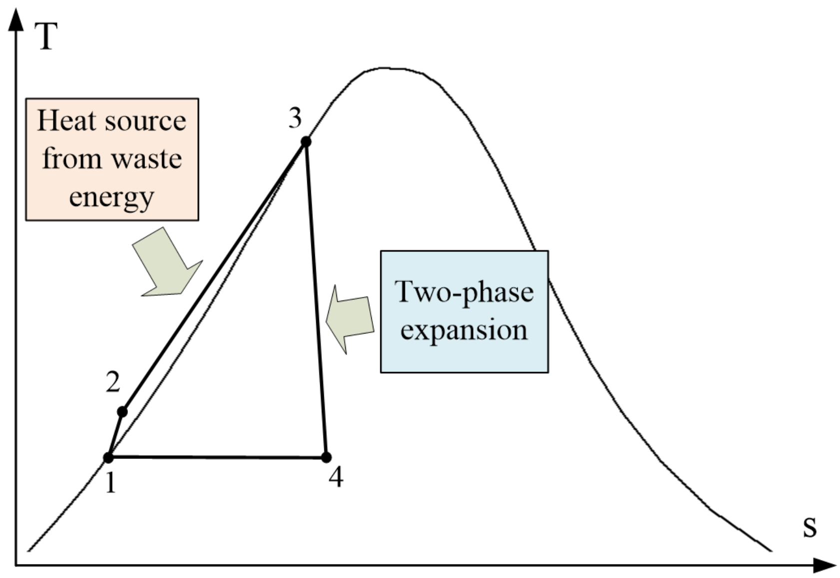

Figure 7.2 - Scheme of a trilateral cycle in the T-s diagram.

Several studies on the two-phase expanders for trilateral cycles were carried out. Smith et al. [43] evaluated the performance of a Lysholm twin-screw expander, reporting an isentropic efficiency of 70%. Kliem [44] investigated the use of a screw expander with water as working fluid. An isentropic efficiency in the range 0.30-0.55 was calculated depending on the inlet temperature. A trilateral cycle with a cyclone separation and a reciprocating expander was studied by Steffen et al. [45]. The results showed that when the rotational speed and the stroke volume increase the injection timing reduces and a reduction of the isentropic efficiency is expected.

In all such systems, as well as the expanders for vapor compression cycles, the behavior of the fluid during the expansion process was not deeply investigated. In adiabatic conditions, a two-phase expansion is called flash evaporation. This process was mainly analyzed by means of experimental tests performed in a constant volume flash chamber without power generation. Saury et al. [46] presented a study on the influence of the initial water head and the pressurization rate on the flash evaporation phenomenon. Dimensionless correlations between the evaporated mass, the initial temperature, the depressurization rate and the initial water head were found. Zhang et al. [47] investigated the steam-carrying effect in static flash evaporation and developed a calculating model according to experimental results. Mutair and Ikegami [48] studied the flash evaporation from superheated water with experimental tests and found that the inflection point and the evaporation end head can be related to the dimensionless Weber, Froude and Jacob numbers.

The available literature dealing with the analysis of a two-phase expansion to generate power is very limited. Kanno and Shikazono [49] analyzed the two-phase adiabatic expansion in a cylinder with a moving piston operating with water at atmospheric pressure (initial condition). An experimental setup was equipped with an insulated cylinder and a piston that was moved by an actuator; a pressure sensor was used to measure the in-cylinder pressure, whereas two thermocouples were used to measure the temperatures of liquid and vapor phases. The results showed a difference between measured and quasi-static pressures that becomes larger with the increase of the piston velocity. They suggest that this pressure difference is caused by the lack of phase change due to the high piston velocity. This behavior is shown in Figure 7.3, where the temperature changes during the experiment are evident. In particular, it can be seen the temperature difference between liquid and vapor. For this reason, a model to predict the pressure change during the expansion was proposed; this model considered the heat exchange between the liquid and the vapor phases and could predict the adiabatic efficiency within the range of about ±2.5%. In addition, they investigated the agitation effect of boiling on the adiabatic efficiency.

Therefore, the mechanism that leads to the reduction of the adiabatic efficiency in two-phase expansion was investigated only with water in atmospheric condition in [49].

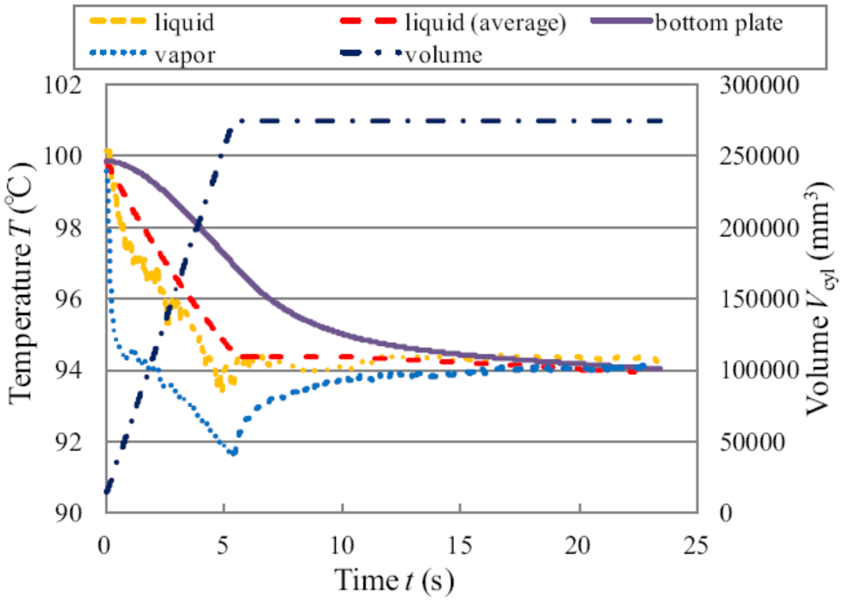

Figure 7.3 - Temperature changes during the two-phase expansion [49].

The previous studies show that the two-phase expansion is not an isentropic process and explained the mechanism that influences the behavior of the fluid during this process. Consequently, these studies were considered so that to explain the trend of the in-cylinder pressure in the tests carried out in this work and to develop a simplified numerical model to predict the behavior of the fluid.

7.3 Development of the numerical model

During the movement of the piston in the expansion phase, the lack of phase change due to the velocity of the piston causes the presence of a hot liquid and a cold vapor in the cylinder. At the beginning, only the vapor phase expands leading to an expansion curve lower than the non-isentropic one, as shown in Figure 7.1. In order to predict the in-cylinder pressure during the expansion phase (i.e. when the valves are closed), a numerical model was developed on the basis of the study presented in [49]. The approach is based on a one dimensional thermal conduction model by applying the correlations used for water in atmospheric conditions to the expansion of pressurized refrigerants. The model was developed with the assumption that saturated vapor is generated from the liquid-vapor interface. In addition, it is assumed that the vapor phase temperature is constant, whereas the liquid temperature has a linear distribution, as schematized in

Figure 7.4. To simplify the model, a single cylinder is taken into consideration and the intake duct is assumed as a dead volume.

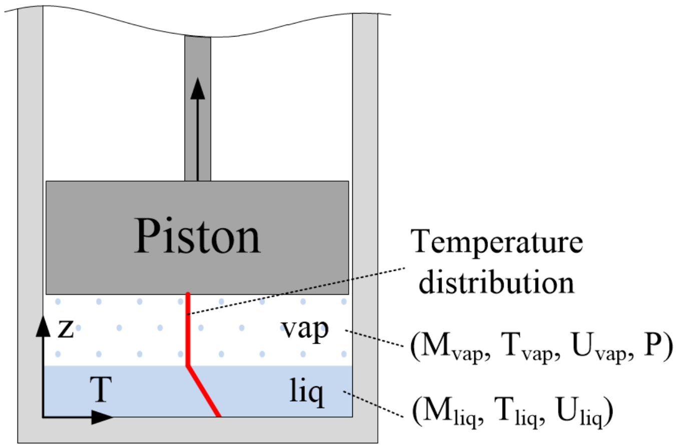

Figure 7.4 - Temperature distribution in the cylinder during the expansion phase.

The model is a quasi-steady model that solves the equations in the fluid volume inside the cylinder for subsequent time-steps. In addition, the model follows a two-step numerical computation, as shown in the scheme of Figure 7.5. First, at each crank angular step that corresponds to an increase of volume, it is considered a sudden expansion only of the vapor phase that reduces its temperature, whereas the liquid does not change its temperature initially. Thus, the mass continuity and the energy equations are solved to obtain the preliminary thermodynamic conditions of the vapor phase inside the cylinder.

Subsequently, a layer of liquid evaporates in order to restore the equilibrium condition in the vapor phase. At the liquid-vapor interface, the latent heat of evaporation due to the evaporated mass is balanced by the heat conduction in the liquid phase (Eq. 7.1).

$$A_{eff} \cdot \lambda_{liq,eff} \cdot \left(\frac{T_{liq} - T_{vap}}{z_{liq}} \right) \cdot dt = M_{ev} \cdot l_v \tag{7.1}$$

Moreover, the actual thermodynamic conditions in the vapor phase are calculated from the mass and energy equations (Eqs. 7.2-7.3).

$$\rho_{vap}^{i} = \frac{M_{vap}^{i-1} + M_{ev}^{i}}{\mathrm{V}_{vap}^{i}} \tag{7.2}$$

$$U_{vap}^{i} = \frac{M_{vap}^{i-1} \cdot U_{vap}^{i-1} + M_{ev} \cdot U_{vap}^{i-1} - p^{i-1} \cdot dV}{M_{vap}^{i}} \tag{7.3}$$

The actual evaporated mass and the in-cylinder pressure at each time step are calculated by solving iteratively the previous equations. By the specific internal energy and the fluid density, the new value of the vapor pressure is obtained by using the property tables. This second step of the procedure is repeated until the difference between two subsequent values of the vapor pressure, which is considered as to the in-cylinder pressure, is negligible. It is important to point out that at the beginning of the expansion (t=0), the temperature in the cylinder is considered constant and the evaporated mass is null. Afterwards, the subsequent liquid temperature is obtained as a consequence of the evaporation from Eq. 7.4.

$$T_{liq}^{i} = \left(\ln(M_{liq}^{i}) - \ln(M_{liq}^{i-1}) + \frac{c_p \cdot T_{liq}^{i-1}}{l_v} \right) \cdot \frac{l_v}{c_p} \tag{7.4}$$

The model of the agitation effect during the expansion phase considers the increase of the interface area between the liquid and vapor due to the boiling bubble. Thus, the liquid effective thermal conductivity can be expressed as a function of the agitation factor β (Eq. 7.5), which depends on the piston diameter, bubble diameter, liquid and vapor density and liquid viscosity:

$$A_{eff} \cdot \lambda_{liq,eff} = (1 + \beta) \cdot A_p \cdot \lambda_{liq} \tag{7.5}$$

The bubble diameter is obtained from the Cole's correlation [50] with the assumption that the bubble departure phenomenon is similar to the pool boiling in atmospheric conditions. By defining the Jacob and Bond numbers in Eqs. 7.6-7.7, the bubble diameter is calculated in Eq. 7.8.

$$Ja = \frac{\rho_{liq} \cdot c_p \cdot (T_{liq} - T_{vap})}{\rho_{vap} \cdot l_v} \tag{7.6}$$

$$Bo^{1/2} = 0.04 \cdot Ja \tag{7.7}$$

$$Bo = \frac{D_b^2 \cdot g \cdot (\rho_{liq} - \rho_{vap})}{\sigma_{liq}} \tag{7.8}$$

The agitation factor is obtained from Eq. 7.9, where the coefficients n_1, n_2 and n_3 are calibrated with the experimental results and depend on the thermodynamic conditions of the fluid.

$$\beta = n_1 \cdot \left(\frac{g \cdot \rho_{liq}^2 \cdot D_b^3}{\mu_{liq}^2} \right)^{n_2} \cdot \left(\frac{D_b}{D_p} \right)^{n_3} \tag{7.9}$$

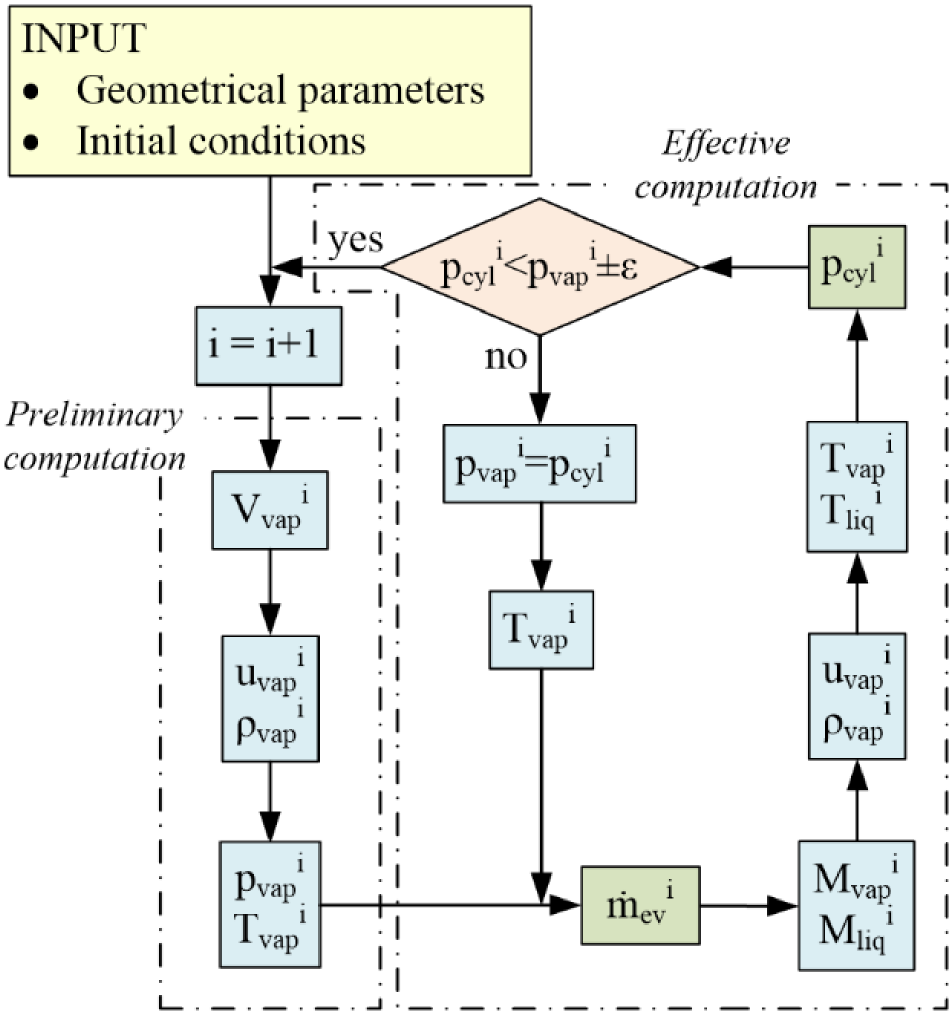

Figure 7.5 - Computational scheme of the numerical model for the prediction of the two-phase expansion.

7.3.1 Comparison with experimental results

The reliability of the two-phase expansion model explained in the previous paragraph was evaluated by comparing the in-cylinder pressure trend obtained by the experimental tests with R134a and the numerical model. In this way, the influence of the inlet thermodynamic condition, in terms of temperature, pressure and quality, and the rotational speed on the behavior of the two-phase fluid was analyzed in detail. In this analysis, the P-V diagram of only one cylinder of the expander is considered for the comparison.

It is important to remark that, at the beginning of the expansion, the value of the fluid quality is different from the inlet quality, due to the losses and the increased volume during the suction phase. Consequently, the numerical results were calibrated to match the experimental trends of the in-cylinder pressure by varying the fluid quality at the beginning of the expansion and the coefficients in Eq. 7.9. These coefficients determine the heat transfer in the cylinder by influencing the bubble diameter. It was found that, in all tests, the value of n_1 deeply changes depending on the thermodynamic conditions, whereas the values of n_2 and n_3 are almost unchanged at 0.1 and 1 respectively. In addition, in order to evaluate the improvement of the in-cylinder pressure prediction by using the non-isentropic two-phase expansion, also the isentropic expansion curve was calculated for every analyzed case by means of the numerical model explained in Chapter 2; in this case, the matching with the starting and final pressures was found by varying only the initial quality.

At first, Figure 7.6 shows the experimental and the numerical expansion curves of an initially saturated liquid at different suction temperatures and 400 rpm expander rotational speed. It was noticed that the initial fluid quality inside the cylinder must be always set at higher values for the calibration of the isentropic model compared to the non-isentropic one, in order to have a satisfactory matching with the experimental data.

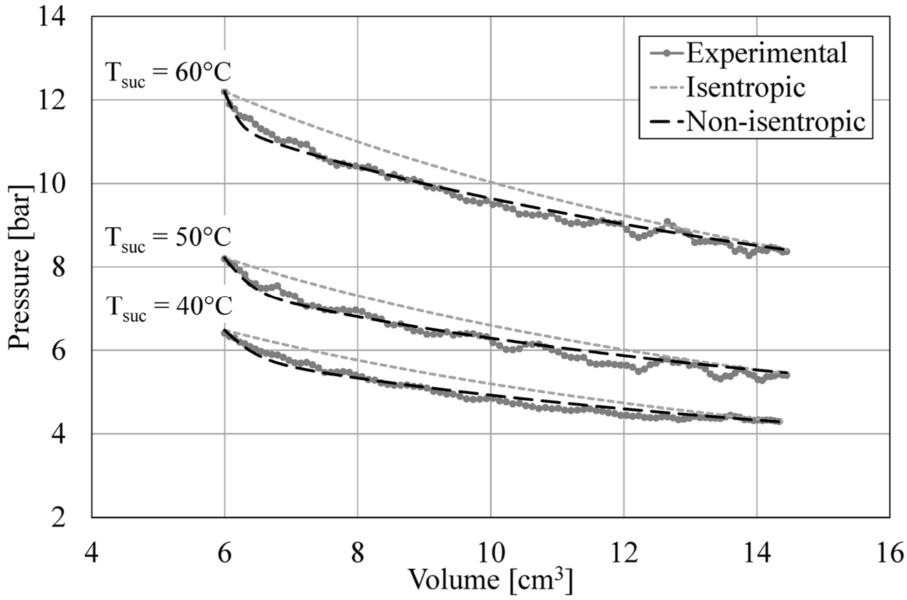

Figure 7.6 - Experimental and numerical trends of the expansion phase for a saturated liquid at different suction temperatures and 400 rpm.

The non-isentropic model predicts with a good accuracy the pressure decrease at the beginning of the expansion and the following less step trend. The expansion starts without boiling bubbles, thus leading to a weak effect of the agitation and, consequently, to a modest heat transfer between the two phases: it results into a rapid decrease of the in-cylinder pressure. Successively, the generated boiling bubbles causes the agitation of the liquid phase, which increases the heat transfer to the vapor phase leading to a moderate pressure reduction. From the calibration of the non-isentropic model, it was found that the coefficient n_I of Eq. 7.9 decreases from 10^8 to 10^6 by reducing the suction temperature, although the initial fluid quality was almost the same. Thus, at the same rotational speed and fluid quality, at higher suction temperature the bubble diameter is larger and thus the effect of the bubble agitation is enhanced.

The behavior of the expansion phase also depends on the inlet quality, as shown in Figure 7.7 that shows the P-V diagrams for different inlet qualities, at 60 °C suction temperature and 500 rpm expander rotational speed.

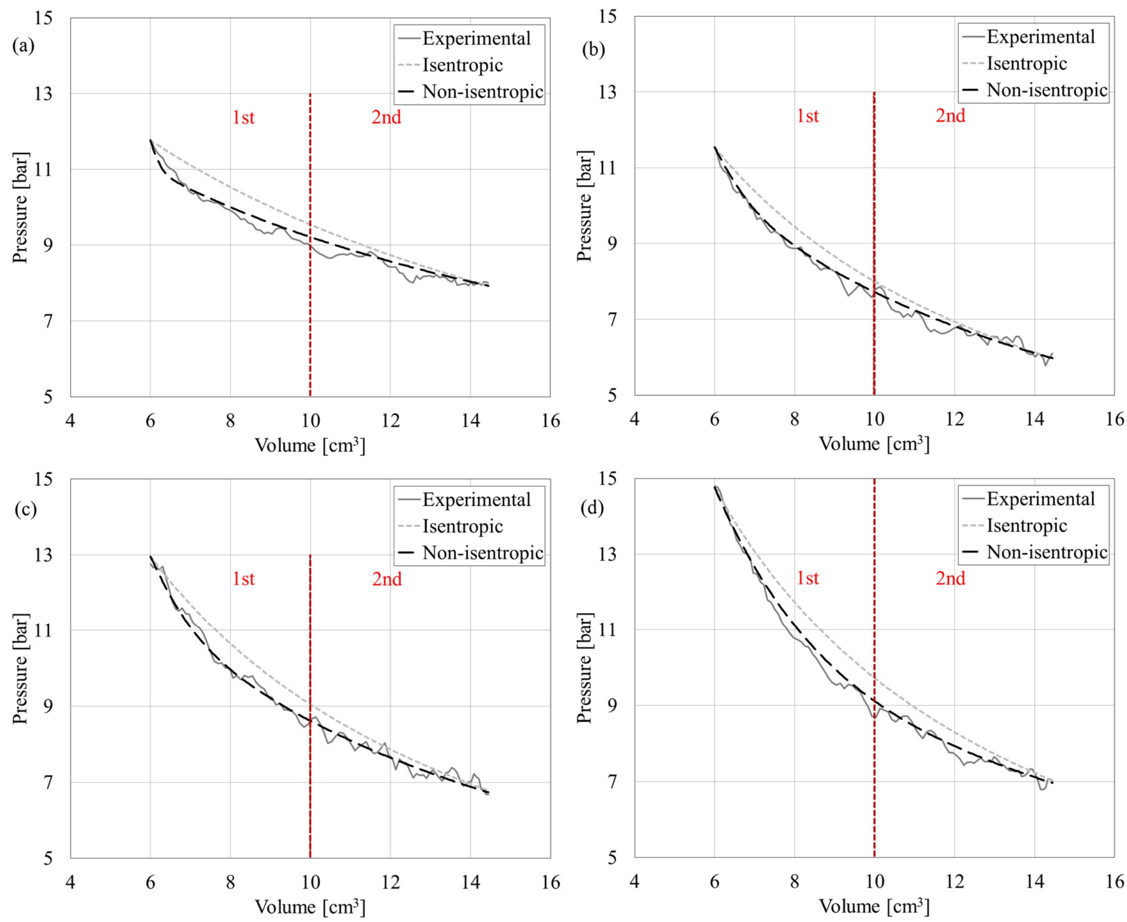

Figure 7.7 - Experimental and numerical P-V diagrams in the expansion at a suction temperature of 60 °C and 500 rpm with an inlet quality of 0 (a), 0.23 (b), 0.56 (c) and 0.8 (d).

At higher values of the inlet quality, the amount of liquid in the cylinder is reduced and the effect of the bubble agitation decreases, leading to a behavior closer to the isentropic expansion. Thus, the difference between the isentropic and the non-isentropic trends at the beginning of the expansion is reduced. This behavior is also explained by the value of the coefficient n_1, which is lower at higher inlet quality (i.e. from 10^8 to 10^4). Summarizing, the higher is the inlet fluid quality, the lower is the bubble diameter, thus the effect of phase change delay is reduced. On the other hand, the influence of the rotational speed on the expansion phase is marginal compared to the other parameters. In fact, as shown in Figure 7.8 that depicts the P-V diagram in the expansion phase for a saturated liquid at 60 °C at the inlet and different rotational speeds, the slopes of the curves are very similar, even though the pressure levels are higher for lower rpms.

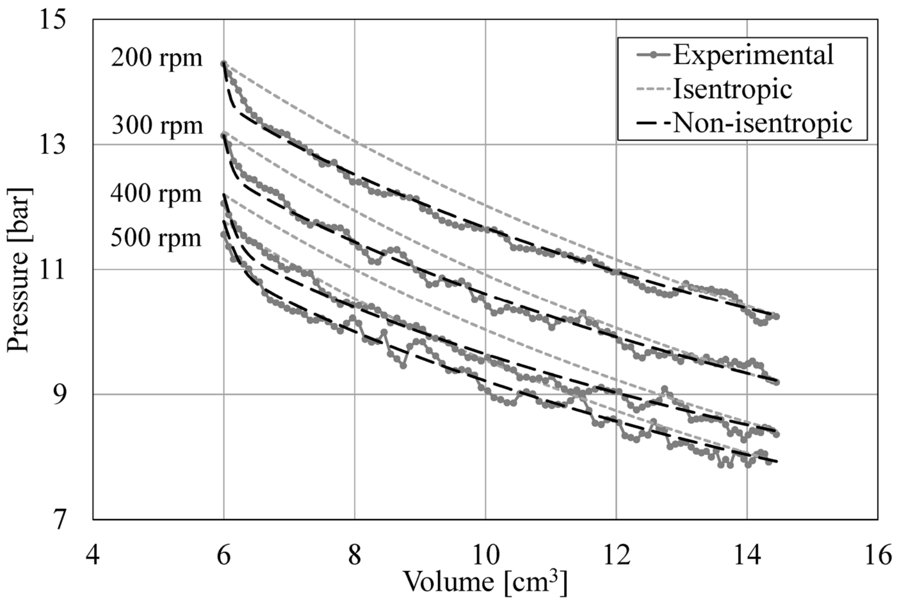

Figure 7.8 - Experimental and numerical trends of the expansion phase for a saturated liquid and 60 °C at the suction and different rpms.

The comparison was carried out by varying the initial fluid quality, which is actually unknown and is different between the isentropic and non-isentropic models. With the same fluid quality fixed at the beginning of the non-isentropic expansion model, which is actually always lower than the isentropic one, the isentropic expansion curve has a moderate slope and an even larger deviation from the experimental data.

The accuracies of the numerical models were evaluated by the R^2 coefficient expressed as (Eq. 7.10):

$$R^2 = 1 - \frac{\sum_{i=1}^{n} (y_i - \hat{y}_i)^2}{\sum_{i=1}^{n} (y_i - \bar{y})^2} \tag{7.10}$$

where y_i is the experimental data, $\bar{y}$ is the average of the experimental data and $\hat{y}_i$ is the calculated numerical value from the model. The accuracy of the model is higher when the value of R^2 is closer to the unity.

Table 7.1 shows the values of R^2 for both models. The estimation was performed separately in two halves of the expansion curve, as depicted in Figure 7.7. The improved accuracy obtained with the non-isentropic model compared to the isentropic one is apparent for the whole curve. It can be noticed that the isentropic model is less accurate with an inlet quality of zero than the other inlet conditions, whereas the accuracy of the non-isentropic model is almost unchanged at all conditions. Moreover, Table 7.1 highlights that the isentropic model predicts the in-cylinder pressure better at the end than the beginning of the expansion phase. On the other hand, the non-isentropic model can predict the in-cylinder pressure with an accuracy almost unchanged during the movement of the piston.

Table 7.1 - Values of R^2 for isentropic and the non-isentropic model and in the first and second parts of the expansion curve at a suction temperature of 60 °C and 500 rpm with different inlet qualities.

	1st		2nd	
	Is	**Non-is**	**Is**	**Non-is**
X_{in} = 0	0.729	0.968	0.890	0.964
X_{in} = 0.23	0.905	0.991	0.958	0.981
X_{in} = 0.56	0.921	0.993	0.967	0.988
X_{in} = 0.8	0.908	0.989	0.950	0.993

In conclusion, the results showed that the expansion of a two-phase expansion can not be modeled accurately with an isentropic model, as usually used in applications with an expansion or compression of a superheated vapor or gas. The developed model that simulates the expansion as a non-isentropic model predicts the process with a higher level of detail and with an increased accuracy, even though it uses the same correlations refereed to the water in atmospheric condition.

Conclusions

In the recent years, the increasing of energy demand for heating and cooling in houses and utility buildings makes these applications a primary component of increasing CO_2 emmisions that cause global warming and air pollution. The environmental and economic policies adopted to abate CO_2 emissions and promote sustainability have led to focus the interest in technologies of high efficiency and energy savings. In particular, many efforts have been made to improve the efficiency of the Vapor Compression Cycles (VCC) that represent the main systems for the production of heat and cold. In these cycles, about 20% of compressor power is consumed by the pressure drop through the throttiling valve or capillary tube. For this reason, a methodology for improving system efficiency and saving energy is the use of new apparatus for reducing the pressure during the expansion phase. With this aim, numerical analyses are needed during the earliest phase of design and experimental tests are needed for the effective characterization of the performance.

The work presented in this Thesis had the purpose of developing an expander in place of the throttling valve in a common VCC unit for power recovery from the expansion phase between the condenser and the evaporator; consequently, an improvement of the cycle efficiency is obtained due to the decrease of the electricity consumed by the compressor and the increase of the cooling capacity in the evaporator. In order to keep the manufacturing costs down and further justify its use, an existing machine already present in the market for other applications was used. In particular, a radial piston expander has been derived from a hydraulic motor that works with oil withstanding pressures up to 300 bar. Both numerical and experimental analyses have been performed to study in detail the performance of the proposed expander inside VCC units working with different fluids.

In the first part of the work, the main issues that influence the expander performance have been evaluated so that to identify how to improve the design without changing the overall architecture of the machine. A fast and flexible approach for reducing the computational costs has been used by developing a 0D quasi-steady numerical model into EES® environment that evaluates the variation of the thermodynamic parameters in the cylinders by solving the mass and entropy equations with time-step progress. Because of the lack of models on expansion of wet fluids in literature, the accuracy of the developed model has been evaluated by comparing its results with those obtained from the commercial software AMESim® that contains validated libraries on compontents such as ducts, orifice and cylinder, and property tables of some refrigerants. The performed numerical analysis have showed that, in comparison to the original version of the machine, some components have needed some modifications related to the valve timing and the dead volume in order to increase the built-in volumetric expansion ratio leading to higher specific powers produced by the expander.

The effective performance of the expander has been measured experimentally in traditional VCC units. For this reason, a test rig has been built and has been composed by the expander, the connection rod instrumented with a torque meter and a rotation sensor, and an electric motor to control the rotational speed through a servo drive. In addition, the expander has been equipped with thermocouples and dynamic pressure sensors so that to measure the working thermodynamic conditions and the time hystories of pressure inside the cylinders. A measurement system has been developed and two purposely LabVIEW® software have been implemented to calculate the power output and the isentropic efficiency, to generate the P-V diagrams and to control the electric motor speed.

In order to evaluate the expander performance inside a widely used VCC unit in residential and industrial applications that works with HFCs, the first tests have been carried out in a test rig with R134a of DORIN. The influence of the thermodynamic conditions at the expander inlet and the rotational speed on the performance has been analyzed in detail. The results have showed that the mechanical losses and the leakages affect negatively the performance, as demonstrated by the isentropic efficiency that reaches at maximum a value of 9% by considering the measured values of power and mass flow rate, and it increases up to a potential value of 40% without considering these sources of losses. As regards the cycle efficiency, the COP improvement increases from a value of almost 1.5% to a potential 8% that is very promising in comparison to the results obtained in literature.

Another important issue that limits the expander performance is the high volumetric expansion ratio required by the expansion of a HFC refrigerant from liquid conditions. For this reason, together with the strong interest towards the use of carbone dioxide as refrigerant in alternative to the synthetic refrigerants, the expander was tested in a test rig at the Department of Industrial Engineering of the University of Florence working with CO_2, which requires a lower expansion volumetric ratio. Higher performance in terms of both indicated and measured isentropic efficiencies has been achieved (i.e. from a measured value of 19% to a potential 60%), despite the greater impact of the mechanical losses due to the high pressure levels reached during the tests. Compared to the HFC cycles, in this case the COP improvement is higher and goes from a measured 8% to a potential 35%.

The experimental tests, especially in terms of indicated cycles, have showed the high potential of the expander when used in VCC cycle. The presence of high mechanical losses and leakages is related to the original application of the machine, which must work with an higher viscosity fluid withstanding high values of pressure (i.e. up to 300 bar). In addition, an assessment of the mechanical losses have showed that the component that mostly affect the friction torque are the bearings and the frontal seal inside the expander. For these reasons, the expander has been redesigned, by maintaining the original concept of the machine so that to reduce the manufacturing costs, whereas modifications have been made for reducing the mechanical losses and increasing the built-in expansion volumetric ratio in order to obtain high performance also with HFCs.

Meanwhile, the issues arised from the experimental tests related to the difficulty of regulating and reaching stable conditions of the cycle has brought to design and build a dedicated cycle for testing the expander. In the developed “hot-gas bypass cycle”, the conditions at the compressor inlet are obtained by mixing the cold two-phase fluid coming from the expansion phase with part of the hot superheated vapor coming from the compressor discharge leading to the remotion of the cooling capacity in the evaporator. This configuration has benefits due to the lower size, smaller number of components, lower costs and higher stability of the cycle. The test rig has been arranged on a portable structure on wheels to facilitate its movement and an acquisition system has been developed to measure pressures, temperatures and the mass flow rate elaborated by the expander. The experimental data with R404A and R410A as working fluids, which are HFC refrigerants with a lower required volumetric expansion ratio, have showed that an improvement of the measured isentropic efficiency has been obtained reaching values over 20%. However, the indicated cycles have showed that a further improvement of the mechanical losses could be reached leading to even higher values of efficiency.

In the last part of the work, the experimental indicated cycles with R134a have been compared with the results obtained by the 0D numerical model in order to assess the accuracy of the developed model. After calibrating the numerical model in order to match the suction and discharge phases (i.e. only by changing the flow coefficient), a difference between the pressure values during the expansion phase has been noticed. This different behavior is due to the lack of phase change during the movement of the piston that causes a temperature difference between the liquid and vapor phases. By applying the same correlations used in literature for water in atmospheric conditions, a non-isentropic model of the two-phase expansion based on a 1D thermal conduction model has been developed to predict the pressure trend with R134a, which considers also the agitation effect of the boiling bubbles. The results have showed that the model can predict the in-cylinder pressures with a good accuracy during the expansion phase in all the tested conditions.

In conclusion, the experimental results obtained by using the proposed radial piston expander, which derived from an hydraulic motor, as energy recovery inside a VCC unit showed very promising results of the performance, despite the high impact of the mechanical losses that have a considerable detrimental effect. The improvement of the expander design led to an increase of the performance, but there is still room for improvement. Moreover, the comparison between the experimental and the numerical cycles showed that the pressure trend during the expansion phase can not be modeled by a isentropic model, as used in case of compression or expansion of fluids in vapor conditions. The use of a 1D thermal conduction model is innovative in this field and leads to an improved accuracy.

References

[1] Perkins, J., 1934. Apparatus for producing ice and cooling fluids. Patent 6662, UK.

[2] Calm, J.M., 2008. The next generation of refrigerants – Historical review, considerations, and outlook. Int. J. Ref. 31, 1123-1133.

[3] Maina, P., Huan, Z., 2015. A review of carbon dioxide as a refrigerant in refrigeration technology. South African Journal of Science 111, 1-10.

[4] Hundy, G.F., Trott, A.R., Welch, T.C., 2008. Refrigeration and Air-Conditioning. 4th ed. Oxford: Butterworth Heinemann.

[5] Lorentzen, G., 1994. Revival of carbon dioxide as a refrigerant. Int. J. Ref. 17 (5), 292-301.

[6] Minh, N.Q., Hewitt, N.J., Eames, P.C., 2006. Improved vapour compression refrigeration cycles: literature eview and their application to heat pumps. International Refrigeration and Air Conditioning Conference at Purdue, West Lafayette, IN.

[7] Preissner, M., 2001. Carbon Dioxide Vapor Compression Cycle Improvements with Focus on Scroll Expanders. Ph.D. Thesis, University of Maryland, College Park.

[8] Domanski, P.A., 1995. Theoretical evaluation of the vapour compression cycle with a liquid-line/suction-line heat exchanger, economizer, and ejector. National Institute of Standards and Technology, US, 1-31.

[9] Qiu, G., Liu, H., Riffat, S., 2011. Expanders for micro-CHP systems with organic Rankine cycle. Applied Thermal Engineering 31, 3301-3307.

[10] Zhang, A., Ma, Y., Li, M., Zhao, L., 2013. Recent advantages of energy recovery expanders in the transcritical CO2 refrigeration cycle. HVAC&R Research 19, 376-384.

[11] Salehi, K.M., Hewitt, N.J., Huang M.J., 2011. Developing a combined compressor expander heat pump – experimental evaluation of the compressor & expander. 26th Int. Congress of Refrigeration, August 21-26 2011, Prague, Czech Republic.

[12] Tøndell, E., 2006. Impulse expander for CO_2. 7th IIR Gustav Lorentzen Conference, Trondheim, Norway.

[13] Stosic, N., Smith, I.K., Aldis, C.A., Brazs, J., Sishtla, V., 1999. Twin screw expanders in large chiller units. Proc. of Int. Conf. on Industrial Compressors and their Systems, September 1999, City University, London.

[14] Huff, H.J., Radermacher, R., Preissner, M., 2003. Experimental investigation of a scroll expander in carbon dioxide air-conditioning system. Int. Congress of Refrigeration, Washington, DC.

[15] Kim, H.J., Ahn, J.M., Cho, S.O., 2008. Numerical simulation on scroll-expander-compressor unit for CO2 trans-critical cycles. Applied Thermal Engineering 28, 1654-1661.

[16] Fukuta, M., Yanagisawa, T., Kosuda, O., 2006. Performance of scroll expander for CO2 refrigeration cycle. Proceedings of International Compressor Engineering Conference at Purdue, West Lafayette, IN.

[17] Fukuta, M., Yanagisawa, T., Higashiyama, M., Ogi, Y., 2009. Performance of vane-type CO_2 expander and characteristics of transcritical expansion process. HVAC&R Research 15, 711-727.

[18] Yang, B., Peng, X., He, Z., Guo, B., Xing, Z., 2009. Experimental investigation on the internal working process of a CO_2 rotary vane expander. Applied Thermal Engineering 29, 2289-2296.

[19] Jia, X., Zhang, B., Pu, L., Guo, B., Peng, X., 2011. Improved rotary vane expander for trans-critical CO_2 cycle by introducing high-pressure gas into the vane slots. International Journal of Refrigeration 34, 732-741.

[20] Li, M., Ma, Y., Tian, H., 2009. A rolling piston-type two-phase expander in the transcritical CO2 cycle. HVAC&R Research 15, 729-741.

[21] Tian, H., Ma, Y., Li, M., Wang, W., 2010. Study on expansion power recovery in CO2 trans-critical cycle. Energy Conversion and Management 51, 2516-2522.

[22] Jiang, Y., Ma, Y., Fu, L., Li, M., 2013. Some design features of CO_2 two-rolling piston expander. Energy 55, 916-924.

[23] Guan, H.Q., Ma, Y.T., Li, M.X., 2006. Some design features of CO2 swing piston expander. Applied Thermal Engineering 26, 237-243.

[24] Nickl, J., Will, G., Quack, H., 2005. Integration of a three-stage expander into a CO2 refrigeration system. Int. J. Refrigeration 28, 1219-24.

[25] Zhang, B., Peng, X., He, Z., Xing, Z., Shu, P., 2007. Development of a double acting free piston expander for power recovery in transcritical CO2 cycle. Applied Thermal Engineering 27, 1629-1636.

[26] Baek, J.S., Groll, E.A., Lawless, P.B., 2005. Piston-cylinder work producing expansion device in a transcritical carbon dioxide cycle. Part I: Experimental investigation. Int. J. Refrigeration 28, 141-151.

[27] Fukuta, M., Anzai, F., Motozawa, M., Terawaki, H., Yanagisawa, T., 2014. Performance of radial piston type reciprocating expander fo CO2 refrigeration cycle. Int. J. Refrigeration 42, 48-56.

[28] He, T., Xia, C, Zhao, Y., Li, L., Shu, P., 2009. An Experimental Study on Energy Recovery by a Pelton-Type Expander in a Domestic Refrigeration System. HVAC&R Research 15, 785-799.

[29] Zhang, Z., Li, M., Ma, Y., Gong, X., 2015. Experimental investigation on a turbo expander substituted for throttle valve in the subcritical refrigeration system. Energy 79, 195-202.

[30] Xia, C., Zhang, W., Bu, G., Wang, Z., Shu, P., 2013. Experimental study on a sliding vane expander in the HFC410A refrigeration system for energy recovery. Applied Thermal Engineering 59, 559-567.

[31] Wang, M., Cao, F., Zhao, Y., Wang, Z., Bu, G., 2013. Comparison between modeling and experiments on a two-stage rotary vane expander for an HFC-410A air conditioning system. Proc IMechE, Part A: J. Power and Energy 227 (2), 193-205.

[32] Hwang, Y., 2009. Expansion work recovery machine: worth using or not? HVAC and R. Res. 15, 671-672.

[33] Subiantoro, A., Ooi, K.T., 2013. Economic analysis of the application of expanders in medium scale air-conditioners with conventional refrigerants, R1234yf and CO2. Int. J. Refrigeration 36, 1472-1482.

[34] Stiaccini, I., Romani, L., Ferrari, L., Ferrara, G., 2015. A Hybrid Time-frequency Domain Approach for Numerical Modeling of Reciprocating Compressors. Energy Procedia 82, 1102-1112.

[35] Ould Didi, M.B., Kattan, N., Thome, J.R., 2002. Prediction of two-phase pressure gradients ofrefrigerants in horizontal tubes. Int. J. Refrigeration 25, 935–947.

[36] Müller-Steinhagen, H, Heck, K, 1986. A simple friction pressure drop correlation for two-phase flow in pipes. Chem Eng Process 20, 297–308.

[37] Chesi, A., Ferrara, G., Ferrari, L., Tarani, F., 2012. Setup and characterisation of a multi-purpose test rig for R744 refrigerating cycles and equipment. Int. J. Refrigeration 35, 1848-1859.

[38] McGovern, J.A., 1984. Analysis of a Refrigerant Compressor Load Stand Incorporating Hot Gas Bypass and a Single Full Condensation Heat Exchangers. Proceedings of International Compressor Engineering Conference at Purdue, West Lafayette, IN.

[39] Bell, I.H, Groll, E.A., Braun, J.E., Horton, W.T., 2013. Experimental testing of an oil-flooded hermetic scroll compressor. Int. J. Refrigeration 36, 1866-1873.

[40] Gessler, P.D., Mathison, M.M., Bowman, A.J., 2014. Modeling of a Hot Gas Bypass Test Block for Centrifugal Compressors. Proceedings of International Compressor Engineering Conference at Purdue, West Lafayette, IN.

[41] Bradshaw, C., 2014. Hot-Gas Bypass Load Stands. Compressor Engineering Conference at Purdue, West Lafayette, IN.

[42] Fischer, J., 2011. Comparison of trilateral cycles and organinc Rankine cycles. Energy 36, 6208-6219.

[43] Smith, I.K., Stosic, N., Aldis, C.A., 1994. Lysholm Machines as Two-Phase Expanders. Proceedings of International Compressor Engineering Conference at Purdue, West Lafayette, IN.

[44] Kliem, B.F., 2005. Grundlagen des Zweiphasen-Schraubenmotors, Fundamentals of the Two-Phase Screw-Type Engine [Dissertation]. Fakultat Maschinenbau der Universitat Dortmund [in German].

[45] Steffen, M., Loffler, M., Schaber, K., 2013. Efficiency of a new Triangle Cycle with flash evaporation in a piston engine. Energy 57, 295-307.

[46] Saury, D., Harmand, S., Siroux, M., 2005. Flash evaporation from a water pool: influence of the liquid height and of the depressurization rate. Int. J. Ther. Sci. 44, 953-965.

[47] Zhang, D., Chong, D., Yan, J., Zhang, Y., 2012. Study on steam-carrying effect in static flash evaporation. Int. J. Heat Mass Transfer 55, 4487–4497.

[48] Mutair, S., Ikegami, Y., 2009. Experimental study on flash evaporation from superheated water jets: influencing factors and formulation of correlation. Int. J. Heat Mass Transfer 52, 5643–5651.

[49] Kanno, H., Shikazono, N., 2015. Experimental and modeling study on adiabatic two-phase expansion in a cylinder. Int. J. Heat Mass Transfer 86, 755-763.

[50] Kim, J., Kim, M.H., 2006. On the departure behaviors of bubble at nucleate pool boiling. Int. J. Multiphase Flow 32, 1269–1286.